

2020-01-01

Spectroscopic Techniques To Characterize And Develop Sensing Methods For Titanium Dioxide Nanoparticles In Water

Reagan Scott Turley
University of Texas at El Paso

Follow this and additional works at: https://scholarworks.utep.edu/open_etd



Part of the [Chemistry Commons](#)

Recommended Citation

Turley, Reagan Scott, "Spectroscopic Techniques To Characterize And Develop Sensing Methods For Titanium Dioxide Nanoparticles In Water" (2020). *Open Access Theses & Dissertations*. 3051.
https://scholarworks.utep.edu/open_etd/3051

This is brought to you for free and open access by ScholarWorks@UTEP. It has been accepted for inclusion in Open Access Theses & Dissertations by an authorized administrator of ScholarWorks@UTEP. For more information, please contact lweber@utep.edu.

SPECTROSCOPIC TECHNIQUES TO CHARACTERIZE AND DEVELOP
SENSING METHODS FOR TITANIUM DIOXIDE
NANOPARTICLES IN WATER

REAGAN SCOTT TURLEY

Doctoral Program in Chemistry

APPROVED:

Jorge Gardea-Torresdey, Ph.D., Chair

Geoffrey Saupe, Ph.D.

Dino Villagrán, Ph.D.

W. Shane Walker, Ph.D.

Paul Westerhoff, Ph.D.

Stephen L. Crites, Jr., Ph.D.
Dean of the Graduate School

Copyright ©

by

Reagan Scott Turley

2020

Dedication

To my parents, my son, my wife and our future children. You make it all worthwhile.

SPECTROSCOPIC TECHNIQUES TO CHARACTERIZE AND DEVELOP
SENSING METHODS FOR TITANIUM DIOXIDE
NANOPARTICLES IN WATER

by

REAGAN SCOTT TURLEY

DISSERTATION

Presented to the Faculty of the Graduate School of

The University of Texas at El Paso

in Partial Fulfillment

of the Requirements

for the Degree of

DOCTOR OF PHILOSOPHY

Department of Chemistry and Biochemistry

THE UNIVERSITY OF TEXAS AT EL PASO

May 2020

Abstract

Titanium dioxide nanoparticles are being used in ever increasing amounts and applications in many consumer products and industrial processes including water treatment. These nanoparticles have not been shown to be toxic to humans via ingestion, but it is worthwhile to develop a portable and rapid detection method to quantify the concentration of nanoparticles in treated drinking water. A preliminary study on how chelating ligands influence the dispersion and ζ -potential of TiO₂ nanoparticles was performed. An additional study was designed to find ligands that would fluoresce when bound to TiO₂ by measuring the level of adsorption but was ultimately unsuccessful. These two studies did, however, show which ligands best improve the suspension of TiO₂ in water.

Photocatalytic nanomaterials are widely utilized in a variety of products including self-cleaning coatings and some water treatment technologies. To support the safe use of photocatalytic nanomaterials, it is essential to have low cost methods to rapidly, preferably in the field, detect residual photocatalysts in water. Current technologies with low detection limits are largely based upon mass quantification rather than functional behavior that is intrinsic to the nanomaterial (e.g., photocatalysis). Current mass-based detection techniques require expensive analytical equipment (e.g., inductively coupled plasma mass spectroscopy, ICP-MS) and often complex sample preparation (e.g., filtration, acidification, microwave digestion). Therefore, we developed a simple and portable method that exploits the photocatalytic reactivity of titanium dioxide (TiO₂) nanoparticles to detect and quantify these materials in various aqueous matrices including synthetic soft and hard waters. Three TiO₂ nanomaterials are used in this study

with various crystalline structure and sizes from 18 nm up to 30 nm. The method quantifies TiO₂ nanomaterials in water at levels comparable to background titanium concentrations in surface waters. Within a 15-minute run time, the detection limit for a NIST reference TiO₂ in distilled water is 0.6 ppb with a quantitation limit of 1.9 ppb. However, these limits increased for soft and hard water due to artifacts associated with dissolved inorganic solids. Detection and quantitation limits were also higher for less photocatalytic materials such as pure anatase and rutile nanoparticles.

Lastly, TiO₂ nanoparticles were studied using single particle ICP-MS in a two-week aging study in synthetic water matrices including distilled, soft, and hard drinking water. This study was designed to quantify the effect of how increasing concentrations of dissolved inorganic solids affect the size distribution and particle number of nanoparticles over an extended period. However, the nanoparticles used in the study were slowly removed from suspension by adhering to the inner walls of the test tubes used to contain each sample solution. Some insights are made on the changes over time in nanoparticle sizes, the influence of dissolved inorganics on these particles, and the influence of particle size and type.

Table of Contents

Abstract.....	v
Table of Contents.....	vii
List of Tables.....	x
List of Figures.....	xi
Chapter 1 : Introduction.....	1
Chapter 2 : Literature Review.....	4
2.1. Titanium Dioxide Nanoparticles.....	4
2.2. Detection Methods for Nanoparticles in Water	5
2.3. Nanoparticles Detection via Fluorescence	7
2.4. Dynamic and Electrophoretic Light Scattering.....	8
2.5. Single Particle Inductively Coupled Plasma – Mass Spectrometry.....	10
Chapter 3 : Insights on Ligand Interactions with Titanium Dioxide Nanoparticles via Dynamic Light Scattering and Electrophoretic Light Scattering	12
3.1. Introduction.....	12
3.2. Experimental	14
3.2.1. Standards and Reagents.....	14
3.2.2. DLS and ELS Measurements.....	15
3.2.3. Solution Preparation.....	16
3.2.4. pH Adjustment.....	16
3.3. Results and Discussion	17
3.4. Conclusions.....	23
Chapter 4 : Effect of Ligand Modification and Probe Sonication on the ζ -potential of Three Forms of Titanium Dioxide Nanoparticles	24
4.1. Introduction.....	24
4.2. Experimental	26
4.2.1. Ligand Selection.....	26
4.2.2. Standards and Reagents.....	27
4.2.3. Sonication	28
4.2.4. Autotitration.....	28

4.2.5. ELS Measurements.....	29
4.2.6. Solution Preparation.....	30
4.3. Results and Discussion	30
4.3.1. Summary of results	30
4.3.2. Influence of Chain Length	33
4.3.3. Influence of Functional Group	34
4.3.2. Effects on ζ -potential of Probe and Bath Sonication	34
4.4. Conclusion.....	37
Chapter 5 : Utilizing Fluorescence of Photocatalytic Probes within a Portable Sensor to Detect TiO ₂ in Simulated Drinking Waters.....	38
5.1. Introduction.....	38
5.2. Experimental	42
5.2.1. Simulated Drinking Water Matrices	42
5.2.2. Standards and Reagents.....	42
5.2.3. Phosphate Buffer	43
5.2.4. UV Irradiation Lamp and Experimental Setup	43
5.2.5. Fluorescence Measurement and Data Processing.....	45
5.2.6. Suspension Preparation	47
5.2.7. Photocatalytic Reactivity Experiments	47
5.2.8. Bandgap Energy Measurement.....	48
5.2.9. Kinetics of 2-hTPA Production and Steady-state Hydroxyl Radical Concentration.....	49
5.3. Results and Discussion	51
5.3.1. Summary of Results.....	51
5.3.1. Agreement with Previously Published Results	55
5.4. Conclusion.....	57
Chapter 6 : Single particle ICP-MS analysis on the aging of P25, rutile, and anatase titanium dioxide nanoparticles in agitated simulated drinking water matrices without sonication.....	60
6.1. Introduction.....	60
6.2. Experimental	62
6.2.1. Nanoparticles	62
6.2.2. Water Matrices	63

6.2.3. Single Particle Inductively Coupled-Plasma Mass Spectrometry (spICP-MS).....	64
6.2.4. Standards.....	65
6.2.5. Experimental Sample Preparation.....	65
6.3. Results and Discussion	67
6.3.1. P25 Concentration Dependence in Distilled, Soft, and Hard Waters	67
6.3.2. Anatase Concentration Dependence	70
6.3.3. Rutile Concentration Dependence	72
6.3.4. Particle Loss via Dissolution, Aggregation, and Adherence to Tube Walls	73
6.4. Conclusion and Future Studies	75
Chapter 7 : Conclusion.....	77
References.....	79
Vita.....	100

List of Tables

Table 3.1. Results of hydrodynamic size for 500 ppm titanium dioxide nanoparticle and ligand solutions and ζ -potential measurements for select ligand-nanoparticle combinations at a concentration of 25 ppm for titanium dioxide nanoparticles and 1 equivalent.....	18
Table 4.1. Characteristics of seven different chemical ligands used for chelation and ζ -potential experiments. pKa values were compiled by Williams <i>et al.</i> ¹³⁸	27
Table 5.1. Formulations for hard and soft waters used in photocatalyst-TPA assays ...	42
Table 5.2. Physical and chemical properties of the three TiO ₂ used in this study	43
Table 5.3. Summary of results for each nanoparticle and water formulation tested in this study including limit of detection (LOD) for each method and limit of quantitation (LOQ).	53
Table 6.1. Physical and chemical properties of the three TiO ₂ used in this study	63
Table 6.2. Formulations for hard and soft waters used in the TiO ₂ aging study	63
Table 6.3. Nanoparticle, matrix, and starting concentration combinations used in experiments. All solutions were produced in triplicate 50 mL samples.....	66

List of Figures

- Figure 2.1.** Diagram displaying a folded capillary cuvette used for ζ -potential measurements and the collection of ions around a negatively charged particle suspended in a dispersion medium and the potential difference as a function of distance from the particle surface 9
- Figure 2.2.** Schematic overview of single particle inductively coupled plasma mass spectrometry. 11
- Figure 3.1.** Effect of pH on the hydrodynamic size of titanium dioxide nanoparticles in aqueous solution. 19
- Figure 3.2.** Effect of pH modification on the ζ -potential of pristine titanium dioxide nanoparticles. A pH of 5 provided the best ζ -potential due to the coordination of positively charged ions with the oxygen atoms in the rutile TiO_2 . However, the charged species in a solution of pH 9 had minimal effect on the ζ -potential of the nanoparticles. The nanoparticles likely have better interactions with positively charged ions at the surface than negatively charged ions..... 20
- Figure 3.3.** Effect of pH modification and ligand addition (for selected ligands) on the ζ -potential of pristine titanium oxide nanoparticles. A pH of 5 provided a positively charged layer or coating for the ligands to interact or coordinate with this improving the ζ -potential and nanoparticle repulsion, thus, inhibiting nanoparticle aggregation and settling. 21
- Figure 4.1.** Structures of ligands used in comparing the increasing numbers of a) hydroxyl groups, b) thiol groups, and c) chain length. 26
- Figure 4.2.** Diagram of autotitrator setup when equipped with folded capillary cuvette for ζ -potential measurements. 29
- Figure 4.3.** ζ -potential autotitration curves for P25 (A), anatase (B), and rutile (C) nanoparticles..... 31

Figure 4.4. ζ -potential alteration by probe sonication vs bath sonication for particles in this study compared to particles used in Doudrick *et al.*⁴² and Suttiponparnit *et al.*¹³² .. 36

Figure 5.1. Experimental apparatus containing UV lamp equipped with 320 nm fluorescent bulb (A), OSB wooden box to contain experiment (B), quartz cuvette with stir bar (C), cuvette holder (D), VWR low profile stir plate (E), fiber optic patch cord (F), and portable spectrophotometer (G). 44

Figure 5.2. Example of fluorescence intensity data collection and inherent noise introduced via the use of a small and portable spectrophotometer. The effect of implementing a moving average of the data is shown as well as the resultant change in linear regression..... 46

Figure 5.3. Mechanistic diagram of TPA hydroxylation and 2-hTPA formation via the hydroxyl radical production by irradiated photocatalytic nanoparticles..... 49

Figure 5.4. Calibration curve for 2-hTPA fluorescence in distilled water. The broadband UV lamp with a maximum of 320nm was used as the excitation source and the fluorescence intensity was recorded at 425 nm. 51

Figure 5.5. Photocatalytic assay results for P25 TiO₂ in distilled water for 10 minutes (A) and 15 minutes (B), soft water for 10 minutes (C) and 15 minutes (D), and hard water for 10 minutes (E) 15 minutes (F). Error bars show the 95% confidence interval for each mean of three replicates..... 52

Figure 5.6. Measured steady state hydroxyl radical concentration using Equation 5.2. for P25 in distilled water after a 15-min run time. Blue squares and blue trendline are from this study while the orange circles and orange trendline are from the Bi and Westerhoff study..... 56

Figure 6.1. Most frequent particle size, mean particle size, and particle mass remaining in dispersion for P25 nanoparticles in distilled water (A), soft water (B), and hard water (C). For P25 NPs, low refers to a concentration of 3 ppb, mid refers to 13 ppb, and high refers to 25 ppb. 68

Figure 6.2. Comparison of most frequent particle size, mean particle size, and particle mass remaining in dispersion for P25 nanoparticles in distilled, soft, and hard water at a concentration of 25 ppb only. 69

Figure 6.3. Most frequent particle size, mean particle size, and particle mass remaining in dispersion for anatase nanoparticles in distilled water (A), soft water (B), and hard water (C). For anatase NPs, low refers to a concentration of 1 ppb, mid refers to 5 ppb, and high refers to 8 ppb. 70

Figure 6.4. Comparison of most frequent particle size, mean particle size, and particle mass remaining in dispersion for anatase nanoparticles in distilled, soft, and hard water at a concentration of 8 ppb only. 71

Figure 6.5. Most frequent particle size, mean particle size, and particle mass remaining in dispersion for rutile nanoparticles in distilled water (A), soft water (B), and hard water (C). For rutile NPs, low refers to a concentration of 0.5 ppb, mid refers to 2 ppb, and high refers to 4 ppb. 72

Figure 6.6. Comparison of most frequent particle size, mean particle size, and particle mass remaining in dispersion for rutile nanoparticles in distilled, soft, and hard water at a concentration of 4 ppb only. 73

Figure 6.7. Comparison of most frequent particle size, mean particle size, and particle mass remaining in dispersion for P25, anatase, and rutile nanoparticles in distilled water (A), soft water (B), and hard water (C). Particle concentration (particles/mL) was 5×10^4 for P25, 2×10^4 for anatase, and 1×10^4 for rutile. 74

Chapter 1 : Introduction

Nanoparticles are a current hot and attractive topic in science and research, and have led to myriads of applications and inventions in many fields.¹ Nanoparticles, or nanomaterials, are defined as a structure or material, either naturally occurring, incidental, or engineered, typically with two lengths or dimensions between 1 and 100 nanometers but sometimes only one dimension as in the case of nanosheets.²⁻⁴ These nanoparticles may contain metals, metal oxides, or carbon compounds and can be functionalized or coated in many different ways including inorganic and organic coatings or functional groups.⁵ Furthermore, their activity and reactivity may be controlled via their crystalline structure, size, and shape, which includes spherical, cylindrical, cubic, octahedral, or planar nanoparticles.^{6,7}

One reason nanoparticles are of great scientific interest is their nano-scale size-dependent properties such as plasmon resonance and superparamagnetism.⁸⁻¹⁰ These novel properties arise, in part, from the high surface area to volume ratio found in nanomaterials and the large proportion of exposed atoms at the surface of these particles. These surface exposed atoms have more energy than that of the internal atoms in other, larger materials (called bulk materials) due to the high-energy bonds found in insufficiently coordinated atoms at the surface.^{7,11,12} These uncoordinated atoms are called surface defects and contribute to the high reactivity and catalytic activity of some nanoparticles.¹³ Bulk materials, on the other hand, often exhibit the same chemical and physical properties at any size.

As the proportion of surface atoms increases with decreasing particle size, materials that would otherwise be inert become highly reactive catalysts. Some size

dependent properties that can alter chemical properties include reactivity and catalysis (resulting in changes in toxicity to live organisms)¹⁴⁻¹⁶, changes in thermal properties such as a reduced melting point for many metal nanomaterials¹⁷⁻¹⁹, changes in mechanical properties including adhesion and capillary forces^{20,21}, changes in optical properties such as absorption and scattering of light^{22,23}, changes in electronic properties such as tunneling current, conductivity and quantum confinement^{24,25}, and magnetic properties such as superparamagnetism.

The growing number of applications for engineered nanomaterials has led to an increase in demand in the production of nanomaterials. In 2013, it was estimated that global production of engineered nanomaterials would be between 260,000 to 309,000 metric tons for a variety of nanomaterials including titanium dioxide, silver, iron and iron oxides, zinc oxide, copper and copper oxides, alumina, cerium oxide, nanoclays, carbon nanotubes, and silica.²⁶ In 2018, via an industrial survey, it was estimated that production of engineered nanomaterials would increase by an average of 5% annually.²⁷ However, these numbers are highly speculative since most companies do not freely publish data on production, products, or formulations for materials. Furthermore, advancements in various products may increase production of certain materials such as quantum dots for electronics or silver nanoparticles in medical devices and packaging when compared to others.²⁸

Suffice it to say that nanomaterials will be produced in growing amounts and incorporated into new or existing products at increasing rates. It is, therefore, vital to develop the science surrounding nanomaterials, their aging in various media, and methods of detection wherein engineered nanomaterials can be properly quantified in

soils, water, air, and waste. Specifically, however, is the incorporation of nanomaterials in products that may be used to treat water or alter the characteristics of food that is to be ingested. Nanotechnology-enabled water treatment is a growing sector of nanomaterial products and is intended to exploit the novel properties of nanomaterials increase the efficiency, efficacy, and selectivity of water treatment processes.²⁹⁻³¹

Of the many varied nanomaterials and composites, nano-titanium dioxide has been used extensively in consumer products and is one of the most produced engineered nanomaterials.²⁶ This dissertation will focus on the chemistry of titanium dioxide interactions with organic molecules and inorganic ions in water. In particular, the interaction of various organic ligands with titanium dioxide nanoparticles, the process and rates of degradation or oxidation of organic compounds that can be used for sensing titanium dioxide, and how various water formulations with varying levels of dissolved organic and inorganic compounds affect the aging, agglomeration, and size of the nanoparticles.

Chapter 2 : Literature Review

2.1. Titanium Dioxide Nanoparticles

Titanium dioxide (TiO_2) powders and materials have been widely used and researched recently due to their usefulness as a light scattering compound³², reactive oxygen species (ROS) generator^{33,34}, food and cosmetic additive³⁵, and photocatalyst among many applications.³⁶ TiO_2 particles with sizes less than 100 nm, classified as nanoparticles, have also increased in production and use.³⁷ Indeed, the applications of titanium dioxide nanoparticles have been increasing year by year at an accelerated pace.³⁸⁻⁴⁰ TiO_2 is now used in numerous solutions, coatings, food products, materials, and catalytic processes. The list extends to reflective paints, self-cleaning coatings, coloring for powdered food products, anti-caking agents, photocatalysis, and water treatment.⁴¹ Furthermore, these particles have high catalytic properties per a given mass and display interesting electronic properties that can be used in water treatment including organic material oxidation and nitrate reduction.^{42,43}

It was estimated in 2011 that TiO_2 nanoparticles were among the top five nanoparticles used in paints and consumer products.⁴⁴ Nanoparticles used in these applications have a wide range of crystallographic compositions, size, shape, and surface coatings.⁴⁵ There are three common crystalline forms of titanium dioxide found in nature: anatase, rutile, and brookite. Brookite is not produced commercially or incorporated in many products and is relatively rare in nature.⁴⁶ Rutile has the highest commercial production and is the most common titanium dioxide bearing mineral found in nature. The next most stable and common form, anatase, is featured in most research on TiO_2

photocatalysts due to its photoactivity.⁴⁷ However, some compounds used commercially are a mixture of rutile and anatase phases (e.g. Aeroxide P25).⁴⁸

Titanium dioxide materials and nanoparticles have been used extensively in water treatment and much research has been performed in that sphere.^{10,41,49} Some examples include photocatalytic nitrate reduction⁴² and advanced oxidation technology (photocatalysis).⁵⁰ Advanced oxidation technologies employ the generation of reaction oxidation species to degrade organic pollutants as shown with bisphenol A⁵¹, trichlorophenol (TCP), 2,4-dichlorophenol (2,4-DCP), and sodium benzoate⁵², methylethylketone⁵³, rhodamine B as a representative dye pollutant⁵⁴, petroleum refinery wastewater⁵⁵, and other model pollutants.⁵⁶

Recently, greater interest has been expressed in the potential toxicity of TiO₂ to human, animal, and plant health.^{46,57,58} Indeed, the French Agency for Food, Environmental and Occupational Health and Safety (ANSES) recently published an article exploring the risks and hazards of titanium dioxide as a food additive.^{59,60} For this reason, there will likely be more research into characterization and detection methods for TiO₂ nanoparticles. Furthermore, an expansion of research into the interactions of TiO₂ and bacteria, plants, and animal cells is likely to occur. Developing a detection method for TiO₂ that provides a rapid and portable means of detecting particles in water is important and worthwhile.⁶¹⁻⁶⁷

2.2. Detection Methods for Nanoparticles in Water

The most commonly used and commercially produced titanium dioxide nanoparticles in water treatment are Aeroxide (Degussa) P25 and Hombikat UV100. As the utilization of nanomaterials increases, release and consequent exposure will be more

likely in the future. Water treatment vessels will be built to prevent the loss of nanoparticles for sustainability and safety reasons; however, no system is perfectly safe, and some release may occur. It logically follows that more nanoparticles will be released into environmental sinks such as water, landfills, soil, and, to a lesser extent, the air.⁶⁸ An increasing number of studies have shown risks to human health from nanoparticle exposure using animal and plant models but the possible hazards cannot be adequately measured at this moment.⁶⁹⁻⁷² However, it is important to detect and quantify nanoparticles in materials that provide an easy path of exposure such as drinking water and especially drinking water that has been treated with nano-enabled water technologies.

The standard for the detection and quantification of most nanoparticles in solution (mainly metal oxides or metal materials) is the single particle-inductively coupled plasma mass spectrometer (spICP-MS). Whereas, scanning electron microscopy and transmission electron microscopy have a high degree of sample preparation and complexity, spICP-MS has very high throughput and extremely high sensitivity.⁷³ However, spICP-MS does not adequately measure the morphology or size of a nanoparticle but instead assumes a shape (selected by the user) to calculate primary particle size.⁷⁴ Dynamic light scattering (DLS) is also a useful technique for measuring the size or presence of nanoparticles in solution but suffers from interference by agglomerates or poly-disperse samples and primarily measures the hydrodynamic size and not the true particle size.⁷⁵ DLS was not designed as a detection technique but as a characterization technique for particles with known composition in suspension.

However, these methods require some level of sample preparation (albeit minimal for ICP-MS and DLS for water samples), are expensive, are not typically rapid and are not portable. Furthermore, except for DLS, the instruments require a high degree of facility support including vacuum pumps, refrigerants, high voltage sources, gas cylinders (such as argon for ICP-MS) and exhaust systems. There is a need for a simple, portable, rapid, and inexpensive technique for determining the concentration of nanoparticles in water samples that can be performed on site or at a lab with minimal facility support or training. The primary way to detect nanoparticles under these parameters are via UV-Vis absorption spectroscopy or fluorescence spectroscopy.

2.3. Nanoparticles Detection via Fluorescence

When comparing UV-Visible spectroscopy and fluorescence spectroscopy, fluorescence techniques have the capability to have a better detection limit due to the active nature of fluorescence vs the passive nature of UV-Vis absorption. Fluorescence measures the active emission of photons from a sample against a “dark” background whereas UV-Visible absorption measures the difference between a blank (typically the solvent) and the light absorbed by a sample. Therefore, it is likely that a highly sensitive technique that can measure nanoparticles in a part per billion (ppb) range would be a fluorescent technique. Indeed, recent publications have shown that UV-Vis absorption or fluorescence spectroscopy could use an indirect method by measuring the loss of a dye, loss of fluorescence, or increase in fluorescence due to oxidation catalyzed by a suspended nanoparticle.^{76,77}

To date, most research involving fluorescence particles or nanomaterials has taken place in the biomedical sphere. Titanium dioxide nanoparticles have been used in

medical imaging and in cancer treatments. These fluorescent nanomaterials are typically functionalized with fluorescein isothiocyanate.⁷⁸ Some questions remain on the stability of the fluorescent labels when attached to nanoparticles that are used in photocatalytic processes. TiO₂ is mainly used in photocatalytic processes that degrade organic matter and molecules in water. To prevent the possibility of a fluorescent tag being degraded, TiO₂ could instead be used to create a fluorescent molecule using its photocatalytic activity. Studies have shown that terephthalic acid can be used as a hydroxyl scavenging molecule which fluoresces upon its reaction with a hydroxyl radical and the formation of 2-hydroxyterephthalate (2-hTPA).⁷⁷

2.4. Dynamic and Electrophoretic Light Scattering

Fluorescent and UV-Vis detection studies cannot, however, be easily performed for materials that tend to agglomerate in solution and fall out of suspension. For example, TiO₂ nanoparticles have a significant tendency to agglomerate in solution, especially aqueous solutions, and settle out. The hydrophobic neutral charge on the surface of TiO₂ is the primary cause for the reversible agglomeration and resulting sedimentation. Removing the neutral charge through surface modification may result in improved aqueous suspensions with lower rates of aggregation and sedimentation.

Dynamic light scattering (DLS) and electrophoretic light scattering (ELS) are both powerful methods that can be used to explore not only the size of particles but the electrical double layer that plays an influential role on the suspension and dispersal of the nanoparticles in aqueous solutions. ELS is a technique used to measure the surface charge of a particle in a suspension as shown in Figure 2.1. By applying a potential to

the solution within a folded capillary disposal cell and observing the movement of particles within that capillary, the surface charge of the particle can be measured.

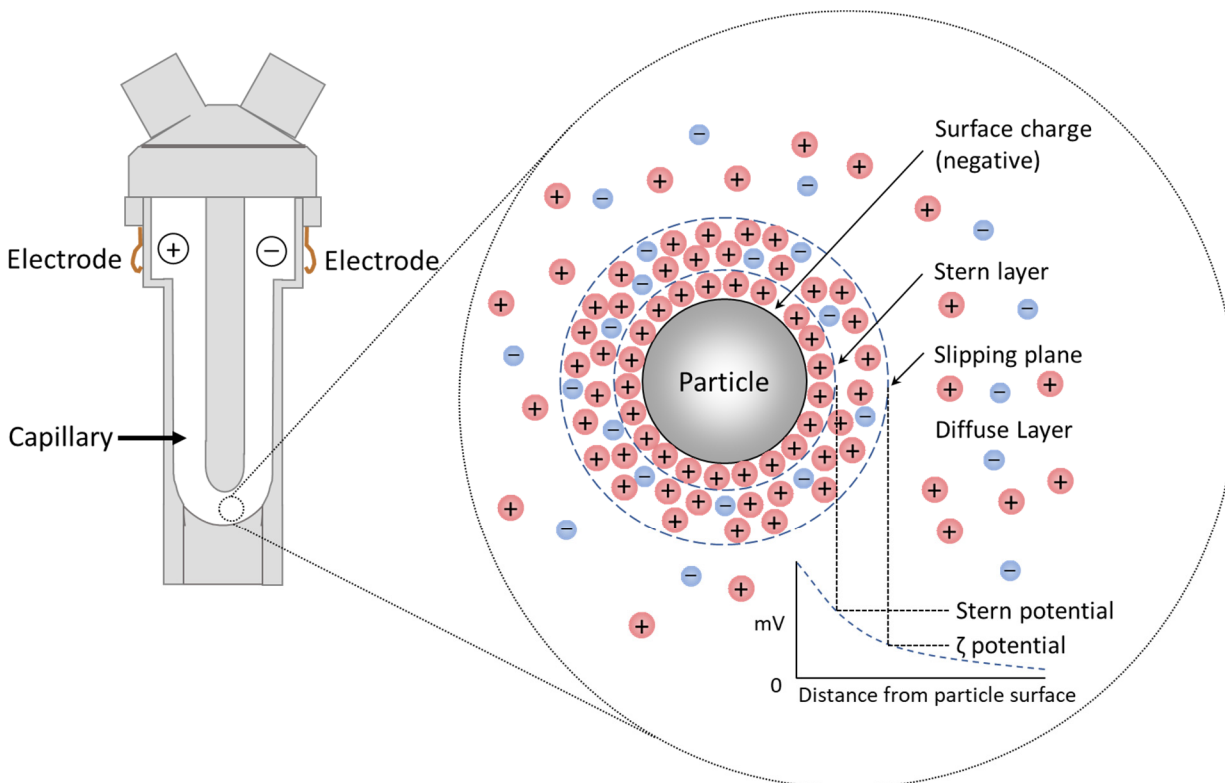


Figure 2.1. Diagram displaying a folded capillary cuvette used for ζ -potential measurements and the collection of ions around a negatively charged particle suspended in a dispersion medium and the potential difference as a function of distance from the particle surface

Using this method, the adsorbed layers of charge can be understood and manipulated to improve suspension and dispersal. These charged layers are responsible for generating repulsive forces within a suspension and are therefore essential for preventing aggregation. DLS and ELS have been used in many studies to investigate the interactions between titanium dioxide nanoparticles and various organic molecules including citric acid, natural organic molecules, dimercaptosuccinic acid, and polyacrylic acid.^{79–81} Simple surface modification by pH variation and ligand coating may provide increased suspension and decreased aggregation thus preserving particle size and surface-dependent properties. Furthermore, green approaches, such as using benign or

non-toxic ligands, are essential in modifying nanoparticles in food related products such as milk, anti-caking agents used in food or food colorants.

2.5. Single Particle Inductively Coupled Plasma – Mass Spectrometry

Single particle ICP-MS is a powerful method for detecting, quantifying, and sizing a wide range of nanoparticles. spICP-MS is an improvement upon ICP-MS wherein particles and ions within water are atomized in an argon plasma and then detected via a quadrupole magnetic analyzer. The improvement lies in the software's ability to discern between ionic atoms and atoms that were part of nanoparticles. Nanoparticles are taken up from the sample solution and introduced to the instrument via a nebulizer and spray chamber. The transport efficiency of particles entering the instrument from spray chamber is typically around six to eight percent so most nanoparticles are lost to waste. After introduction to the torch, the particles are ionized in the argon plasma. The ion deflector selects for the mass of interest as well as the mass analyzer which direct a stream of ions to the detector. After detection, the data can be processed and particle diameter can be calculated as shown in Figure 2.2.

Running in this mode, the instrument is able to detect pulses of ions on a particle to particle basis and quantify the amount of atoms within an individual particle. Advancements in this technique have widely stemmed from an increase in the acquisition speed of newer instruments. The dwell time of an instrument refers to the period of time when a measurement is occurring and can be compared to the integration time of a spectrometer or the exposure of a photograph. Indeed, just as cameras with fast shutter speeds and low exposure times can capture an image of something moving very quickly through the frame, a spICP-MS has a dwell time of such a short duration,

on the scale of tens of microseconds, that it can capture or measure the amount atoms within a nanoparticle.⁸² However, due to the high sensitivity of the instrument, particle samples must be diluted to extremely low concentrations in the microgram per liter, or parts per billion, range. Environmental samples, which are already at a very low level, can be measured without preconcentration techniques or methods, yielding a high throughput method for particle characterization.⁸³ In Chapter 6 of this work, spICP-MS will be put to use by measuring the amount of particles in simulated drinking waters and how they transform in size and particle concentration over time.

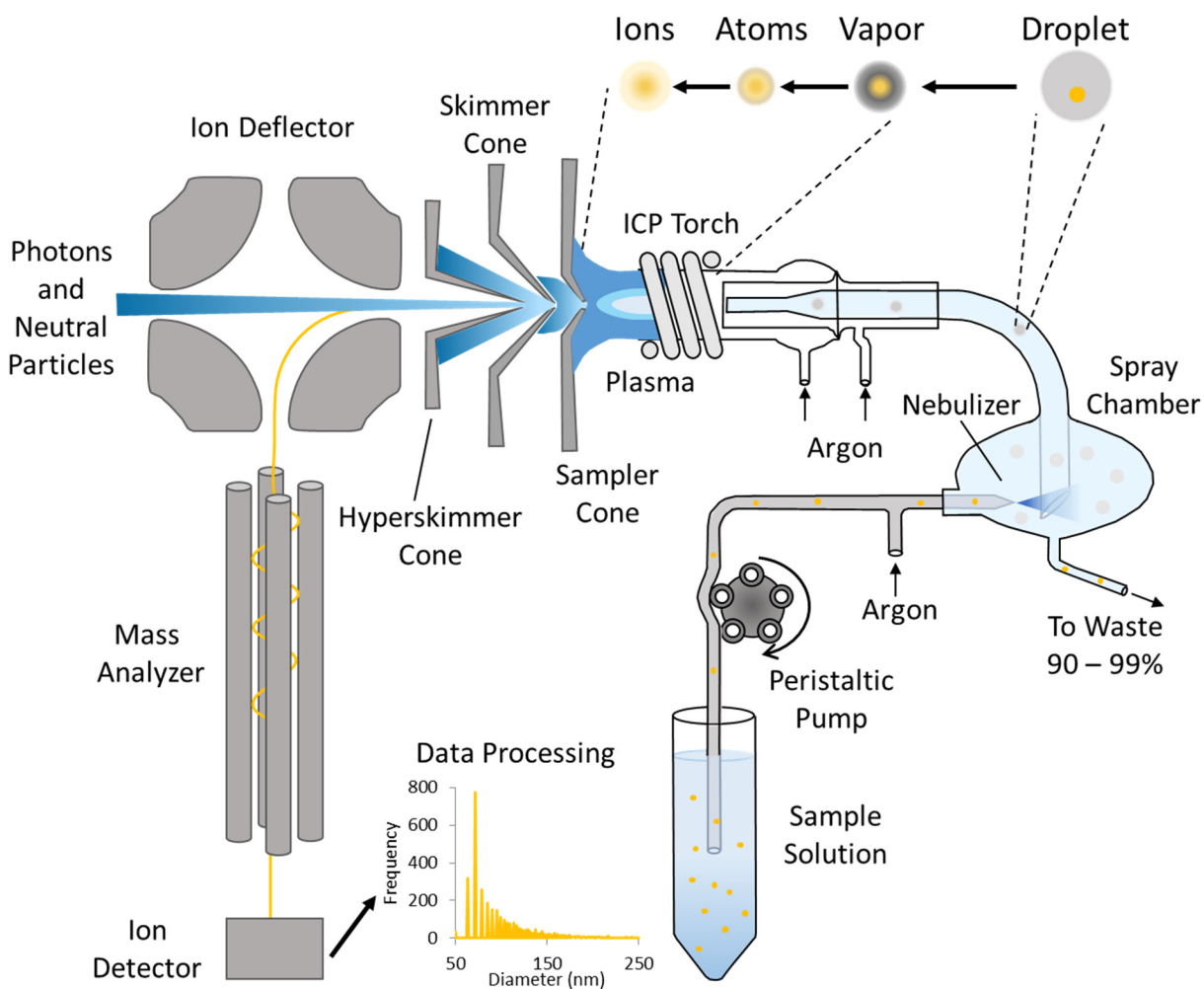


Figure 2.2. Schematic overview of single particle inductively coupled plasma mass spectrometry.

Chapter 3 : Insights on Ligand Interactions with Titanium Dioxide Nanoparticles via Dynamic Light Scattering and Electrophoretic Light Scattering¹

3.1. Introduction

Titanium dioxide (TiO₂) nanoparticles have been widely used and researched recently due to their usefulness as a light scattering compound,⁸⁴ reactive oxygen species (ROS) generator,^{85,86} food and cosmetic additive,⁸⁷ and photocatalyst among many other applications.⁸⁸ Nanoparticles used in these applications have a wide range of crystallographic compositions, size, shape, and surface coatings. However, TiO₂ nanoparticles have a significant tendency to aggregate in solution, especially aqueous solutions, and settle out.⁸⁹ The hydrophobic neutral charge on the surface of TiO₂ is the primary cause for the aggregation and resulting sedimentation.⁹⁰ Removing the neutral charge through surface modification may result in better aqueous suspensions.⁹¹

Recently, using nanoparticles for pollutant and foulant removal or transformation via oxidation has gained strong interest in the field of water remediation.²⁹ TiO₂ nanoparticles have been used photo-catalytically in self-cleaning and anti-fouling water treatment membranes,⁹² formation of singlet oxygen states and consequent destructive oxidation of organic pollutants,^{93–97} and the reduction of oxoanions in water.^{43,98} Lately, reactors have been designed by affixing TiO₂ nanoparticles to optical fibers attached to LEDs.⁹⁹ Treatment vessels such as these could be used for efficient water treatment

¹ This chapter has previously appeared as an article in *Microchemical Journal*. The original citation is as follows: Turley, R. S.; Benavides, R.; Hernández-Viezcas, J. Á.; Gardea-Torresdey, J. L. Insights on Ligand Interactions with Titanium Dioxide Nanoparticles via Dynamic Light Scattering and Electrophoretic Light Scattering. *Microchemical Journal* **2018**, 139, 333–338. <https://doi.org/10.1016/j.microc.2018.03.015>.

while preventing nanoparticle escape. Other promising applications of titanium dioxide are in the bioremediation of oil in contaminated soils¹⁰⁰ and the photocatalytic degradation of air-borne organic compounds.¹⁰¹ However, questions arise on how the nanoparticles will preserve their properties in complex matrices such as water and soil.^{102–104} Exploration of nanoparticle suspensions via dynamic and electrophoretic light scattering are essential in understanding a material's properties.

Dynamic light scattering (DLS) and electrophoretic light scattering (ELS) are both important methods that can be used to explore not only the size of particles but the electrical double layer that plays an influential role on the suspension and dispersal of the nanoparticles in aqueous solutions. Electrophoretic light scattering is a technique that measures the surface charge of a particle in a suspension. By applying a potential to the solution within a folded capillary disposal cell and observing the movement of particles, within that capillary, the surface charge of the particle can be calculated. Through this method, the adsorbed layers of charge can be understood and manipulated to improve suspension and dispersal. These charged layers are responsible for generating electrostatic repulsive forces within a suspension and are, therefore, essential for preventing aggregation.¹⁰⁵ DLS and ELS have been used in several studies to investigate the interactions between titanium dioxide nanoparticles and various organic molecules including citric acid,¹⁰⁶ natural organic molecules,⁹⁰ dopamine,^{85,107,108} other enediol ligands,^{109,110} dimercaptosuccinic acid,¹¹¹ and other larger surfactants.^{112,113}

Previous reports have focused on thiolation or coordination of TiO₂ nanoparticles using dimercaptosuccinic acid, urea, oleic acid, and citric acid.^{80,106,114–118} Mohan et al. synthesized TiO₂ nanoparticles in conjunction with stearic acid dispersed in toluene.⁸¹

The capped nanoparticles of around 7 nm in size were then functionalized with 2,3-dimercaptosuccinic acid, which made them easily suspended in water. Similarly, Seo et al. synthesized hydrophobic TiO₂ nanoparticles and modified them in a solution of toluene and dimercaptosuccinic acid dissolved in methanol. The resulting nanoparticles were easily dispersed in water after recovery.¹¹¹ Most studies focused on nanoparticles with sizes typically between 5 and 20 nm and all were below 50 nm. No existing study experimented with ligand interactions of TiO₂ nanoparticles that were larger than 50 nm.

Simple surface modification by pH variation and ligand coating may provide increased suspension and decreased aggregation, thus, preserving particle size and surface-dependent properties.^{105,118,119} Furthermore, green approaches, such as using benign or non-toxic ligands, are essential in modifying nanoparticles in food related products such as milk, anti-caking agents used in food, or food colorants. Therefore, some ligands in this study were selected primarily due to their non-toxic nature. For example, DMSA is already administered orally and intravenously to humans for the treatment of heavy metal toxicity.¹²⁰ It can also be easily purchased over-the-counter as an oral supplement.¹²¹ Herein, we present the results of various surface modifications of TiO₂ nanoparticles by complexation with nineteen ligands over a range of pH values, ligand equivalents, and nanoparticle concentrations. We also investigated the mechanisms pertaining to why some ligands work better than others in TiO₂-ligand systems.

3.2. Experimental

3.2.1. Standards and Reagents

The following chemicals were purchased and used in the experiments: uncoated

rutile titanium dioxide nanoparticles with a size of 50 ± 25 nm (US Research Nanomaterials, Inc. <http://www.us-nano.com/inc/sdetail/7710>), hydrochloric acid (SCP Science), sodium hydroxide pellets (Mallinckrodt), citric acid, oxalic acid, lactic acid (racemic), diethyldithiocarbamic acid, malic acid, mandelic acid, citramalic acid, gallic acid, potassium D-gluconate, dimethylethanolamine (DMEA), and diethylenetriaminepentaacetic acid (Sigma Aldrich), sodium citrate, ethylenediaminetetraacetate tetrasodium salt (EDTA), urea, and dimethylglyoxime (Fisher Scientific), and dimercaptosuccinic acid (DMSA), ammonium oxalate monohydrate, 3-(N-Morpholino) propanesulfonic acid sodium salt, and L-glutamine (Alfa Aesar). High resistivity (>18.2 M Ω) water was provided by a Millipore filtration apparatus and used to prepare all aqueous solutions.

3.2.2. DLS and ELS Measurements

Particle size and ζ -potential measurements were made using a Malvern Zetasizer Nano ZS-90. Disposable polystyrene cuvettes purchased from Malvern were used for the dynamic light scattering measurements. The scattering angle of the measurement was 90° with refractive index of the particles of 2.61. All measurements used water as the dispersant with a refractive index of 1.330. Each sample was allowed to equilibrate inside the instrument for 120 s before measurement with an equilibration of 25.0 ± 0.1 °C. Three measurements were made for each solution with each measurement averaged over 70 s. Via this method, aggregation of the sample could be determined over a relatively short period of time.

ζ -potential was measured using the same instrument as the DLS experiments, which employs a laser Doppler electrophoresis procedure. Via this method, mobility

within a capillary is measured from which the ζ -potential can be calculated using Smoluchowski's approximation. Disposable folded capillary cells were used for the ζ -potential measurements and sonicated solutions were loaded with a syringe to ensure no air bubbles were trapped in the folded capillary. Each end of the capillary tube were capped to prevent further gas exchange with the atmosphere during measurement. The equilibration temperature was 25.0 ± 0.1 °C for each measurement.

3.2.3. Solution Preparation

For the initial particle size measurements, 10 mg of TiO₂ nanoparticles were added to 50 mL centrifuge tubes along with the appropriate mass of ligand. One, two, and three equivalents by mole of ligand were added to each centrifuge tube followed by 20mL of water resulting in a 500 mg·L⁻¹ TiO₂ solutions. Centrifuge tubes containing solutions were placed on tube rockers for 24 h to allow time for adequate ligand association. After thorough mixing, solutions were removed from tube rockers and samples were drawn promptly for analysis. The samples from each solution were added to the proper cuvette for measurement using DLS on the Zetasizer instrument.

When measuring the ζ -potential of the nanoparticles in solution, 1:20 dilutions were made using the prepared 500 mg·L⁻¹ TiO₂ solutions resulting in 25 mg·L⁻¹ solutions. These dilutions were necessary when measuring ζ -potential to prevent multiple scattering effects that could obscure results. However, the dilutions were not made too dilute, which would introduce error via other particulate matter inadvertently introduced into the solution from the stock compounds used.¹²²

3.2.4. pH Adjustment

pH adjustments were made using 0.1, 0.01, and 0.001 M solutions of sodium

hydroxide and hydrochloric acid. pH measurements were made using an Orion pH meter model 420A. Additions were minimized to less than a half a millimeter to maintain solution concentrations. Three solutions were made for each ligand at 1 equivalent by diluting the original 500 ppm solutions down to 25 ppm TiO₂ and adjusting pH to between 4 and 5.5, 6.5-7.5, and 8.5-10 each. After another 24-hour mixing session, ζ-potential and dynamic light scattering measurements were taken to determine suspension stability and particle size.

3.3. Results and Discussion

When measuring nanoparticles using DLS, all Z-averaged hydrodynamic diameters were much larger than the reported numbers given by the manufacturer. This is partly due to the excessive influence that aggregates have on the signal and, therefore, the calculation of average particle size within a solution.^{123,124} In many of the measurements conducted, the size distribution was multi-modal and was polydisperse. This is partly due to the fact that the particle properties or chemical interactions are not directly measured using DLS or ELS but are rather inferred based on their motion due to either Brownian motion or electrophoretic behavior.¹²⁵ However, DLS is useful in observing general trends of ligand-TiO₂ interaction and not necessarily the true size of the nanoparticles in solution. Considering this, data presented in Table 1 should be viewed comparatively and not as an absolute measurement of the nanoparticles size in solution.

Table 3.1. shows a few general trends that were observed across the series of ligands used in these experiments. Overall, ligand equivalency did not affect aggregation and often increased aggregation and particle size at higher ligand equivalencies. The

surface of nanoparticles is likely saturated with ligand interactions at below unity ligand equivalencies and increasing the amount of ligand in solution does nothing to help particle separation. The higher concentrations of dissolved organic molecules in the solution increase the ability of the nanoparticles to aggregate and, in so doing, prevent the chelators intended effect.

Table 3.1. Results of hydrodynamic size for 500 ppm titanium dioxide nanoparticle and ligand solutions and ζ -potential measurements for select ligand-nanoparticle combinations at a concentration of 25 ppm for titanium dioxide nanoparticles and 1 equivalent

Ligand added	500 ppm Size Measurements (nm)			25ppm ζ - potential (mV)		
	1 equivalent	2 equivalents	3 equivalents	pH 5	pH 7	pH 9
Control (no addition)	242	262	210	31	10.9	-7.9
Citric acid	2316	2493	2686	-29.9		
Oxalic acid	1892	1692	1907	-28.8		
Lactic acid	364	562	1230	6.3		
Ethylenediaminetetraacetic acid	545	1984	3050	-16.3		
Sodium citrate tribasic	302	416	437	-35		
Dimercaptosuccinic acid	599	534	951	-40.7		
Urea	264	314	261	-13.3		
Ammonium oxalate	1575	1609	1890	-26		
Dimethylethanolamine	198	192	188	32.3	-5.9	1.9
MOPS Sodium salt	306	411	1244	20.3		
Pentetic acid	1622	1372	1540	23.3		
Diethyldithiocarbamic acid	312	355	431	-6.7	-27	-27
Malic Acid	2055	1714	2274	-22		
Mandelic acid	820	1691	1479	-0.5		
Citramalic acid	1547	1551	1696	-15		
Dimethylglyoxime	229	247	227	28	-5	-15.8
Gallic acid	520	724	918	-25		
Potassium gluconate	418	841	868	-15		
L-glutamine	364	562	1230			

Depending on the structure of the ligand and resulting pKa values, acidic pH improved ζ -potential for most ligands and basic pH improved ζ -potential only for diethyldithiocarbamic acid as shown in Table 3.1. Indeed, when TiO₂ is alone in solution, a departure from neutral pH preserves particle size and prevents aggregation (see Figure

3.1. and Figure 3.2.). This is likely due to the increase of charged particles surrounding the nanoparticles and weakly coordinating with the negatively charged oxygen atoms within TiO_2 in the case of positive charges in acidic pH solutions or coordinating with titanium within the crystal structure for negative charges in basic pH solutions. This pH dependent suspension ability of TiO_2 proves what is already known about hydrophobic pristine TiO_2 nanoparticles: inducing a charge on the surface of the nanoparticle improves repulsion and decreases aggregation.¹²⁶

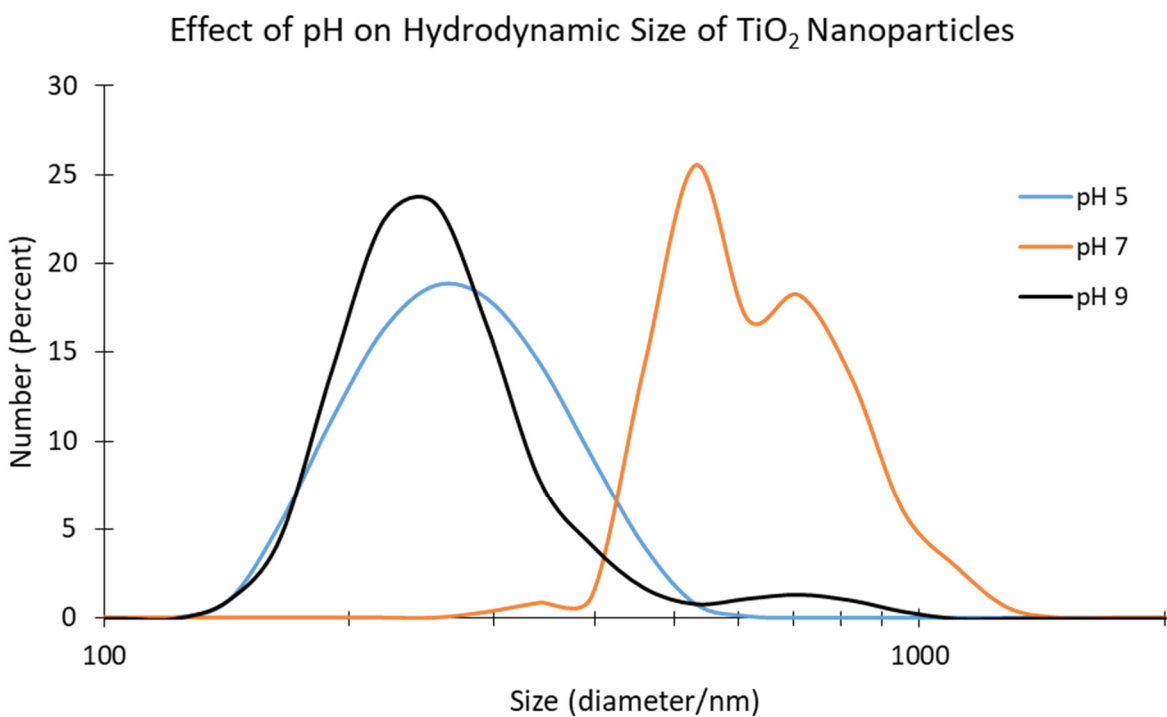


Figure 3.1. Effect of pH on the hydrodynamic size of titanium dioxide nanoparticles in aqueous solution.

The structure and pKa dependency of the chelating compound can be elucidated from the results of sodium citrate, DMSA, and diethyldithiocarbamic acid solutions when paired with TiO_2 nanoparticles in acidic pH. Figure 3.3. shows the ζ -potential at pH 5 of select ligands that improved the suspension of TiO_2 . DMSA, sodium citrate, and DMEA improved suspension beyond that of pH modification alone. Citric acid and oxalic acid

improved suspension beyond the zone of instability and incipient aggregation between -30 mV and 30 mV but not beyond that of pH modification along. Dimethylglyoxime also improved suspension but may not be far enough from 0 mV to prevent aggregation. The other ligands tested had ζ -potential curves well inside the zone of instability.

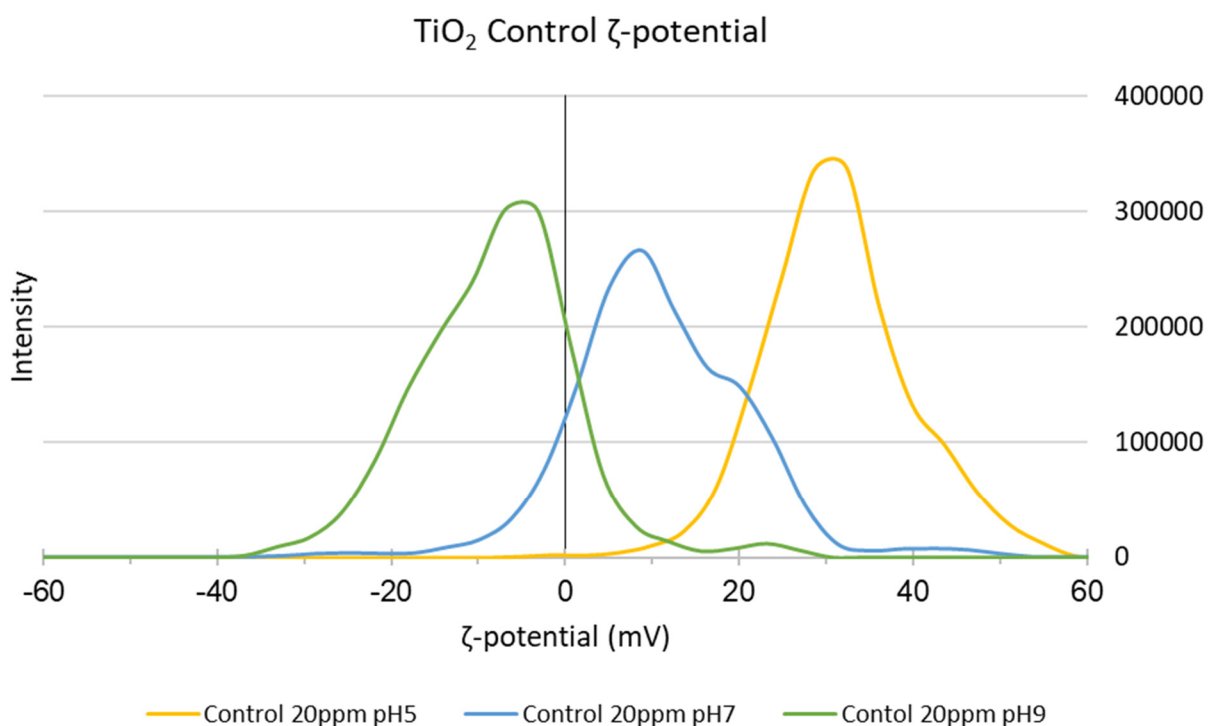


Figure 3.2. Effect of pH modification on the ζ -potential of pristine titanium dioxide nanoparticles. A pH of 5 provided the best ζ -potential due to the coordination of positively charged ions with the oxygen atoms in the rutile TiO₂. However, the charged species in a solution of pH 9 had minimal effect on the ζ -potential of the nanoparticles. The nanoparticles likely have better interactions with positively charged ions at the surface than negatively charged ions.

A possible mechanism implies the complexation of the nanoparticle with a positive charge under acidic conditions and then coordination with chelating molecules to this positive charge. For this to happen, the chelating molecules must have a negative charge on their residuals, which is accomplished via deprotonation under basic conditions. Sodium citrate has three pKa values one of which is at 6.40 which deprotonates one of the carboxyl groups and forms a negative charge available for coordination.¹²⁷ The thiol

groups of dimercaptosuccinic acid deprotonate at a pKa of 9.68 and 11.14 implying that for coordination of a bidentate fashion to be uniform, neutral to slightly acidic conditions are required.¹²⁰ The same low pH conditions are required for diethyldithiocarbamic acid. Even though a pH of 2 or 3 was not reached in these experiments, enough of the ligands must have been deprotonated to allow for chelation of the nanoparticles and consequent particle size stabilization at a pH of 5.

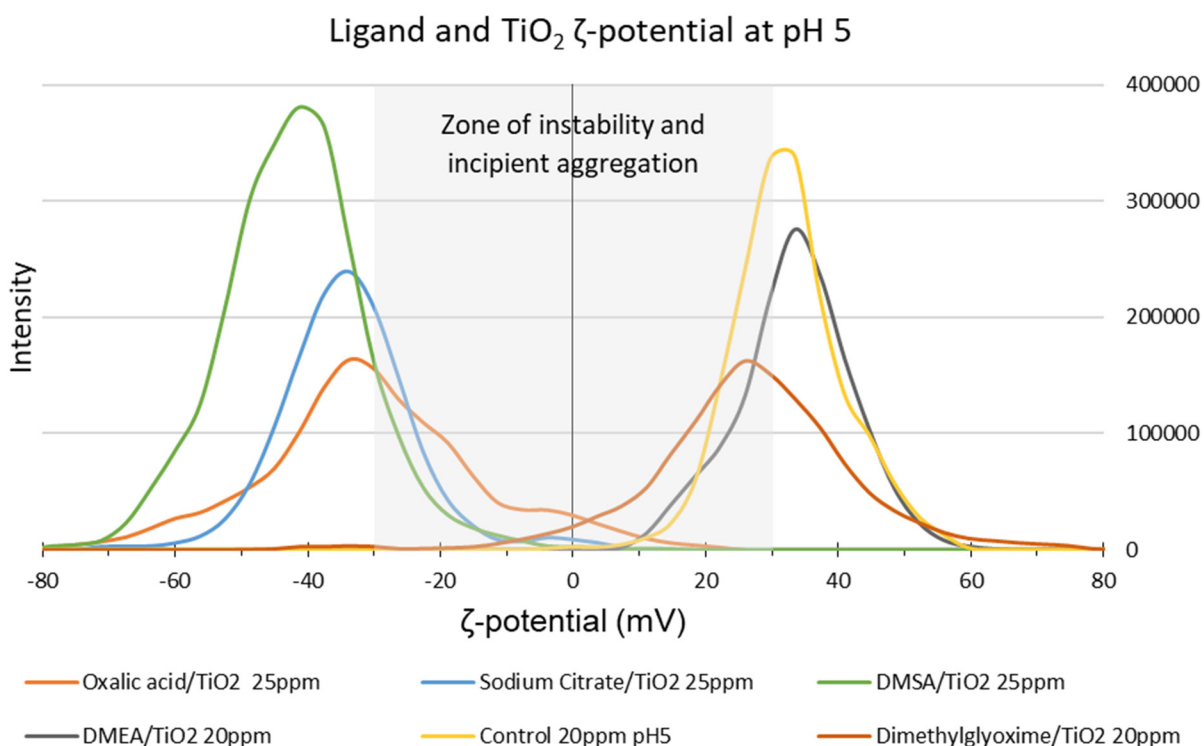


Figure 3.3. Effect of pH modification and ligand addition (for selected ligands) on the ζ-potential of pristine titanium oxide nanoparticles. A pH of 5 provided a positively charged layer or coating for the ligands to interact or coordinate with this improving the ζ-potential and nanoparticle repulsion, thus, inhibiting nanoparticle aggregation and settling.

Future studies might include ligand equivalencies at fractional molarities of the TiO₂ nanoparticles at levels of a quarter equivalency or half. Even one equivalency may be excessive when considering the smaller surface area of nanoparticles when compared to single molecules and more than one point of chelation. If single molecules or metal centers were used then multiple equivalencies may have been appropriate but for larger

particles where most of the atoms are embedded inside the particle, equivalencies may be a meaningless evaluation.

When investigating the stability of a suspension of particles in any liquid, DLS is well complimented by ELS, which measures ζ -potential of a suspension. ζ -potential is a measure of the collection of charges around and repulsion between particles in a suspension. It is very important in designing suspensions that are stable in the selected solvents. A ζ -potential outside the range of -30 to 30 mV signifies a stable solution in water. Within the range, the stability ranges from moderate around ± 20 to ± 30 mV and very unstable the closer to zero the suspension is measured to be.¹¹³ Pristine TiO₂ nanoparticles are known to be very hydrophobic and quickly aggregate and settle out of aqueous solutions. To expand their usefulness and extend the design of aqueous systems and suspensions, a nanoparticle that can easily be suspended and remain so is important and beneficial. Testing several coatings and chelating ligands, such as in this paper, can be developed via electrophoretic light scattering and ζ -potential measurement.

While many ligands and synthesis mechanisms may provide a stable hydrophilic TiO₂ nanoparticle, our simple addition and pH adjustment scheme showed that the addition of sodium citrate, DMEA, and DMSA improved the ζ -potential and the stability of the comparatively large nanoparticles in solution (>50 nm). By providing an increase in charge around the nanoparticle, aggregation is decreased, and repulsion is increased. The solution was also noticeably cloudy (due to the scattering of light by suspended TiO₂) for an extended period (up to 3 days) as compared to other samples that aggregated and settled out of solution in a span of hours.

3.4. Conclusions

Our results indicate that the simple pH modification of TiO₂ in solution provides a substantial increase in the absolute value of ζ -potential and an improvement in hydrodynamic size. Inclusion of ligands such as sodium citrate, DMEA, DMSA, dimethylglyoxime, and oxalic acid also improve suspension in solution and increase repulsion between nanoparticles of size 50 ± 25 nm. Dimethylethanolamine improved the hydrodynamic size beyond that of simple pH modification alone. These results show that lowering the pH of a solution provides a positively charged coating or layer around nanoparticles, which then allows organic ligands with negatively charged groups to associate to the surface of nanoparticles. Hindrance and repulsion can then be active within suspensions of nanoparticles, which can prevent or substantially delay aggregation and loss of suspension.

Chapter 4 : Effect of Ligand Modification and Probe Sonication on the ζ -potential of Three Forms of Titanium Dioxide Nanoparticles

4.1. Introduction

Nanoparticle and micron sized TiO_2 particles tend to aggregate in water dispersions, especially in distilled water, leading to loss of surface area, activity, and eventual sedimentation from the suspension.¹²⁸ Typically, titanium dioxide nanoparticles are used in slurries with intense mixing to inhibit agglomeration.¹²⁹ But preventing agglomeration via chelation, and consequent sedimentation, may lead to improved properties, higher levels of homogeneity in dispersions, and improved efficiency for processes involving titanium dioxide.¹³⁰ Modifying nanoparticle TiO_2 with organic ligands may help to increase their suspension ability across a range of pH values.^{131,132}

One property of nanoparticles that can be readily modified and customized to suit the needs of a particle suspension is the surface charge and surrounding charge layer of a nanoparticle which is referred to as ζ -potential.¹³³ ζ -potential is the electrical potential of ionic species surrounding a particle in a colloidal suspension.¹³⁴ The surface charge of a particle will attract positive or negative ions within the dispersion medium eventually leading to a buildup of charge dependent on the availability of charge within a medium and the amplitude of surface charge on a particle. This collection of charge can be measured indirectly by the electrophoretic mobility of a particle under an oscillating electric field. The mobility can then be used to calculate the ζ -potential. As ζ -potential moves away from zero in either direction (in other words, as the absolute value of ζ -potential increases), particles have an increase of charge around them which will repel similarly charged particles. The repulsion of particles prevents agglomeration and

sedimentation. ζ -potential can be measured using electrophoretic light scattering (ELS), which is related to dynamic light scattering, but employs a folded capillary cuvette and an application of an oscillating electrical potential to induce the oscillation of particles and, by collecting the light scattered by the particles from a laser light source, a measurement of their mobility. One general principle to consider when measuring the ζ -potential of particles is that a ζ -potential value between -30 and +30 mV is insufficient to maintain a dispersion of the particles.¹³⁵ Between these two values, the charge surrounding particles is inadequate for repulsion and agglomeration prevention. A good particle dispersion will have a ζ -potential either greater than 30 mV or less than -30 mV and excellent dispersion will have a magnitude greater than 60 mV.¹³⁶ Modifying nanoparticles with ligands, changing pH, and/or changing the ionic strength of a solution may improve the ζ -potential and therefore colloidal stability.

In this study, three types of TiO₂ nanoparticles are suspended in separate solutions, mixed with solutions of various ligands, and their ζ -potentials are measured as the pH is increased from a value of 3 to 10. The first of the three nanoparticles, Aeroxide P25, was chosen based on its application in water treatment and photocatalysis. The remaining two nanoparticles, 18 nm anatase TiO₂ nanoparticles and 30 nm rutile nanoparticles, were chosen to enable a comparison of nanoparticles based on their size and crystalline structure. Improvements in ζ -potential can lead to improvements in dispersion and, therefore, uninhibited application of these important photocatalytic nanoparticles. All three nanoparticles chosen for the study showed improvements in ζ -potential for all ligands tested. However, DMSA, citric acid, and MSA showed the greatest improvements to nanoparticle ζ -potential.

4.2. Experimental

4.2.1. Ligand Selection

From a previous paper using large TiO₂ sizes (>50 nm), it was determined that the best ligands for complexing TiO₂ and improving ζ -potential of particles are DMSA, citric acid, and oxalic acid.¹³⁷ Based on these results, four other carboxylic acids were chosen to test the complexation of TiO₂ nanoparticles with a primary size of 30 nm and smaller. These compounds will allow the comparison of number and type of functional group (thiol and hydroxyl) and chain lengths as shown in Figure 4.1. For chain length

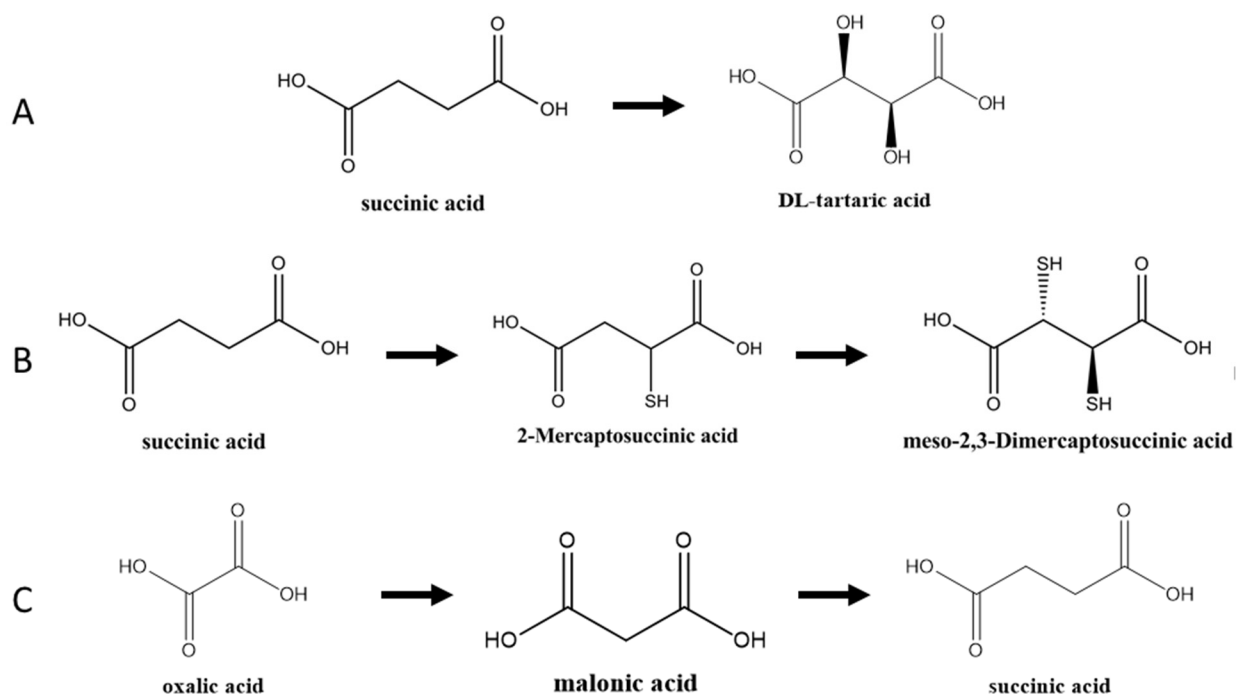
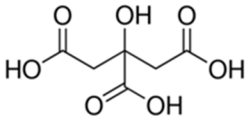
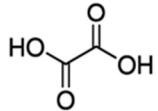
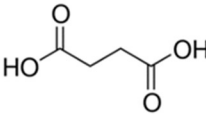
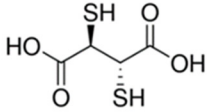
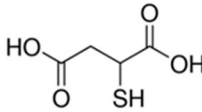
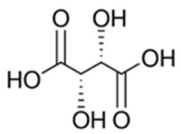
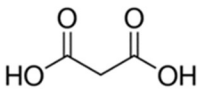


Figure 4.1. Structures of ligands used in comparing the increasing numbers of a) hydroxyl groups, b) thiol groups, and c) chain length.

dependent effects, oxalic acid, malonic acid, and succinic acid were chosen. To measure effects of thiol groups, 2-mercaptosuccinic acid and meso-2,3-dimercaptosuccinic acid were chosen and compared to succinic acid. Hydroxyl group effects were tested using DL-tartaric acid, when compared to succinic acid. Citric acid was also included as a positive control and benchmark due to its good complexation

ability of TiO₂ observed in previous experiments. Additional chemical characteristics for these compounds is listed in Table 4.1.

Table 4.1. Characteristics of seven different chemical ligands used for chelation and ζ-potential experiments. pKa values were compiled by Williams *et al.*¹³⁸

Chemical Substrate	Chemical Structure	Chemical Formula	Molecular Weight (g/mol)	pKa Values
Citric Acid		C ₆ H ₈ O ₇	192.12	3.09, 4.75, 5.41
Oxalic Acid		C ₂ H ₂ O ₄	90.03	1.25, 4.14
Succinic acid		C ₄ H ₆ O ₄	118.09	4.19, 5.48
<i>meso</i> -2,3-Dimercaptosuccinic acid (DMSA)		C ₄ H ₆ O ₄ S ₂	182.21	2.40, 3.46, 9.44, 11.82
Mercaptosuccinic acid (MSA)		C ₄ H ₆ O ₄ S	150.15	3.30, 4.60, 10.38
D,L-Tartaric acid		C ₄ H ₆ O ₆	150.09	3.03, 4.45
Malonic acid		C ₃ H ₄ O ₄	104.06	2.83, 5.69

4.2.2. Standards and Reagents

Three TiO₂ nanoparticle powders were acquired and used in the study each with a different size and crystalline makeup. Aeroxide P25 was acquired from Sigma Aldrich. Aeroxide P25 is a mixture of anatase and rutile crystal structures with a primary particle size of 21 nm. 18nm anatase and 30 nm rutile nanoparticles were also purchased (US

Research Nanomaterials, Inc.) The following organic compounds were purchased for the study and prepared in 10 mM solutions: citric acid, oxalic acid, malonic acid, (Sigma Aldrich), dimercaptosuccinic acid (Alfa Aesar) DL-tartaric acid, 2-mercaptosuccinic acid, succinic acid. 0.5 M NaOH and HCl solutions were also prepared as titrants for the autotitrator. NaOH pellets were purchased from Mallinckrodt and a concentrated HCl solution was purchased from SCP Science. A Millipore filtration apparatus was used to prepare all aqueous solutions with high resistivity water (> 18.2 MΩ and less than 3 ppb dissolved organic matter).

4.2.3. Sonication

For all nanoparticle and ligand combinations, a Crest Ultrasonics bath sonicator was used for nanoparticle dispersion. To test the effect and difference of probe sonication, a BioLogics Model 300VT ultrasonic homogenizer with a probe equipped with a 19 mm tip was used for the preparation and suspension of TiO₂ nanoparticle dispersions without added ligands. The probe sonicator was calibrated according to NIST standard protocol 1200-2 to ensure delivered power of 50 watts to each dispersion.^{139,140} The sonicator was operated at an 80% pulsed operation mode for 15 min.

4.2.4. Autotitration

A Malvern MPT-2 was used for the autotitration of each solution. Solutions were prepared using 5 mL of TiO₂ dispersion and 5 mL of each ligand solution or water blank. Solutions were used 30 minutes after combination to provide adequate time for equilibration and initial adsorption of compound to particle. 0.50 M NaOH and HCl solutions were prepared and used as titrants. The instrument would initially adjust the pH of the solution to a beginning pH of 3. Measurements would begin at that pH and continue

at increments of approximately 0.5 until a pH of 10 was achieved. The pH range of 3 to 10 was chosen according to the manufacturer's recommendation for the folded capillary cuvettes. Total added volume of the titrants was generally below 0.5 mL to prevent dilution effects. A schematic diagram of the autotitration setup is shown in Figure 4.2.

4.2.5. ELS Measurements

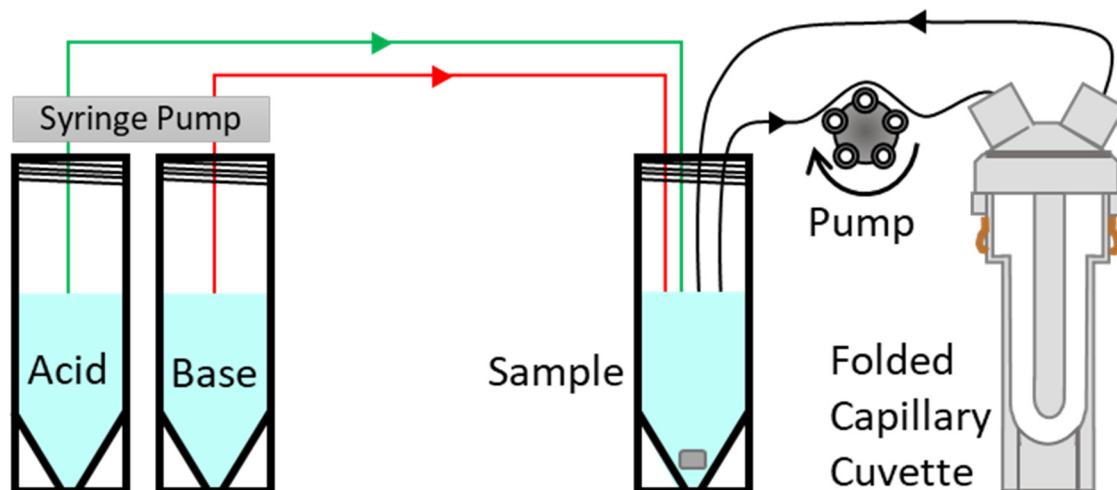


Figure 4.2. Diagram of autotitrator setup when equipped with folded capillary cuvette for ζ -potential measurements.

ζ -potential of each solution in the pH range of 3 to 10 was measured using a Malvern Zetasizer Nano ZS-90. Calculations were made using water as the dispersant with a refractive index of 1.330 and a particle refractive index of 2.61. Cuvette holder temperature was set to the ambient temperature for the laboratory (22.0 ± 0.1 °C) as most of the solution was equilibrated to room temperature during the experiment. Laser doppler electrophoresis acquired data in automatic mode and results were calculated using Smoluchowski's approximation. Transfer lines and the folded capillary cell were carefully filled using the onboard peristaltic pump to displace any air in the lines and remove any trapped air bubbles. Visual inspection was necessary to ensure no air bubbles were present in the capillary cell prior to measurements.

4.2.6. Solution Preparation

2 mg of each nanoparticle powder was added to 50 mL of water to produce solutions of 40 ppm for each solution. This concentration is appropriate for the autotitration and ζ -potential measurement using electrophoretic light scattering. Before each measurement, each TiO₂ suspension was sonicated using a bath sonicator and a probe sonicator for the blank only according to NIST Special Publication 1200-3 to explore probe sonicator effects.¹⁴¹ TiO₂ nanoparticles were weighed using an analytical balance and 50 mL of water was added using a volumetric pipette. After sonication, dispersions were used in experiments and the remaining dispersion was either stored in a cabinet away from ambient light or in amber borosilicate glassware to minimize light exposure. Ligand solutions were prepared to a concentration of 10 mM. Solutions with solids that did not dissolve immediately were placed on a tube rocker for further agitation. However, due to the low solubility of meso-DMSA in water, the pH was raised using a 0.5 M NaOH solution to improve solubility. The final pH for this solution was around 4.5 while the other ligand solutions were at a native pH typically less than 5.

4.3. Results and Discussion

4.3.1. Summary of results

Of the three types of particles examined in this study, 18 nm anatase had the greatest improvement in ζ -potential across the pH range of 3 to 10 when modified with chelating organic molecules and 30 nm rutile had the least improvement (Figure 4.2). Furthermore, the addition of ligands to dispersions of rutile nanoparticles produced a very minor increase in ζ -potential amplitude in solutions with a pH of 8 to 10. Below a pH of

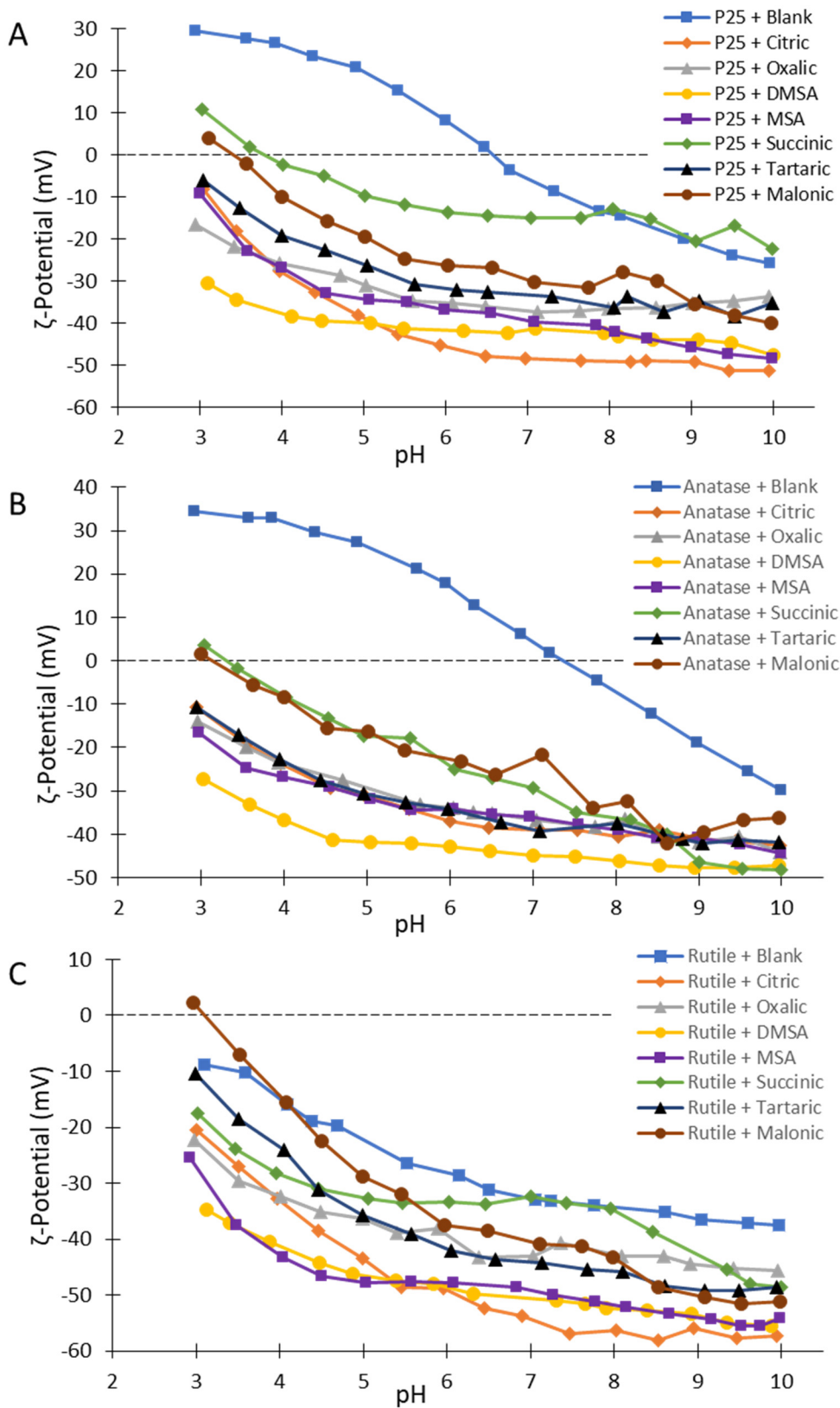


Figure 4.3. ζ -potential autotitration curves for P25 (A), anatase (B), and rutile (C) nanoparticles.

7, only DMSA and MSA increased the ζ -potential amplitude by more than 40%. Pristine 30 nm rutile TiO_2 had ζ -potential value of approximately -10 at a pH of 3 but increased in amplitude rapidly to a ζ -potential of -46 mV at a pH of 11. Within the crucial pH 6 to 8 range, the ζ -potential was around -30 mV to -35 mV. Citric acid, DMSA, and MSA increased the magnitude of the ζ -potential to -50 within this range for DMSA and MSA and nearly -55 mV for citric acid. This is a large improvement in the surface charge on the particle and in the surrounding layer especially at a neutral pH. This large improvement in ζ -potential results in a reduced likelihood of agglomeration of the nanoparticles making them more available to chemical or photocatalytic processes. It would also enable a better dispersion of 30 nm rutile nanoparticles within suspensions or coatings. However, most ligands did not improve the ζ -potential as significantly. Malonic acid, succinic acid, tartaric acid and oxalic acid, did not improve the ζ -potential by more than 20% on average. Malonic acid had a negative effect on rutile nanoparticles below a pH of 4 and presented an isoelectric point around a pH of 3.

One very widely used and well understood TiO_2 nanoparticle product is Aeroxide P25. It is an 80/20 mix of anatase and rutile, has good photocatalytic properties, and its uses have recently spread to water treatment. Unmodified P25 had a typical ζ -potential curve, when compared to the literature, beginning at 30 mV at a pH of 3 and ending at -26 at a pH of 10 with an isoelectric point of 6.53.^{42,132} However, modification with solutions of citric acid and MSA increased the ζ -potential throughout a pH range of 3 to 10. DMSA increased the ζ -potential to below -30 mV at a starting pH of 3 and further increased the ζ -potential by 60% down to a ζ -potential of -48 mV at a pH of 10. These results also show that P25 is vulnerable to agglomeration and sedimentation between the pH values of 5

and 8. However, adding low concentrations of DMSA can improve the ζ -potential to an acceptable value of -30 beginning at a pH of 3 until a pH of 5 where citric acid is the more favorable ligand. Similar to the rutile nanoparticles, succinic, malonic, and tartaric acid showed the least improvement in ζ -potential across the pH range tested and succinic acid had a lower value of ζ -potential in magnitude at a pH less than 8 than rutile alone.

Unmodified anatase nanoparticles had a very similar ζ -potential curve to P25 nanoparticles with an isoelectric point (IEP) at a pH of 7.3. All ligands lowered the ζ -potential across the pH range with only succinic acid and malonic acid modified nanoparticles having IEPs. DMSA had the highest negative ζ -potential from a pH of 3 to 9 and improved the ζ -potential at a pH of 7 from 2 to -44. This large increase in charge around the nanoparticles would surely decrease aggregation and ensure a stable dispersion. Citric acid, MSA, DMSA, and oxalic acid all had very similar ζ -potential curves beginning at around -15 mV at a pH of 3 and ending at a value of around -40 mV at a pH of 10.

4.3.2. Influence of Chain Length

Carboxylic acids of increasing chain length were used in the study to examine any connection increasing number of carbons had on the ζ -potential of TiO₂ nanoparticles. The shortest ligand used was oxalic acid, followed by malonic acid, and finally succinic acid. There was no appreciable difference in the effects that each ligand had on the nanoparticles. The impacts across the three nanoparticle types showed a random order in the change of ζ -potential for the nanoparticles. For instance, with 30 nm rutile TiO₂, oxalic acid improved the ζ -potential the most when compared to malonic acid and then succinic acid. But for 18 nm anatase nanoparticles, oxalic acid improved ζ -potential better

than the other two but succinic and malonic acid were very similar in their effects and succinic acid improved ζ -potential more after a pH of 8.5 than oxalic acid did. For P25 nanoparticles, oxalic acid had the best ζ -potential curve among the three compared here followed by malonic and then succinic acid. These results show a non-conclusive influence of chain length on ligand modification of TiO₂ nanoparticles.

4.3.3. Influence of Functional Group

To study the impact of functional groups on the ζ -potential of TiO₂ nanoparticles, ligands with an increasing number of hydroxyl or thiol groups were used. Starting with succinic acid for each type of functional group with zero, the number was increased to one with mercaptosuccinic acid (thiol) followed by an increase to two functional groups within the carboxylic end groups, tartaric acid (hydroxyl) and dimercaptosuccinic acid (thiol). Except in the case of 18 nm anatase nanoparticles, MSA and DMSA had very similar effects but were a clear improvement over succinic acid. In 18 nm anatase suspensions, DMSA improved ζ -potential 10 mV beyond that of MSA, on average, but was an effect only observed in that particular suspension. Tartaric acid modified nanoparticles had a higher magnitude ζ -potential overall than dispersions with succinic acid but the compounds containing thiol groups had a greater improvement overall than tartaric acid.

4.3.2. Effects on ζ -potential of Probe and Bath Sonication

Some of the most important results are shown in Figure 4.4., which highlights the difference in results between particles that underwent bath sonication or probe sonication. Probe sonication is very effective at dispersing agglomerated nanoparticles and is often used to prepare nanoparticle suspensions. Indeed, NIST protocols specify probe

sonication in the preparation of TiO₂ suspensions.^{139,140} However, probe sonication resulted in significantly different ζ -potential curves for P25 and anatase nanoparticles in this study when compared to bath sonication and publications from other researchers.^{42,132} For P25 nanoparticles, probe sonication had the effect of a much more negative ζ -potential across the pH range of 3 to 10 and no IEP. The IEP of titanium dioxide in water is generally accepted to be between a pH of 6 and 7, which has been confirmed by dozens of publications.¹⁴² Likewise, anatase nanoparticles had an IEP of 3.1 using probe sonication but an IEP of 7.3 using bath sonication. A similar study using anatase nanoparticle of 16 nm had an IEP of 5.8.¹³² However, when comparing rutile nanoparticles sonicated via probe and bath to those of another study, no significant variation is found.

Previous studies have also observed the differential effects of probe sonication as compared to bath sonication.^{143–147} Some studies showed changes in ζ -potential after prolonged probe sonication of 15 minutes as compared to 3 minutes but the changes were not statistically significant.¹⁴³ However, the same study observed that prolonged sonication times may increase the dissolution of metal nanoparticles such as ZnO and Mn NPs. Roebben *et al.* reported that CeO₂ nanoparticles reversed ζ -potential from positive to a negative value upon sonication.¹⁴⁴ They posited that sonication may affect the electrical double layer surrounding the particle and, therefore, the consequent ζ -potential value but did not present an explanation. Karlsson *et al.* observed similar changes to ζ -potential of CuO, Cu, and Cu-Zn nanoparticles dependent upon sonication strength and delivered energy.¹⁴⁵ CuO nanoparticles had an increase in ζ -potential from +27 mV to +40 mV after probe sonication and Cu nanoparticles increased from near-

neutral values to +10 mV after probe sonication. Finally, Betts *et al.* noted that there is a potential for metal contamination when using direct (probe) sonication.¹⁴⁷ This observation is especially pertinent for the study presented here due to the fact that the probe used is titanium and the particles are titanium dioxide. However, further research is required to determine if titanium particles or ions due to probe contamination had an effect on TiO₂ ζ -potential measurements.

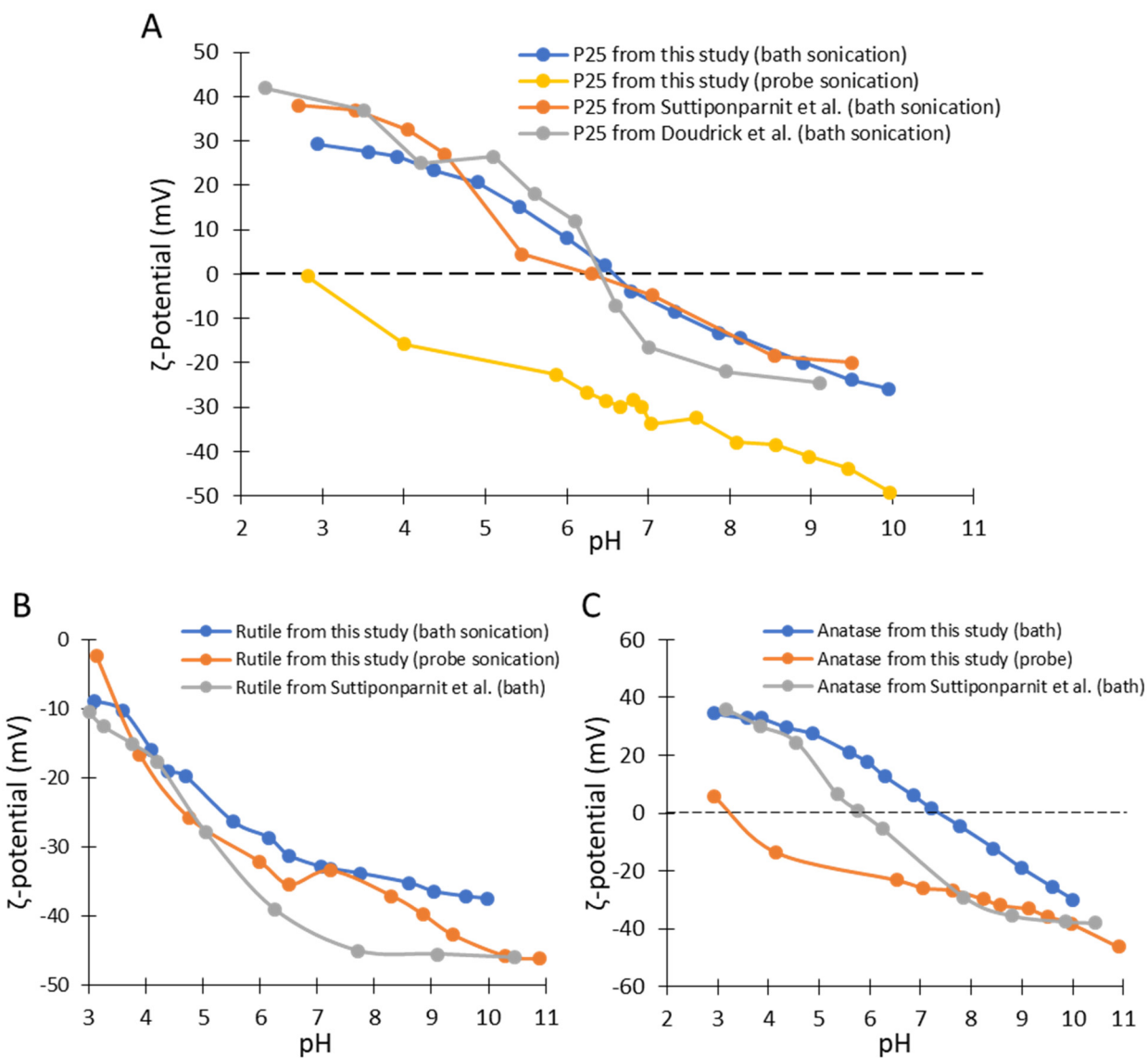


Figure 4.4. ζ -potential alteration by probe sonication vs bath sonication for particles in this study compared to particles used in Doudrick *et al.*⁴² and Suttiponparnit *et al.*¹³²

4.4. Conclusion

The modification of three dispersions of TiO₂ nanoparticles of similar sizes with organic compounds can increase the charge around a nanoparticle, which will lead to a decrease in agglomeration and sedimentation. DMSA, citric acid, and MSA increased the charge, and therefore the ζ -potential, around the nanoparticles to the greatest degree as compared to the other ligands used and the unmodified suspensions of each nanoparticle. Furthermore, there was no identifiable relationship between the increase in ζ -potential and chain length of the various double carboxylic acid ligands used in the study. However, there was a noticeable effect on ζ -potential of TiO₂ nanoparticles when modifying them with ligands that contained additional thiol or hydroxyl groups. The greatest increase in ζ -potential as pH was increased was observed with ligands with thiol groups, namely dimercaptosuccinic acid and mercaptosuccinic acid. Finally, probe sonication disrupted the pH- ζ -potential curve at pH values > 7 and altered the measured IEP for anatase and P25 nanoparticles. It is for this reason that future research focused on ζ -potential measurements of particles in aqueous suspensions should employ bath sonication rather than direct sonication.

Chapter 5 : Utilizing Fluorescence of Photocatalytic Probes within a Portable Sensor to Detect TiO₂ in Simulated Drinking Waters²

5.1. Introduction

Titanium dioxide (TiO₂) particles with sizes less than 100 nm, classified as nanoparticles, have significantly increased in production and use.³⁷ TiO₂ is used in a myriad of aqueous solutions, aerosols, coatings, plastic products, food products, and catalytic processes.³⁵ One field where nanomaterials of all kinds have seen increased application and utilization is in the purification of drinking water or industrial wastewater.^{29,30,148,149} Due to the high surface area to volume ratio and electronic properties, TiO₂ particles have high catalytic properties per a given mass that can be used in water treatment including organic micropollutant oxidation or nitrate reduction.^{42,43,55,150,151} Specific organic micropollutants include pesticides, pharmaceuticals, and other emerging contaminants of concern.^{152–154} Like other advanced oxidation processes such as the use of hydrogen peroxide, ozone, or UV irradiation^{155,156}, TiO₂ based systems have shown equal promise as an advanced oxidation process (AOP) and is differentiated because it provides an opportunity for heterogeneous catalysis where localized surface reactions can lead to enhanced pollutant degradation.¹⁴⁸ Beyond photocatalysis, TiO₂ is used to adsorb pollutants (e.g., arsenic) and nanoparticles of TiO₂ can be incorporated into macroscale granulars and placed in packed bed filters.^{157,158} In all these cases, there has been relatively little

² This chapter has been submitted as an article in ACS Sensors. The original submission is as follows: Turley, R. S.; Bi, Y.; Flores, K.; Hernández-Viezcas, J. Á.; Westerhoff, P.; Gardea-Torresdey, J. L. Utilizing fluorescence of photocatalytic probes within a portable sensor to detect TiO₂ in simulated drinking waters. *ACS Sensors*, **Submitted**.

information available on release of TiO₂ from associated nano-enabled water treatment devices.

TiO₂ enabled water treatment devices have been widely researched^{159–161} and numerous commercial systems exist that either separate and recirculate TiO₂ slurries using in-line ceramic membranes^{162–164} or TiO₂ is immobilized on highly porous and fibrous meshes.¹⁶⁵ Researchers are exploring ways of immobilizing nanoparticles within water treatment devices such as through impregnation in carbon block¹⁶⁶, immobilization onto sand or fibers^{99,129,167}, paints or coatings^{168,169}, or capture via magnetic nanomaterials.¹⁷⁰ However, nanomaterials used in water treatment devices can potentially be released into produced drinking water, industrial wastewater or discharged to surface waters. Additionally, TiO₂ is used in many sunscreens and enter water systems directly by bathers, and there has been interest in quantifying TiO₂ from recreational water uses.^{171–175} Occasionally, industrial spills of TiO₂ have occurred¹⁷⁶, and a field measurement device to detect TiO₂ would provide rapid-response monitoring opportunities. Because titanium dioxide has been shown in some rodent studies to cause cellular stress^{177–180}, concerns exist related to potential releases of TiO₂ from engineered treatment systems. While this risk appears low⁴⁹, based upon limited measurements, improved analytical techniques for TiO₂ analysis are needed for routine monitoring and safe operations of water treatment processes using TiO₂.

Background concentrations of titanium in rivers and lakes are on the order of 1 to 10 parts per billion (ppb or µg/L).⁴⁹ The most reliable and accurate method of detecting nanomaterials at these low concentrations is through the use of inductively coupled plasma mass spectrometry (ICP-MS) or more recently, single particle ICP-MS, which

allows for the quantification and detection of TiO₂ nanomaterials in the part per trillion to part per quadrillion range.^{181–183} However, the equipment required for the analysis can be prohibitively expensive, involves hazardous chemicals (e.g., hydrofluoric, nitric and hydrochloric acids) and high temperature/pressure microwave digestion, requires knowledge and experience to operate, is located only in centralized laboratories that result in days to weeks before TiO₂ concentration data becomes available. Several colorimetric methods have been proposed for TiO₂ detection in various matrices including water, food, and other products. For example, Bulbul *et al.* developed a photocatalytic and paper-based method for TiO₂ detection using methylene blue deposited onto filter paper.¹⁸⁴ This method, while novel, detected TiO₂ in the ppm range, which is not environmentally relevant. Yoe and Armstrong designed a colorimetric method using disodium-1,2-dihydroxybenzene-3,5-disulfonate and was shown to have a detection limit for titanium of 10 ppb.¹⁸⁵ This method, however, was specific to titanium ions in solution; TiO₂ analysis would, therefore, require an acid digestion step prior to analysis. Lastly, Hamano *et al.* established a colorimetric method using diantipyrylmethane for TiO₂ detection in foods.¹⁸⁶ The minimum level of TiO₂ required for determination was measured at 5 µg/g, but, similar to the previously discussed method, required acid digestion to liberate titanium ions from TiO₂ compounds.

In this paper, we integrate a fluorescent assay into a novel device that can be used to quantify TiO₂ nanoparticles in water at concentrations as low as 2 ppb. This method has several potential applications including (i) monitoring the change in photocatalytic reactivity of known nanoparticles in various water matrices, (ii) screening for the accidental release or loss of nanoparticles from water treatment or other products

where TiO₂ nanoparticles are being utilized, and (iii) screening for the occurrence of unknown photocatalytic nanomaterials, such as ZnO or TiO₂ released from sunscreens, that may be present in water samples.^{174,187,188} This preliminary screening, similar to other developed assays, could then be followed up by more advanced analytical methods including ICP-MS for accurate quantification of number and size concentrations.⁷⁶

Three types of TiO₂ nanoparticles were chosen for the study based on their use in commercial activities and crystalline structure. One of the three TiO₂ nanoparticles (Aeroxide P25) was chosen based on the application in water treatment and photocatalysis and use in previous photocatalytic studies⁷⁷ and use as a NIST reference material. The other two nanoparticles were chosen to enable a comparison of nanoparticles based on their size and crystalline structure. These include 18 nm anatase nanoparticles and 30 nm rutile nanoparticles. P25 is a mixture of the two crystalline states of TiO₂ while the remaining two samples are homogeneous. TiO₂ nanoparticles were dispersed and suspended in synthetic waters representative of treated drinking water and then irradiated with a 320 nm compact fluorescent tube light source to produce hydroxyl radicals (HO[•]). The HO[•] then oxidize a probe compound, terephthalic acid (TPA), which is often employed as a HO[•] sensor in biological assays.^{189–192} Upon hydroxylation of TPA, detectable by a fluorescent sensor. The goal in using this method was to detect TiO₂ nanoparticles near the levels of background titanium concentrations in water (1 to 10 ppb). Ultimately, the concentration of TiO₂ can be determined at a P25-equivalent level with a limit of detection of 0.6 ppb and limit of quantitation as low as 1.9 ppb dependent on the nanoparticle/water formulation combination used.

5.2. Experimental

5.2.1. Simulated Drinking Water Matrices

To measure the capabilities of the photocatalyst-TPA assay in quantifying the concentration of NPs in drinking water matrices, we used two drinking water formulations including distilled water to test for interferences. Simulated drinking waters provide a standardized chemical matrix that allows future comparison across different analytical method platforms. Soft drinking water was composed of sodium bicarbonate, calcium chloride, and magnesium chloride salts with a TDS of 141.6 mg/L with an equivalent of 50 mg/L as CaCO₃.¹⁹³ The hard water formulation was composed of sodium bicarbonate, calcium chloride, and magnesium sulfate salts with a total dissolved solid of 486.3 mg/L or the equivalent of 150 mg/L as CaCO₃. The amount of each salt in mg/L and mM is shown in Table 5.1. Each water solution was prepared in high resistivity water (> 18.2 MΩ) as a 2-liter solution at a temperature of 20 ± 2.5 °C with a pH adjusted using HCl of 7.5 ± 0.1. Sonication was required for the hard water solution.

Table 5.1. Formulations for hard and soft waters used in photocatalyst-TPA assays

Salt	Soft	Hard	Soft	Hard
	mmol/L		mg/L	
NaHCO ₃	0.75	3	63.0	252.0
CaCl ₂	0.25	1	27.7	110.9
MgSO ₄ · 7 H ₂ O	----	0.5	----	123.2
MgCl ₂ · 6 H ₂ O	0.25	----	50.8	----
Equivalent as CaCO ₃			50	150

5.2.2. Standards and Reagents

The following compounds were purchased for the study and used to prepare various synthetic drinking solutions. Sodium hydroxide pellets, magnesium chloride

hexahydrate, and sodium phosphate di-basic anhydrous were purchased from Mallinckrodt. A concentrated hydrochloric acid solution (32-35%) was purchased from SCP Science. Sodium bicarbonate, calcium chloride anhydrous, magnesium sulfate heptahydrate were purchased from Fisher Scientific. Sodium dihydrogen phosphate dihydrate, P25 titanium dioxide nanoparticles, TPA, and 2-hydroxyterephthalic acid (2-hTPA) were purchased from Sigma-Aldrich. 18nm anatase and 30nm rutile titanium dioxide nanoparticle powders were purchased from US Research Materials, Inc. A Millipore filtration apparatus was used to prepare all aqueous solutions with high resistivity water (> 18.2 MΩ and less than 3 ppb dissolved organic matter). Table 5.2. summarizes key characterization parameters for the TiO₂ nanoparticles.

Table 5.2. Physical and chemical properties of the three TiO₂ used in this study

Material	Rutile: anatase (mol:mol) ^b	Bandgap energy (eV) ^a	Primary size (nm) ^b
P25	24:76	3.66	19 to 21
Anatase	0:100	3.59	18
Rutile	100:0	3.31	30

^a Estimated from Tauc plot of reflectance data

^b Characterization from manufacturer

5.2.3. Phosphate Buffer

A buffered solution proved to be vital for not only the stability of TPA in solution but also to maintain the pH, which may affect the photocatalytic rates. Terephthalic acid is weakly soluble in water and will precipitate in acidic solutions. Therefore, TPA solutions, TiO₂ solutions, distilled, soft, and hard water solutions were all prepared with the addition of the required amounts of monobasic and dibasic phosphate followed by an adjustment to a pH of 8 ± 0.05 using a 0.5 M NaOH solution and/or a 0.5 M HCl solution.

5.2.4. UV Irradiation Lamp and Experimental Setup

An 18-watt UV lamp kit (Way Too Cool LLC; Glendale, AZ) can produce light

centered at different wavelengths. For our application, only the UVB lamp was used and was installed in the center of the lamp enclosure (in house built) between the two other lamps. This allowed it to be centered directly over the cuvette for maximum irradiation of the assay solution. The UVB lamp has a broad emission spectrum from 300 nm to 400 nm centered at 320 nm. This source allows for the excitation of a range of materials with various bandgaps that are UV excitable (i.e., < 380 nm). The use of a broad light source provided light for not only the photocatalytic activation of suspended TiO_2 but also for the excitation of 2-hTPA and consequent fluorescence within the solution.

Figure 5.1. illustrates the experimental apparatus that consisted of a fabricated box that fit the lamp snugly to prevent stray light from entering the box and to prevent UV light from escaping. However, the box was not lined with any reflective material. Ozone

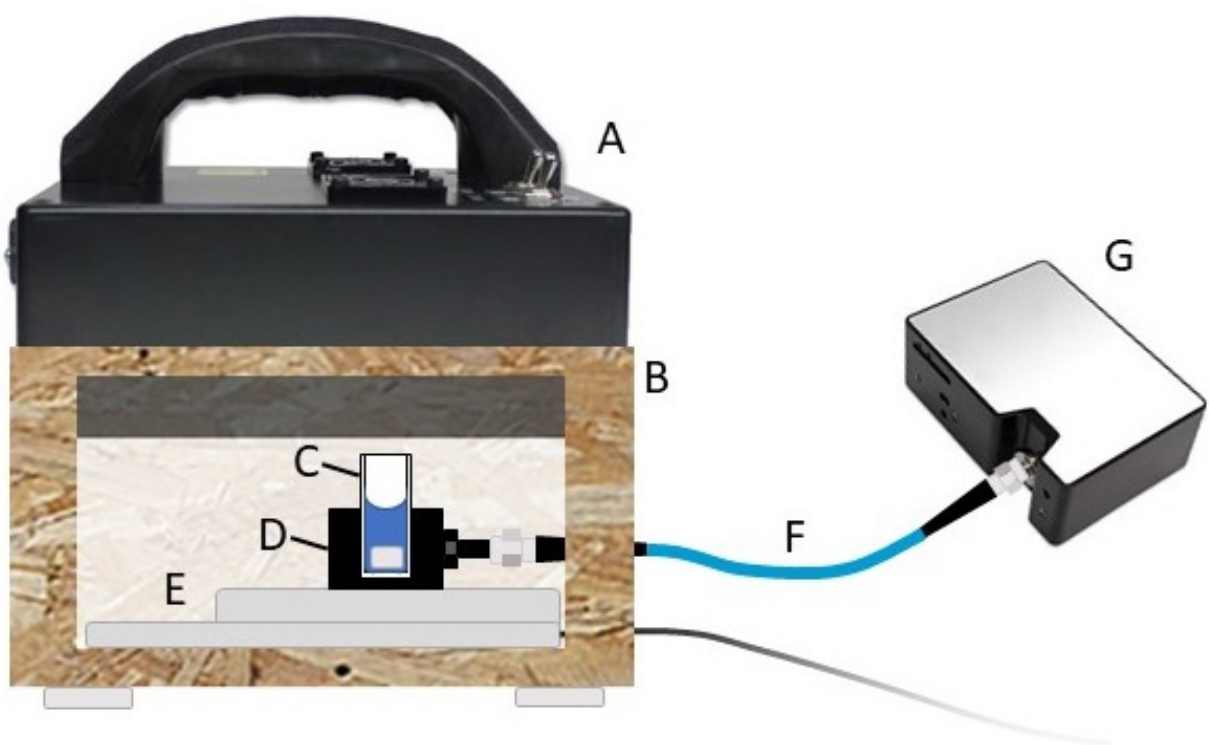


Figure 5.1. Experimental apparatus containing UV lamp equipped with 320 nm fluorescent bulb (A), OSB wooden box to contain experiment (B), quartz cuvette with stir bar (C), cuvette holder (D), VWR low profile stir plate (E), fiber optic patch cord (F), and portable spectrophotometer (G).

is a reactive oxygen species produced under UV irradiation and is thought to not directly react with TPA.¹⁹⁴ However, to reduce the opportunity for ozone accumulation and possible reactions, the bottom of the box had holes as well as a 5-volt USB fan on the side opposite to the technician for ventilation and to maintain the temperature within the box. Inside the box, the cuvette holder was placed on a low profile stir plate (VWR catalog number 10153-690) to allow for mixing of the solution within the cuvette during irradiation. Holes were drilled in the sides of the box for patch cord passthrough from the cuvette holder to the detector and for the stir plate's power cord.

5.2.5. Fluorescence Measurement and Data Processing

The fluorescent detector ((FLAME-T-UV-VIS, Ocean Optics Flame spectrophotometer) had a 200 to 850 nm range. Oceanview™ software was used to collect all spectra. Within the software, the integration time was set at 100 ms with 20 scans averaged for each reported value. Total time for each measurement was therefore 2 seconds. These settings helped to reduce noise and increase precision. The spectrometer was equipped with a 200 μm width slit and a patch cord with a fiber core size of 600 μm and a length of 250 cm. The slit and fiber core size combination were ideal for collecting low levels of 2-hTPA fluorescence with acceptable signal to noise ratios.

To collect the increase in fluorescence over time, the software was setup to monitor the emission of light at 425 nm (the emission maximum for excited 2-hTPA) and record measurements every 2 seconds as previously described. This measurement was automatically saved in real-time to a *.txt* file for future processing and analysis. Measurements for the experiments presented herein ranged from 10 minutes to 60

minutes. After the experiment had been performed and recorded, a moving average was applied to the fluorescence signal to smooth the signal. This moving average is used in Figure 5.2. for illustrative purposes and the rate for each experimental run was calculated using the raw data acquired from the spectrometer. However, as can be seen in Figure 5.2., the moving average used to smooth the data improves the correlation coefficient but does not change the slope of the linear regression by any appreciable amount.

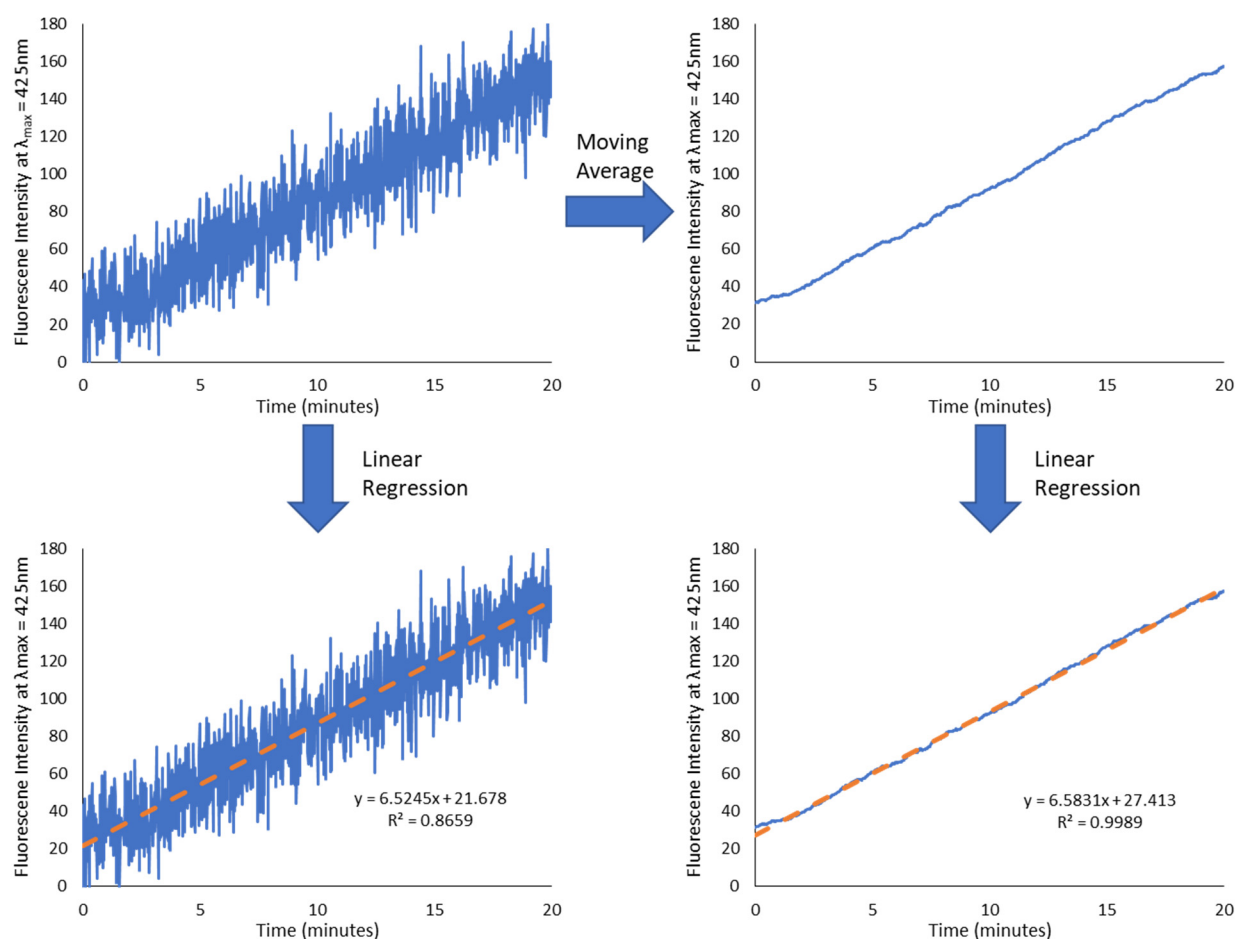


Figure 5.2. Example of fluorescence intensity data collection and inherent noise introduced via the use of a small and portable spectrophotometer. The effect of implementing a moving average of the data is shown as well as the resultant change in linear regression.

To calculate the amount of 2-hTPA formed in the photocatalytic reaction, a calibration curve for 2-hTPA fluorescence intensity was required. A standard was purchased and used to create suspensions of 2-hTPA in phosphate buffered water at a

pH of 8 similar to the solutions used in the experiments, including distilled, hard, and soft water. Eleven solutions were made for each water formulation, starting with the blank and increasing by 100 nanomolar from 100 nM up to 1000nM (or 1 μ M). Readings were taken in the same conditions that the experiments were conducted in, namely, the use of the UV lamp as an excitation source, the same quartz cuvettes used in the experiment including stir bar, and the same integration time of 100 ms, 20 scans averaged, and intensity reading at 425 nm.

5.2.6. Suspension Preparation

TiO₂ nanoparticles were weighed using an analytical balance and dispersed in 50 mL of water to produce 50 ppm stock solutions. Each dispersion was sonicated according to NIST SP 1200-3.¹⁴¹ A BioLogics Model 300VT ultrasonic homogenizer with a probe equipped with a 19 mm tip was used for the preparation and suspension of TiO₂ nanoparticle dispersions. The probe sonicator was calibrated according to NIST standard protocol 1200-2 to ensure delivered power of 50 watts to each dispersion.¹⁴⁰ The sonicator was operated at a 90% pulsed operation mode for 5 min. After sonication, dispersions were used immediately in experiments and the remaining dispersion was either stored in a cabinet away from ambient light or in amber borosilicate glassware to minimize light exposure. Stock solutions were stored in this way before use and experimental solutions were prepared via dilution with a 5mM phosphate-buffered water of either distilled, soft, or hard variety. The final pH for solutions was 8 ± 0.1 .

5.2.7. Photocatalytic Reactivity Experiments

As described, we investigated the photocatalytic reactivity of TiO₂ NPs in the presence of TPA using a UV light source to activate the NPs and excite produced 2-hTPA.

Each stock suspension was prepared as previously described in either distilled, soft, or hard water. To prepare the working suspensions, stock TiO₂ solutions, a 1 mM TPA stock solution and buffered water were used. Each working suspension was 10 mL to provide ample volume for three replicate runs. The final concentration for TPA was 50 μM for all working suspensions and the final concentration of TiO₂ is the same as the reported concentration in the results. These working suspensions were allowed to equilibrate for 30 minutes in the dark on a tube rocker for mixing (Thermolyne Speci-Mix M26125). Before each run, the tube was vortexed briefly to ensure oxygen was dissolved into the solution. Then 2 mL was added to a quartz cuvette containing a magnetic stirrer and placed in the enclosure. The UV lamp was turned on, the OceanView software set to record the fluorescence at 425 nm, and the reaction proceeded for 15 minutes. After conclusion of the experiment, the cuvette was rinsed, cleaned, and prepared for the next sample. As each set of three replicates required 45 to 50 minutes, the solutions were prepared at an interval of 1 hour to ensure the equilibration time was the same between the experiments. A blank experiment was run before any other experiments to ensure that the cuvette and stir bar had been cleaned sufficiently to remove any adhered or remaining TiO₂ nanoparticles. Each blank run contained the same concentration of TPA in either distilled, soft, or hard water (all phosphate buffered) but without nanoparticles.

5.2.8. Bandgap Energy Measurement

To further understand the possible reasons behind the differing photocatalytic reactivities of the three TiO₂ nanomaterials used in this study, the bandgap for each material was estimated using a Tauc plot collected via reflection.¹⁹⁵ A reflection/backscatter probe purchased from Ocean Optics was used to collect

reflectance spectra for each material used in the study. A high reflectivity standard was used to calibrate the Ocean Optics Flame spectrophotometer. The reflectance standard had a PTFE diffusing material with >98% reflectivity in the range of 250 to 1500 nm. The bandgap was calculated following the procedure outlined by Lopez and Gomez using $(F(R) \times E)^2$ for indirect allowed transitions.

5.2.9. Kinetics of 2-hTPA Production and Steady-state Hydroxyl Radical Concentration

As reported by Bi and Westerhoff⁷⁷, the results presented herein show that the reaction rate of 2-hTPA formation follows zero-order kinetics when TPA is in excess within the solution. Referring to Figure 5.2., the increase in fluorescence is highly linear with an R^2 coefficient of 0.9989 after smoothing for that particular experiment. Most experiments besides those at low concentrations with a high level of noise had very similar coefficients.

Figure 5.3. shows a schematic diagram of the TPA hydroxylation reaction and hydroxyl radical production mechanism by UV irradiated TiO_2 and the change in fluorescence exhibited over time due to 2-hTPA production. The emission of 2-hTPA exhibits a maximum (λ_{max}) at 425 nm. As a result of the highly sensitive nature of

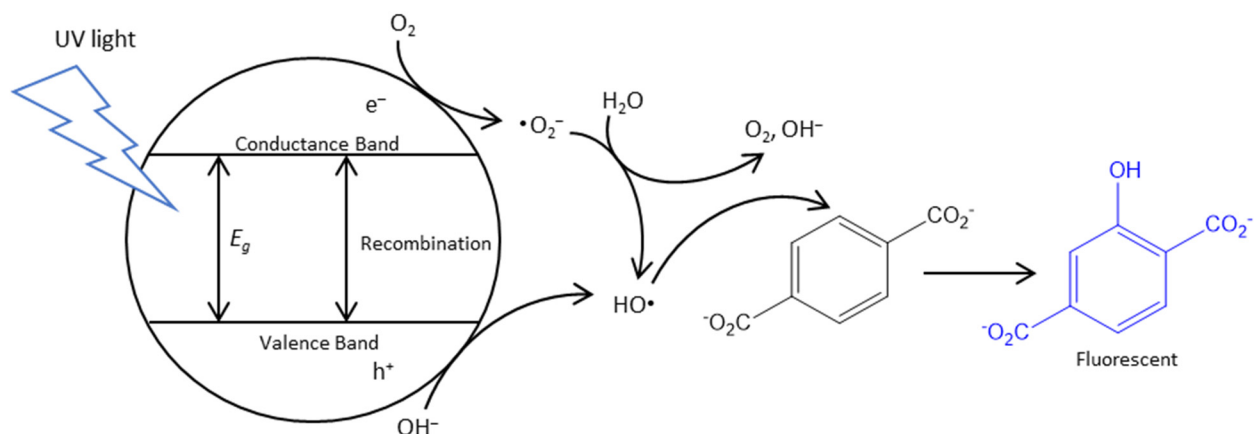


Figure 5.3. Mechanistic diagram of TPA hydroxylation and 2-hTPA formation via the hydroxyl radical production by irradiated photocatalytic nanoparticles.

fluorescence measurements, the concentration of TiO₂ can be detected at ppb concentrations. However, to calculate and compare various TiO₂ NPs to one another and in different water matrices, it is essential to calculate not only the rate of 2-hTPA production over time but also the steady-state concentration of hydroxyl radicals (M), [HO·]_{SS}. As proposed by Page et al., the calculation of the zero-order rate constant is shown in Equation 1.¹⁸⁹

$$k_{app} = \frac{d[2-hTPA]}{dt} = k_{OH,TPA}[TPA][HO \cdot]_{SS}Y \quad (5.1.)$$

$k_{OH,TPA}$ is the rate constant of TPA hydroxylation by hydroxyl radicals (M⁻¹ s⁻¹) within the solution. This value was previously determined by Page et al. via γ radiolysis of water to be 4.4×10^9 M⁻¹ s⁻¹. In the same study, Y , which is the yield of 2-hTPA via TPA hydroxyl attack, was determined to be 0.35 or 35%.¹⁸⁹ $[TPA]$ is the beginning concentration of TPA in moles, which for this study is 5×10^{-5} M. Finally, k_{app} is the zero-order rate constant of 2-hTPA generation or as shown here, the change in 2-hTPA over the change in time. To solve for the steady-state hydroxyl concentration, Equation 5.1. can be rewritten as shown in Equation 5.2.:

$$[HO \cdot]_{SS} = \frac{k_{app}}{k_{OH,TPA}[TPA]Y} \quad (5.2.)$$

Parameters in Equation 5.2. are known or determined from experimental measurements (k_{app}), and thus enable calculation of [HO·]_{SS}. To obtain k_{app} , the 2-hTPA calibration curve is required to know the change in fluorescence due to the change in 2-hTPA concentration. The slope of the calibration provides a conversion factor between the fluorescence and 2-hTPA concentration at any given point in an experiment. Figure 5.4. shows the calibration curve of 2-hTPA fluorescence in distilled water. The slope of the linear regression calculated can be thought of as $\frac{d[FI]}{d[2-hTPA]}$, where FI is the fluorescence

intensity. Likewise, the increase in fluorescence intensity in each experimental run is $\frac{d[FI]}{dt}$.

Therefore, dividing $\frac{d[FI]}{dt}$ by $\frac{d[FI]}{d[2-hTPA]}$ yields $\frac{d[2-hTPA]}{dt}$, which is equal to k_{app} .

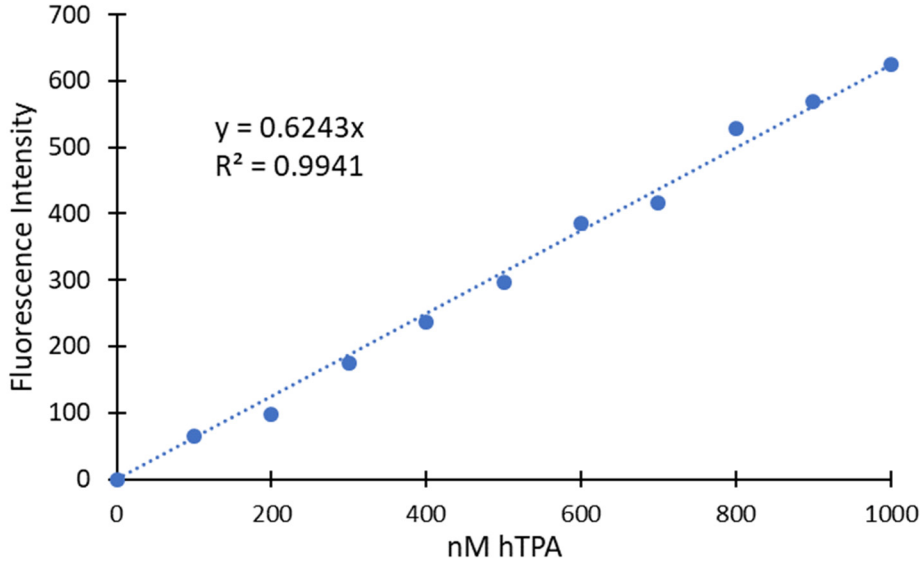


Figure 5.4. Calibration curve for 2-hTPA fluorescence in distilled water. The broadband UV lamp with a maximum of 320nm was used as the excitation source and the fluorescence intensity was recorded at 425 nm.

5.3. Results and Discussion

5.3.1. Summary of Results

The efficacy and usefulness of the 2-hTPA photocatalytic reactivity assay can be determined by comparing the limit of detection (LOD) and the limit of quantitation (LOQ) for each nanoparticle in each water matrix used. A series of calibration experiments were performed to calculate LOD and LOQ values. The LOD and LOQ values were then calculated using the standard deviation of the lowest concentration tested as shown in Equations 5.3. and 5.4.:

$$LOD = \frac{3(\sigma_{2-hTPA})}{|k_{2-hTPA, TiO_2}|} \quad (5.3.)$$

$$LOQ = \frac{10(\sigma_{2-hTPA})}{|k_{2-hTPA, TiO_2}|} \quad (5.4.)$$

where σ_{2-hTPA} is the standard deviation of the rate of 2-hTPA production for the lowest

concentration tested and k_{2-hTPA, TiO_2} is the production rate of 2-hTPA per concentration of TiO_2 suspended in solution which is the slope of the linear fit for all the runs tested for a specific NP/water matrix combination as shown in Figure 5.5.

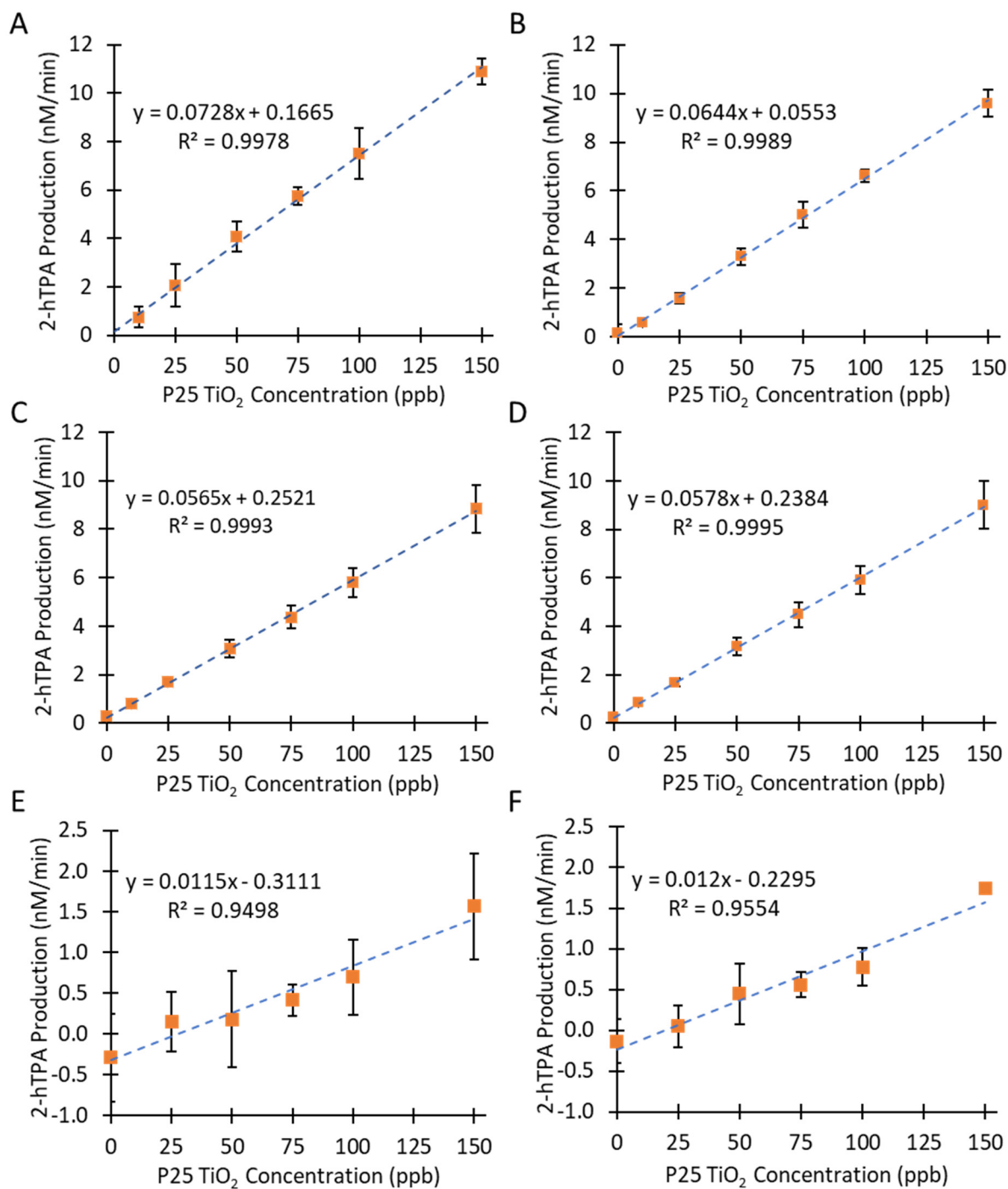


Figure 5.5. Photocatalytic assay results for P25 TiO_2 in distilled water for 10 minutes (A) and 15 minutes (B), soft water for 10 minutes (C) and 15 minutes (D), and hard water for 10 minutes (E) 15 minutes (F). Error bars show the 95% confidence interval for each mean of three replicates.

In Table 5.3., the LOD and LOQ values are listed for 10 min experimental runs and 15 min experimental runs. In the case of P25 nanoparticles, the LOD ranges from as low as 0.6 ppb and 3.1 ppb for 15 min runs in distilled and soft water, respectively, up to 96 ppb for a 10-minute run in hard water. For anatase, the LOD and LOQ were similar to those found for P25 in distilled and soft water but a magnitude higher likely due to the reduced photocatalytic activity displayed by anatase as compared to P25. Rutile had a much higher LOD and LOQ, in the 0.5 to 4 ppm range, due to the substantially decreased photocatalytic reactivity of rutile. The detection limits for P25 in distilled and soft water are comparable to those obtained from ICP-OES after acid digestion, but higher than those obtained from ICP-MS.¹⁹⁶ Additionally, the presented method does not require the expense of an ICP-OES or the required expertise. However, the respectable LOD rises quickly with increasing concentrations of dissolved inorganic compounds.

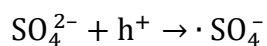
Table 5.3. Summary of results for each nanoparticle and water formulation tested in this study including limit of detection (LOD) for each method and limit of quantitation (LOQ).

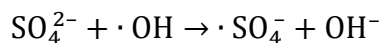
TiO ₂ Nanoparticle	Matrix	10 min	15 min	10 min		15 min	
		k ₂ -hTPA, TiO ₂	k ₂ -hTPA, TiO ₂	LOD (ppb)	LOQ (ppb)	LOD (ppb)	LOQ (ppb)
P25	Distilled	0.0728	0.0644	4.7	16	0.6	1.9
	Soft	0.0565	0.0578	3.4	11	3.1	10
	Hard	0.0115	0.0120	96	319	64	214
Anatase	Distilled	0.0188	0.0067	14	46	39	131
Rutile	Distilled	0.0008	0.0003	454	1510	1110	3690

The difference in photocatalytic activity, and therefore HO_{ss} production is, in part, due to rutile being a direct band gap semiconductor while anatase is an indirect band gap semiconductor. The photo-excited electrons and consequent holes in indirect band gap anatase would possess a longer lifetime than those in direct bandgap semiconductors such as rutile, which would extend the amount of ROS production time before

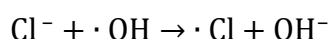
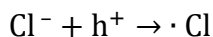
recombination as shown in Figure 5.3.^{197,198} The differences in measured band gaps (Table 5.2.) would not necessarily affect the results as the energies of the emitted light used in the experiment were sufficient to excite electrons within each material. In a drinking water treatment scenario, a calibration curve would be developed using the actual commercial or proprietary TiO₂ used in the drinking water device. Thus, a calibration curve for this specific TiO₂ material could be readily developed. The data presented in Table 5.3. suggest that the proposed photocatalytic assay can detect TiO₂ NPs in treated drinking water as well as ultrapure distilled water in a simple and repeatable manner.

There was interference imparted by inorganic compounds dissolved in soft and hard water in these experiments. The rate of 2-hTPA production over 10 minutes, k_{2-hTPA,TiO_2} , in soft water decreased by 22.4% as compared to P25 in distilled water, and in hard water decreased by 84.2% as compared to P25 in distilled water. These interferences and lower 2-hTPA production consequently increased the detection limits and introduced higher deviation into the acquired data. Multiple factors could influence the reduced value of k_{2-hTPA,TiO_2} . This could include photo-aggregation of TiO₂ due to localized charging and presence of divalent cations (e.g., calcium)¹⁶², wherein the aggregate has less TiO₂ surface area exposed to UV light. Additionally, the lower steady-state hydroxyl radical concentration is in part due to the formation of other radical ions in water including chloride and sulfate. According to Burns et al., sulfate ions that are bound to the surface of TiO₂ could react with the valence band holes or, alternatively, to a hydroxyl radical and form a sulfate radical.¹⁹⁹





Similarly, chloride ions in solution can also interfere with hydroxyl radical production by a similar mechanism as reported by Lutze et al.²⁰⁰



These processes would lead to competitive interference with not only hydroxyl radical production but also the reaction of hydroxyl radicals with TPA to form 2-hTPA. Furthermore, the increased amount of inorganic ions within solution could block active sites on TiO₂ nanoparticles leading to decreased production of hydroxyl radicals overall.²⁰¹

5.3.1. Agreement with Previously Published Results

Bi and Westerhoff⁷⁷ used multi-well plates for a high-throughput method of quantifying the photocatalytic reactivity of nanoparticles in water. That study used not only terephthalic acid, but also methyl orange, methylene blue, and NADH to determine the photocatalytic activity of certain nanoparticles. While similar, our study exploits the photocatalytic activity of nanoparticles to quantify the mass concentration in solution rather than quantifying their reactivity. The multi-well plate method, while superior in throughput and the number of samples that can be analyzed concurrently, lacked the ability to record real-time changes in the fluorescence increase of produced 2-hTPA in solution. The well plate method required irradiation, followed by a brief pause to move the plate to a fluorescent plate reader, and then back to the light source for irradiation. This pause may result in a reported steady state hydroxyl radical concentration different than the actual concentration. Furthermore, the short pathlength in the 96-well plates

restricted the study to concentrations > 1 ppm and limited the dynamic range.

The method presented here, while only allowing one sample to be studied at a time, provides a method for continuous irradiation and continuous monitoring of 2-hTPA fluorescence. Additionally, the well plate method lacked a way to mix the contents of each well for thorough mixing, which may lead to sedimentation of nanoparticles at elevated concentrations or upon photo-aggregation. The online and real-time analysis of photocatalytic reactivity presented here is a superior method to sampling a test solution at intervals, which requires shutting off the light source for a period of time so as not to irradiate the scientist conducting the experiment. Our method has the capability to be used in a variety of photocatalytic experiments whenever the degradation of model pollutants is required. Figure 5.6. shows that the solid-state hydroxyl radical concentration for this work and the Bi and Westerhoff study have good agreement, and therefore validates the device and method developed here. Using the solid-state hydroxyl

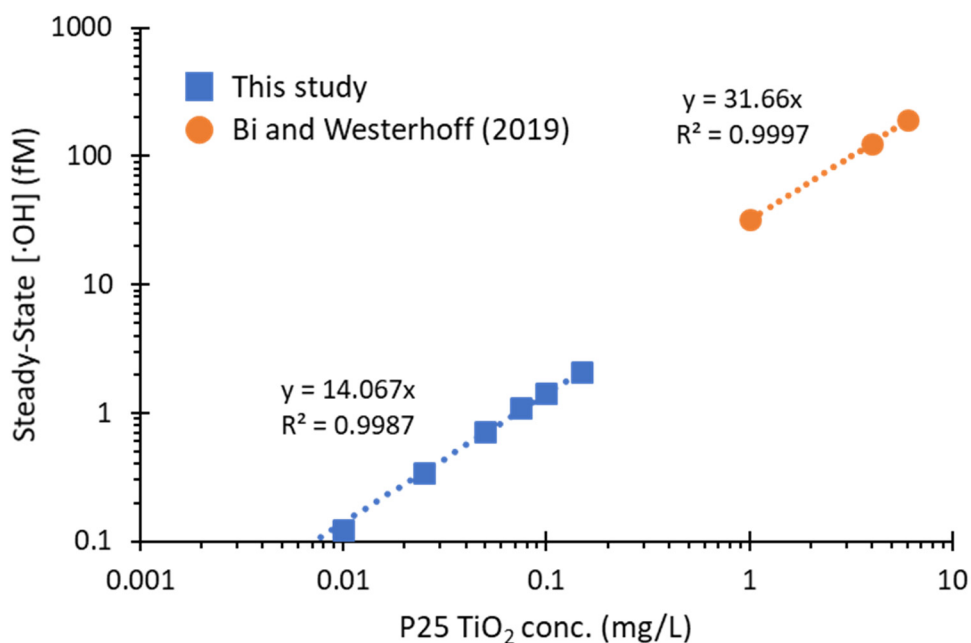


Figure 5.6. Measured steady state hydroxyl radical concentration using Equation 5.2. for P25 in distilled water after a 15-min run time. Blue squares and blue trendline are from this study while the orange circles and orange trendline are from the Bi and Westerhoff study.

radical concentration is the best metric for comparing similar studies since it pertains directly to the creation of hydroxyl radicals from photocatalytic materials and not to a reaction of hydroxyl radicals and another molecule. HO_{ss} concentration can also enable comparison between studies such as this one using TPA and others that calculate HO_{ss} from the degradation rates of other molecules such as methylene blue.²⁰²

5.4. Conclusion

We have shown that a simple, rapid, and affordable method and device can be developed for quantifying and detecting TiO_2 nanoparticles in water. The findings agree with prior work using 96-well plate reader technology. The method presented here is sufficiently sensitive when detecting TiO_2 nanoparticles in the low parts per billion range and uses commercially available reagents. The method described here employs terephthalic acid as a hydroxyl radical scavenger and consequent fluorescent probe upon creation of 2-hydroxyterephthalic acid. This procedure is aimed at detecting nanoparticles in treated drinking water to monitor and demonstrate negligible release from drinking water devices. Given background titanium concentrations of 1 to 10 ppb, our device has detection limits adequate to differentiate released TiO_2 from background levels. For example, in one study we observed up to 100 ppb of TiO_2 , detected using ICP-MS, for a TiO_2 system with a ceramic membrane, when the system was not operating to full capacity (i.e., only two of four UV lamps were operational).¹⁶² The background, influent water to the TiO_2 system, was ~8 ppb. Our device shown herein would have readily detected 100 ppb of TiO_2 in the TiO_2 system effluent.

Future work will focus on the application of this method to environmental waters including lakes and rivers, and possibly to wastewater streams entering and exiting

wastewater treatment plants. This method could also be applied to other photocatalytic nanomaterials such as zinc oxide, but the detection limits would be wholly reliable on the reactivity of said materials. Whereas the TiO₂ composition (i.e., crystallinity) is known for engineered treatment systems that employ TiO₂ and calibration curves can be readily developed to detect release of the TiO₂, such may not be the case for detection of “unknown” TiO₂ in rivers – which may have originated from stormwater runoff, reactional use of the water by bathers wearing sunscreens, treated wastewater discharges, or other sources. These releases are predicted to result in TiO₂ concentrations of 0.53 ppb in surface waters and 16 ppb in sewage treatment plant effluent.²⁰³ Each source of TiO₂ may have different crystal structures or even surface coatings (e.g., alumina or silica oxides or PEG coatings that are used on sunscreens), which influence photoreactivity. In applying our device to these samples, the intent is to understand potential ecological impact from “photocatalytic processes”, rather than quantifying a mass concentration of TiO₂. Such indirect measurements are common in environmental analysis, where the process or outcome is more important than mass concentrations of individual pollutants. In such cases, surrogate assays are often used, and the response recorded as equivalent units. Two examples include estrogenic activity from bioassays or algal toxin activity from receptor binding assays, wherein final activity is reported in equivalent units (e.g., EE2 equivalents/L or microcystin-LR equivalents/L). In the same way, we recommend reporting photocatalytic activity as mgP25-TiO₂ equivalents/L when using our device. A similar approach has been taken for reporting chemical redox activity of nanoparticles in water (e.g., mg of 50 nm gold-NP equivalents / L).^{76,204} Overall, the assay presented here

is a reliable, sufficiently sensitive, and accurate method for detecting TiO₂ nanoparticles in water using affordable and portable instrumentation.

Chapter 6 : Single particle ICP-MS analysis on the aging of P25, rutile, and anatase titanium dioxide nanoparticles in agitated simulated drinking water matrices without sonication

6.1. Introduction

Engineered nanomaterials (ENMs) are widely used in consumer products, commercial activities, and industrial processes.²⁰⁵ These materials are often finely tuned to have well controlled properties for specific applications. One application that has drawn increased attention is their application to water treatment.^{29,206,207} Water treatment devices have been nano-enabled for more than a decade with promising results.^{31,208,209} These devices promise to have higher efficiency using lower amounts of active materials and can be tuned for specific pollutants and feed waters. This is possible due to the chemical and physical properties unique to nano-sized materials. These materials have increased surface area to volume for increased activity, for example, maximum adsorption capacity or photocatalytic reactivity.^{210,211}

Due to the ever-increasing use of nanomaterials in industry and consumer products, ENMs will inevitably be released into the environment.¹ Some of these materials are known to be toxic to aquatic organisms and mammals.^{86,212–215} In the realm of drinking water treatment, these materials could be released by nano-enabled devices through either free particle release, immobilization failure, or through aging effects. However, the concentration of these released materials in the environment will be very low and recent publications show a concentration of $< 1 \mu\text{g L}^{-1}$ or 1 part per billion.^{169,174,216} However, release of materials into drinking water streams from nano-enabled devices may be a magnitude higher. Not only could this lead to ingestion of materials by

consumers but possible transformation of materials while in storage within water heaters, pressure vessels, pipes, etc. These water matrices can be extremely complex and include not only inorganic compounds but also dissolved organic matter and microbes.

Research into nanoparticle transformation water matrices are often limited by the capabilities of analytical instrumentation, including complex sample preparation for methods such as electron microscopy, detection limits in instruments, such as inductively coupled plasma – optical emission spectroscopy (ICP-OES), and often require extensive data analysis.¹²³ To properly characterize the materials used, multiple methods are often required to measure the aggregation or dissolution kinetics, size over time, and changes in chemical composition.^{217–219} However, many of these methods require much higher concentrations of ENMs than is environmentally relevant on the scale of 50 $\mu\text{g L}^{-1}$ to 500 $\mu\text{g L}^{-1}$, depending on the method.^{220,221} These concentrations are significantly higher than expected in product water from particles lost from water treatment devices and will therefore skew dissolution or transformation results. Some of these changes include increased nanoparticle to nanoparticle interactions and higher ENM to dissolved inorganic solid ratios. Previous studies have explored nanoparticle transformation at 100 $\mu\text{g L}^{-1}$ and shown the changes to be different from studies at 1000 $\mu\text{g L}^{-1}$.^{222,223} At present, no study has been published on the transformations of titanium dioxide ENMs at concentrations that are not only environmentally relevant but also relevant to the incidental release of materials into drinking water from nano-enabled water treatment devices.

This work uses single particle inductively coupled mass spectrometry (sp-ICP-MS) to quantify changes in three types of titanium dioxide nanoparticles. These changes

include size, size distribution, and the particle concentration over two weeks at realistic concentrations. The three materials used in this study include Aeroxide P25, which is a mixture of two crystalline states of TiO₂, rutile and anatase, while the remaining two are pure rutile or pure anatase. The work presented here explores the transformations in simulated drinking water matrices of soft and hard varieties including ultrapure distilled water.

6.2. Experimental

6.2.1. Nanoparticles

The P25 nanoparticles used in this study were purchased from Sigma Aldrich and 18 nm anatase and 30 nm rutile were purchased from US Research Materials, Inc. P25 nanoparticles are a mixture of the two crystalline structures, rutile and anatase, but in a mix between 70:30 and 80:20 mole to mole ratio as rutile : anatase. P25 NPs from Sigma Aldrich were used after suspension and dilution between 5×10^4 and 4×10^5 particles mL⁻¹ for experiments. The corresponding solution concentrations were approximately 3 to 25 ppb ($\mu\text{g L}^{-1}$). Anatase NPs from US Research Materials, Inc. were used after suspension and dilution between 2×10^4 and 1×10^5 particles mL⁻¹ for experiments. The corresponding solution concentrations were approximately 1 to 8 ppb ($\mu\text{g L}^{-1}$). Rutile NPs were used after suspension and dilution between 7×10^3 and 2×10^4 particles mL⁻¹ for experiments. The corresponding solution concentrations were approximately 0.5 to 4 ppb ($\mu\text{g L}^{-1}$). Table 6.1. displays some relevant characteristics of the three TiO₂ nanoparticles used in this study.

Table 6.1. Physical properties of the three TiO₂ nanoparticles used in this study

Material	Rutile: anatase (mol:mol)	Primary size (nm)	Density (g/cm ³)
P25	24:76	19 to 21	3.87
Anatase	0:100	18	3.78
Rutile	100:0	30	4.23

6.2.2. Water Matrices

To determine how various water matrices affect size and particle concentration of suspended nanoparticles over time, distilled water, a synthetic soft water, and a synthetic hard water were used in the experiments. The synthetic soft water formulation was composed of calcium chloride, sodium bicarbonate, and magnesium chloride salts. The synthetic hard water formulation was composed of calcium chloride, sodium bicarbonate, and magnesium sulfate salts.²²⁴ Soft water had a total dissolved solid (TDS) of 141.6 mg/L with an equivalent of 50 mg/L as CaCO₃ using Equation 6.1.¹⁹³ Hard water had a TDS of 486.3 mg/L or the equivalent of 150 mg/L as CaCO₃. The amount of each salt in mg/L and mM is shown in Table 6.2. Ultrapure water was used to prepare the soft and hard water solutions (> 18.2 MΩ) with a pH adjusted using HCl of 7.5 ± 0.1 at a temperature of 20 ± 2.5 °C.

$$[CaCO_3] = 2.5 \times [Ca^{2+}] + 4.1 \times [Mg^{2+}] \quad (6.1.)$$

Table 6.2. Formulations for hard and soft waters used in the TiO₂ aging study

Salt	Soft	Hard	Soft	Hard
	mmol/L		mg/L	
NaHCO ₃	0.75	3	63.0	252.0
CaCl ₂	0.25	1	27.7	110.9
MgSO ₄ · 7 H ₂ O	----	0.5	----	123.2
MgCl ₂ · 6 H ₂ O	0.25	----	50.8	----
Equivalent as CaCO ₃			50	150

6.2.3. Single Particle Inductively Coupled-Plasma Mass Spectrometry (spICP-MS)

All spICP-MS data was collected using a Perkin Elmer NexION 1000 ICP Mass Spectrometer in single particle mode using the Syngistix Nano Application Module within the Syngistix software. The sample uptake rate over 2 weeks varied from 0.293 to 0.268 mL min⁻¹. Instrument conditions for data acquisition were set at a dwell time of 100 μs, an acquisition time of 120 s and an RF power of 1600 W. The transport efficiency also varied over the two-week time period from 8.73% down to 6.57%. The measured analytes for titanium were ⁴⁹Ti and for gold, ¹⁹⁷Au. ⁴⁹Ti is not the most abundant isotope of titanium but is used by the instrument to prevent isobaric interferences for the most prevalent isotope of titanium ⁴⁸Ti from ⁴⁸Ca.²²⁵ The Nano Application in Syngistix reported particle concentration, particle size, mean size, most frequent size, and the concentration of dissolved (ionic) species in solution.

Solutions were sampled directly after being removed from their place on an incubator/shaker. The sample uptake probe was dipped in a water rinse solution and before sampling to prevent acidification of samples by remaining nitric acid from the wash solution. A one-minute wash cycle was performed between each sample to clean the introduction system before each measurement. The rinse cycle guaranteed the removal of inorganic salts in each solution from the instrument and sampling system to prevent an inadvertent buildup of salts that could not only clog the nebulizer and sample introduction system but could alter the transport efficiency. The wash cycle used a 2 to 3 % nitric acid solution followed by a short immersion in distilled water that was replaced daily.

In spICP-MS analysis, the instrument measures one element at a time with settling time between elements to change the quadrupole and QID for the next element.

However, in this experiment, only titanium was analyzed so the settling time was 0 μ s. The Nano application estimated particle size for each material and calculated the corresponding particle concentration, mean size, and most frequent size for each sample. A straightforward calculation was used to determine the mass concentration for each sample as changes in particle concentration can be misleading when combined with changes in mean size. The calculation for mass concentration is as follows:

$$C_{\text{NP}}^{\text{M}} = \frac{4}{3} \pi \left(\frac{d}{2}\right)^3 \rho N_{\text{NP}} \quad (6.2.)$$

where C_{NP}^{M} is the mass concentration for the nanoparticles in each sample, d is the calculated mean diameter size for the nanoparticles, ρ is the nanoparticle density for each nanoparticle (as shown in Table 6.1.), and N_{NP} is the number concentration of nanoparticles calculated by the Nano software for each sample.²²⁶

6.2.4. Standards

Ionic gold and titanium standards with concentrations of 1, 5, 10, and 20 $\mu\text{g L}^{-1}$ were used for the ionic calibration of titanium and for the transport efficiency calculation for gold nanospheres. Titanium ionic standards were diluted using 2 to 3% nitric acid and gold ionic standards were diluted using 2 to 3% hydrochloric acid. 60 nm Au NPs were purchased from Nanocomposix (NanoXact Citrate coated Gold Nanospheres) and used to calculate the transport efficiency of the instrument sampling system at a particle concentration of 1.5×10^5 particles mL^{-1} .^{227,228}

6.2.5. Experimental Sample Preparation

As previously mentioned, experiments were performed in two synthetic water formulations and in distilled water. Each solution containing nanoparticles and soft, hard, or distilled water had an initial volume of 50 mL and were stored in VWR PerformR High

Performance Centrifuge tubes. The tubes are made of polypropylene and a polyethylene cap. The conditions of the experiment including temperature, light/dark cycles and agitation using a REVCO incubator shaker in an environmental growth chamber on a 16/8 h light dark cycle at 22 °C and equipped with photosynthetic lamps. While these conditions may mimic environmental conditions^{229,230} and not necessarily the conditions in drinking water storage and production, they were chosen to maintain consistency

Table 6.3. Nanoparticle, matrix, and starting concentration combinations used in experiments. All solutions were produced in triplicate 50 mL samples.

Particle	Matrix	Mass Conc. ($\mu\text{g L}^{-1}$)	Number Conc. (particles mL^{-1})
P25	Distilled Water	3	5×10^4
		13	2×10^5
		25	4×10^5
	Soft Water	3	5×10^4
		13	2×10^5
		25	4×10^5
	Hard Water	3	5×10^4
		13	2×10^5
		25	4×10^5
Anatase	Distilled Water	1	2×10^4
		5	6×10^4
		8	1×10^5
	Soft Water	1	2×10^4
		5	6×10^4
		8	1×10^5
	Hard Water	1	2×10^4
		5	6×10^4
		8	1×10^5
Rutile	Distilled Water	0.5	7×10^3
		2	1×10^4
		4	2×10^4
	Soft Water	0.5	7×10^3
		2	1×10^4
		4	2×10^4
	Hard Water	0.5	7×10^3
		2	1×10^4
		4	2×10^4

across the samples and across the time period required. Samples were in 50 mL centrifuge tubes and were placed horizontally on the shaker to allow for agitation across the test tube. Experiments were performed in triplicate for each nanoparticle in each water matrix and for each concentration as listed in Table 6.3. Test tubes were sampled at time intervals of 0, 24, 48, 72, 96, 120, 144, 168, 192, and 216 hours. Each sampling event consumed about 1.5 mL of sample so over the 2-week period 16.5 mL was lost from each sample or a loss of about a third by the end of the study. Samples were removed from the shaker and environmental chamber in sets of nine tubes, analyzed, and returned to the shaker.

6.3. Results and Discussion

Particle size and number concentration for titanium dioxide nanoparticles were monitored over two weeks to determine the degree of transformation in each respective water matrix. These transformations may include homo-aggregation or hetero-aggregation, dissolution, or loss of nanoparticle by adherence to tube walls. Aggregation was exhibited by an increase in particle size accompanied by a decrease in particle concentration and dissolution could be detected by the increase of dissolved nanoparticles in the single particle results. However, loss of nanoparticles to sedimentation or adherence to tube walls is not easily detected and may have been reversible through sonication.¹⁴⁰

6.3.1. P25 Concentration Dependence in Distilled, Soft, and Hard Waters

P25 nanoparticles were prepared with three distinct initial concentrations of 5×10^4 , 2×10^5 , and 4×10^5 . Similar recent experiments used concentrations similar to the highest concentration used here for dissolution and aggregation studies.^{222,231,232}

The lower end on the concentration range was selected as being environmentally relevant and also relevant to the slow release potential of nanoparticles from water treatment devices. As shown in Figure 6.1., the concentration for each water formulation didn't affect the changes in part size, mean size, and particle mass

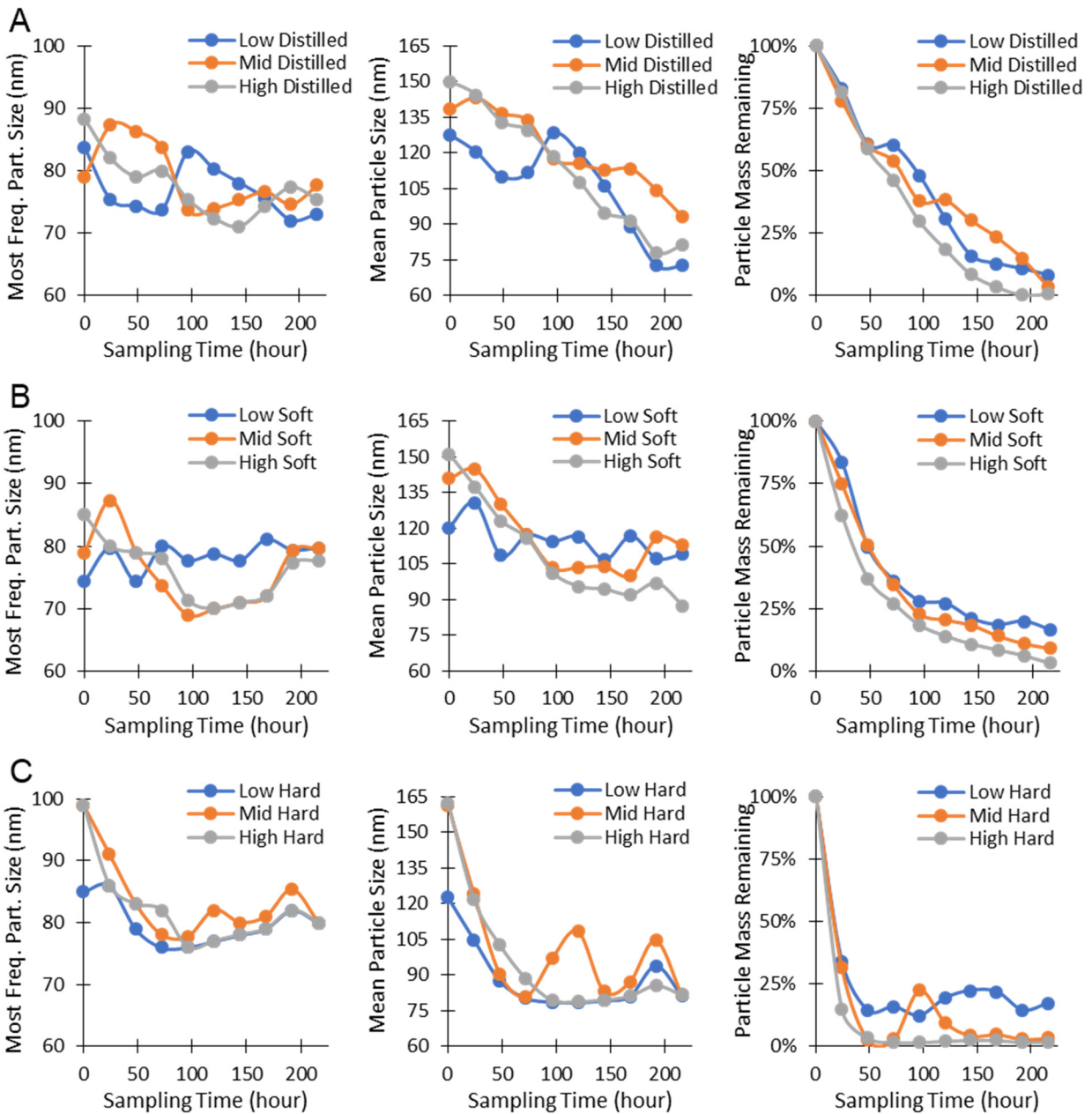


Figure 6.1. Most frequent particle size, mean particle size, and particle mass remaining in dispersion for P25 nanoparticles in distilled water (A), soft water (B), and hard water (C). For P25 NPs, low refers to a concentration of 3 ppb, mid refers to 13 ppb, and high refers to 25 ppb.

remaining as much as the water formulation did. Interestingly, as the remaining mass of particles in solution decreased, the most frequent particle size skewed towards approximately 80 nm for particles in all water formulations. However, mean particle size decreased rapidly towards 80 nm for distilled and hard water formulations but not for soft water formulations. Nanoparticles in distilled and soft water had a higher mean particle size and most frequent particle size for low concentrations than mid or high concentrations. This is likely due to increased agglomeration for higher concentrations of nanoparticles due to the higher likelihood of particle-particle interactions.

When comparing the highest concentration in each water formulation, shown in Figure 6.2., water hardness had a significant effect on particle loss with the mass of particles remaining in hard water dropping precipitously followed by soft and then distilled water suspensions. However, most frequent particle size for each matrix followed a similar pattern and settled in around 80 nm. Mean particle size followed a similar trend to particle mass remaining in suspension likely due to falling particle numbers and therefore lower opportunity for agglomeration. By the end of the study, an equal percentage of particles were longer suspended in all water formulations and final mass concentration was between 0.2 and 0.7 ppb.

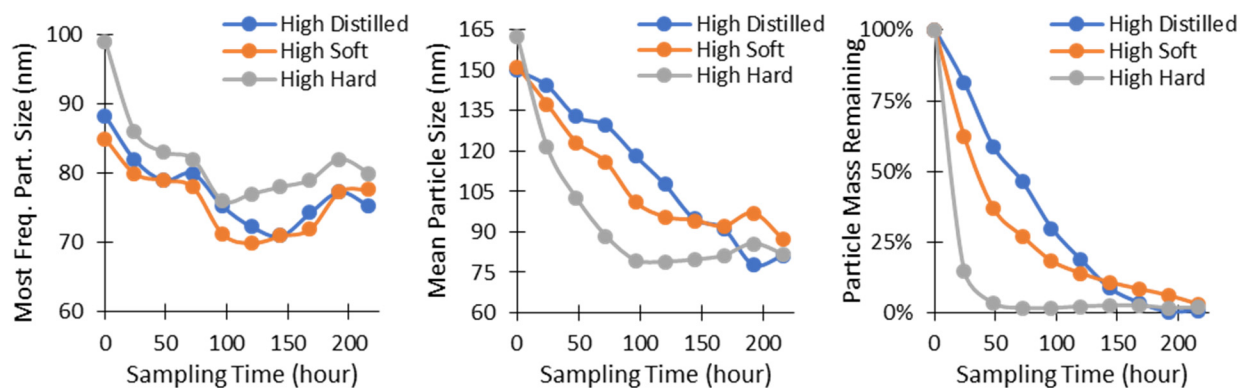


Figure 6.2. Comparison of most frequent particle size, mean particle size, and particle mass remaining in dispersion for P25 nanoparticles in distilled, soft, and hard water at a concentration of 25 ppb only.

6.3.2. Anatase Concentration Dependence

The initial concentration of anatase nanoparticles were 2×10^4 , 6×10^4 , and 1×10^5 corresponding to mass concentrations of 1, 4, and 8 $\mu\text{g/L}$. Similar trends were observed for anatase nanoparticles as in P25 nanoparticles except that the lowest

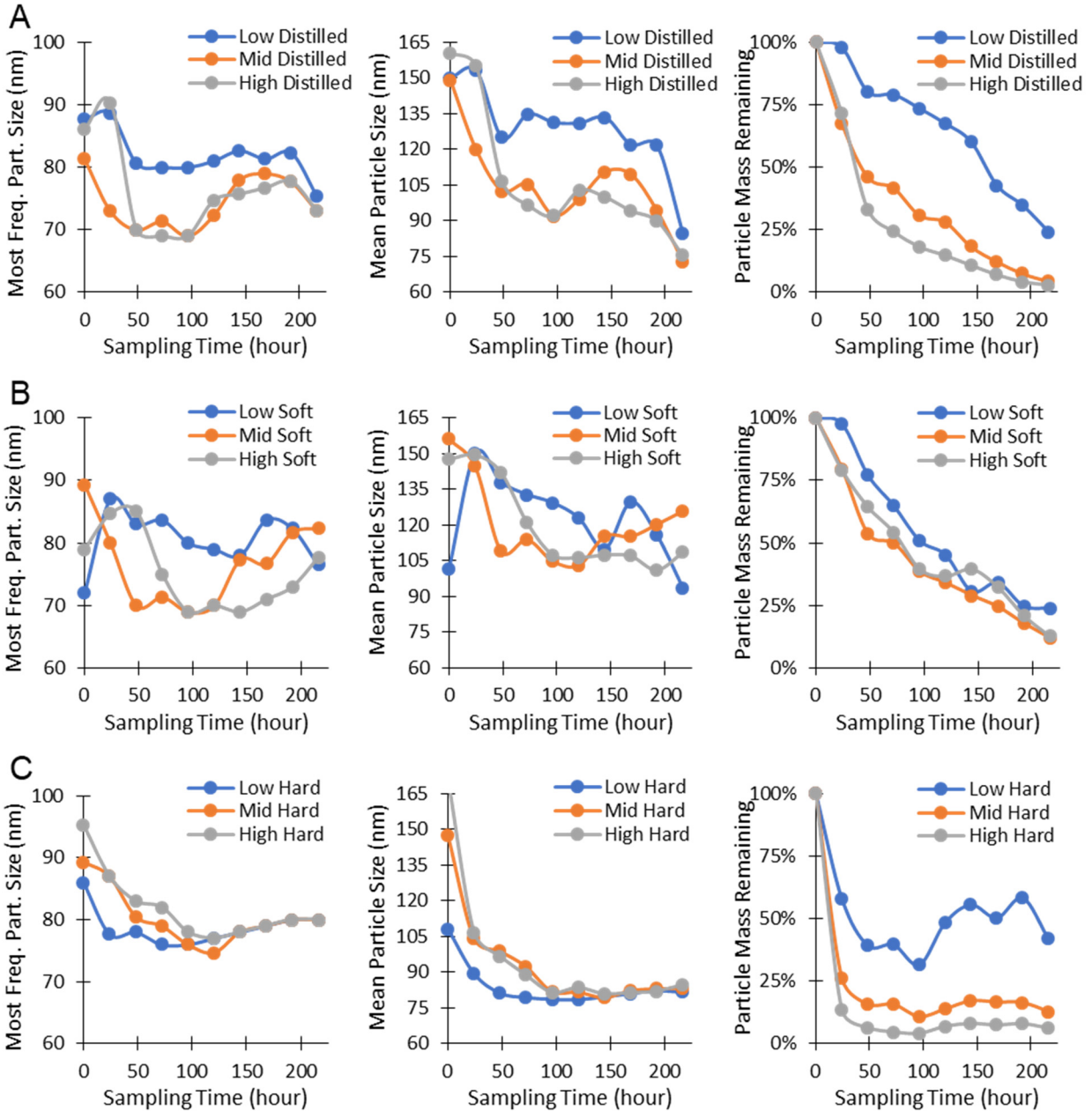


Figure 6.3. Most frequent particle size, mean particle size, and particle mass remaining in dispersion for anatase nanoparticles in distilled water (A), soft water (B), and hard water (C). For anatase NPs, low refers to a concentration of 1 ppb, mid refers to 5 ppb, and high refers to 8 ppb.

concentration in each water formulation did not follow the general trend of the next highest concentrations except in soft water. For distilled water, the lowest concentration had higher most frequent particle size, mean particle size, and particle mass remaining over time. For hard water, the lowest mass concentration followed the same trends as the mid and high concentrations in most frequent particle size and mean particle size but not in the particle mass remaining. 42% of the starting mass concentration remained suspended in hard water for the lowest concentration at the conclusion of the study as opposed to 12% for the middle concentration and 6% for the highest concentration.

In comparing the highest concentration, 8 ppb, in each water formulation, a similar trend is seen to that of P25 as shown in Figure 6.4. The particle mass remaining dropped quickly for each suspension, but soft water had a more gradual decline. By the end of the study, however, only 12% of the beginning mass concentration of particles was remaining for soft water, as compared to 6% and 3% for suspensions in hard and distilled water, respectively. Mean particle size also remained higher on average for suspensions in soft water and this is likely due to more interactions between the particles as the remaining concentration of particles remaining elevated.

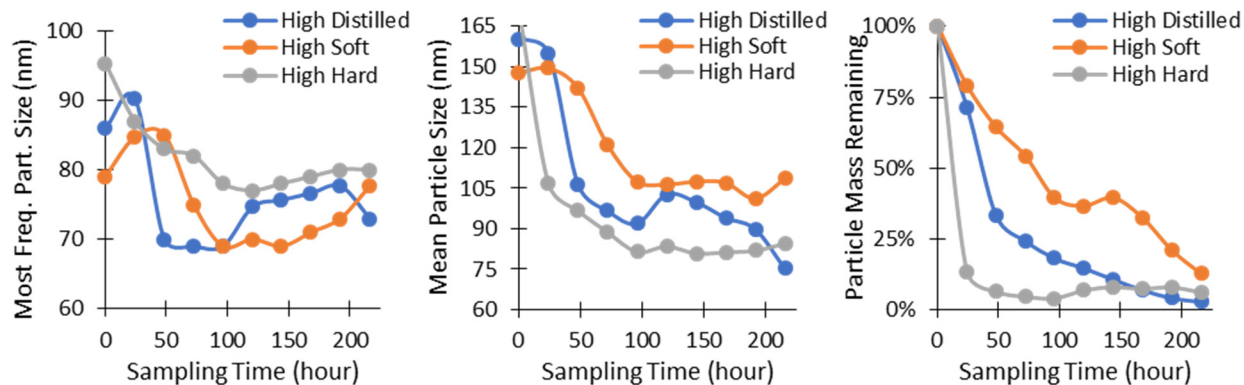


Figure 6.4. Comparison of most frequent particle size, mean particle size, and particle mass remaining in dispersion for anatase nanoparticles in distilled, soft, and hard water at a concentration of 8 ppb only.

6.3.3. Rutile Concentration Dependence

The initial concentration of rutile nanoparticles for the studied suspensions were 7×10^3 , 1×10^4 , and 2×10^4 corresponding to mass concentrations of 0.5, 2, and 4 $\mu\text{g/L}$. Rutile nanoparticle trends in most frequent size, mean size, and particle mass

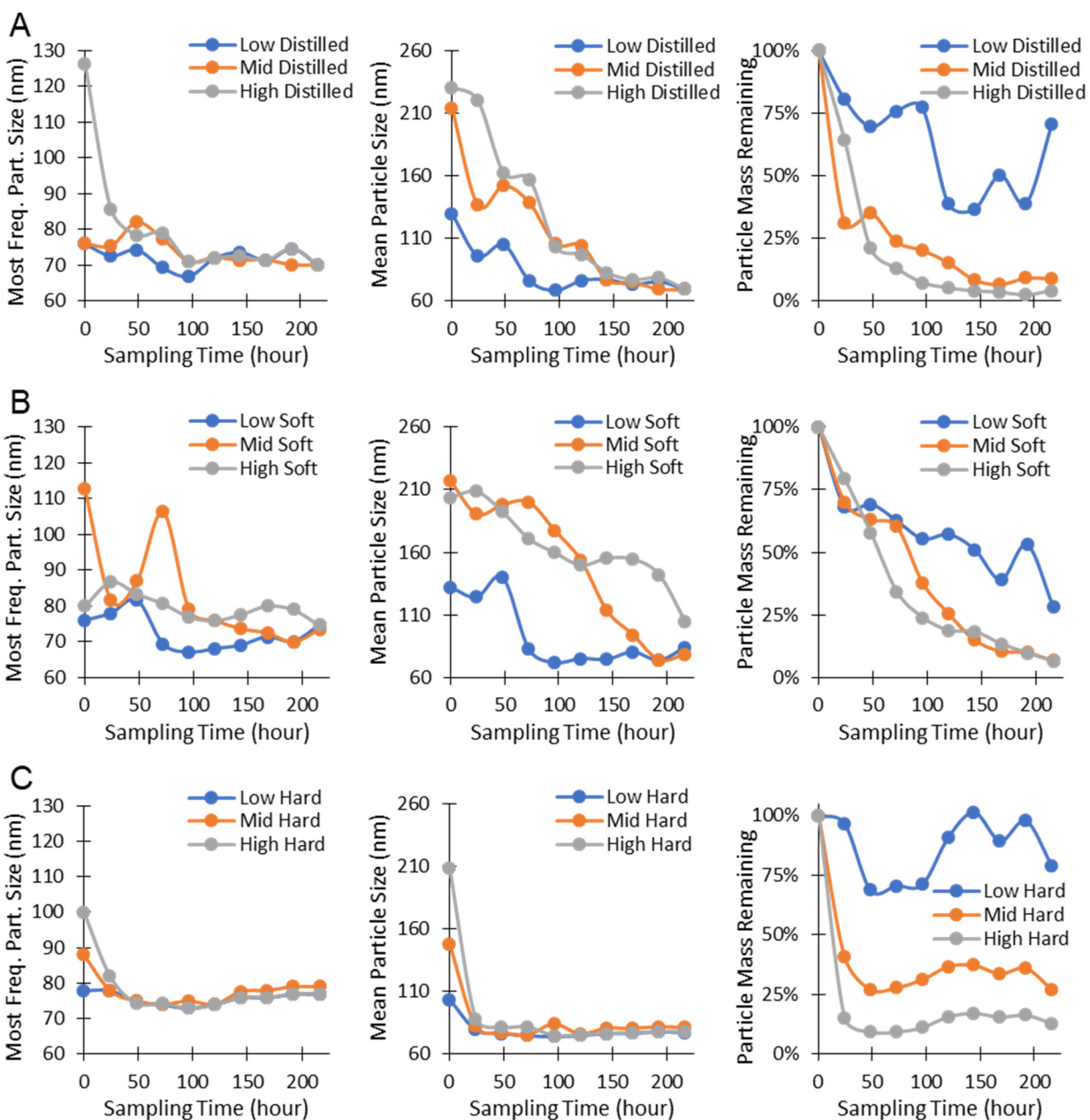


Figure 6.5. Most frequent particle size, mean particle size, and particle mass remaining in dispersion for rutile nanoparticles in distilled water (A), soft water (B), and hard water (C). For rutile NPs, low refers to a concentration of 0.5 ppb, mid refers to 2 ppb, and high refers to 4 ppb.

remaining suspended better matched the trends observed for anatase particles than for P25. However, the lowest concentration in each water formulation continually showed higher fractions of particles remaining suspended than the other particles. For hard water, the percentage of particles in suspension had a minimum value of 68% and was at 79% at the conclusion of the study. In distilled and soft water, the mean particle sizes for the lowest concentrations were consistently lower than the higher concentrations which indicates lower agglomeration and may explain the higher percentage of particles remaining suspended.

In comparing the highest concentration, 4 ppb, for each water formulation, particles suspended in soft water had a higher mean particle size but also had a higher percentage of particles remaining suspended. As seen in other particle/water combinations as the percentage of particles remaining suspended decreased, mean particle size likewise decreased. This is likely due to less particle interactions as particle concentration decreased. The comparison between water matrices using the highest concentration of rutile nanoparticles is shown in Figure 6.6.

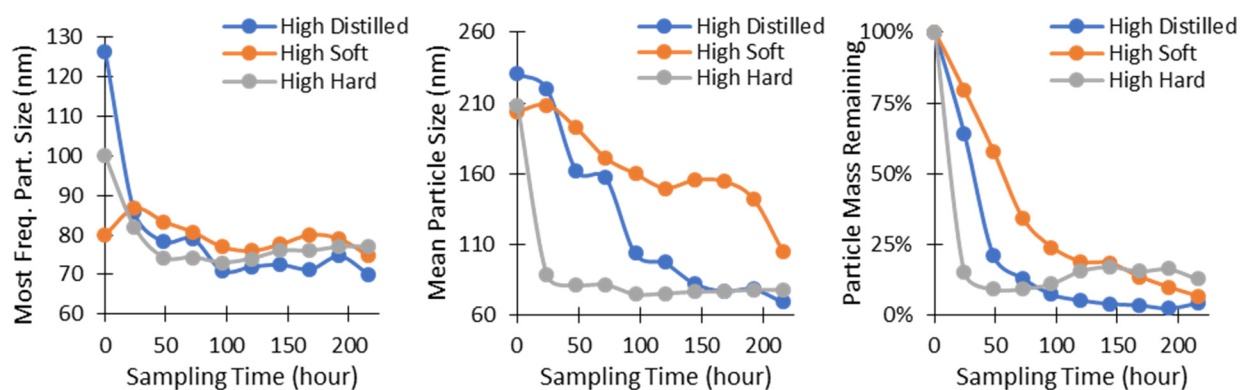


Figure 6.6. Comparison of most frequent particle size, mean particle size, and particle mass remaining in dispersion for rutile nanoparticles in distilled, soft, and hard water at a concentration of 4 ppb only.

6.3.4. Particle Loss via Dissolution, Aggregation, and Adherence to Tube Walls

It is evident from the data presented thus far that particles were lost from

suspension through either dissolution, agglomeration and consequent sedimentation, or adherence to the walls of the polypropylene tubes. Throughout the study, the concentration of dissolved titanium ions was measured continuously by the spICP-MS instrument and no detectable increase was observed throughout the study. This

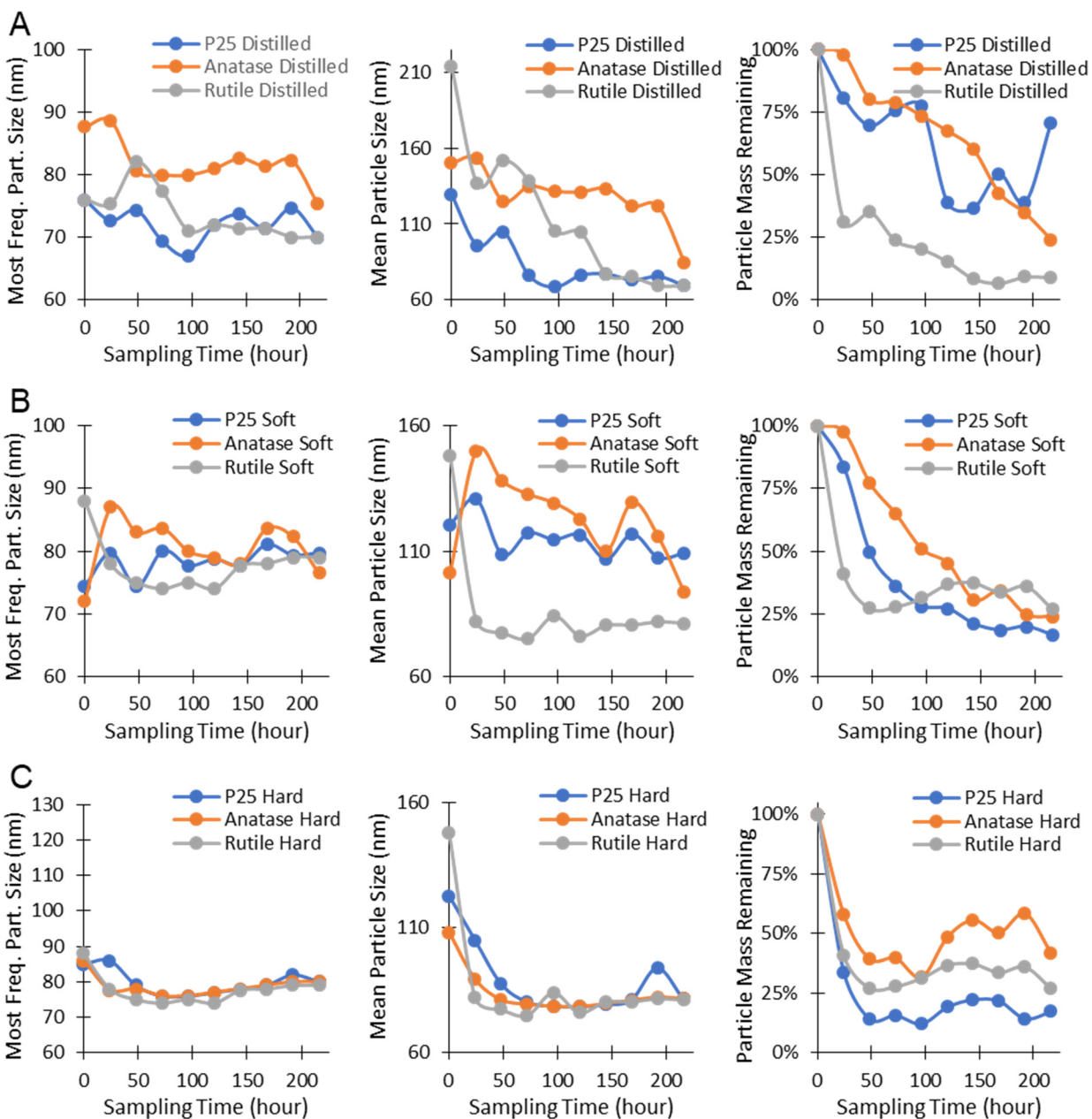


Figure 6.7. Comparison of most frequent particle size, mean particle size, and particle mass remaining in dispersion for P25, anatase, and rutile nanoparticles in distilled water (A), soft water (B), and hard water (C). Particle concentration (particles/mL) was 5×10^4 for P25, 2×10^4 for anatase, and 1×10^4 for rutile.

indicates that TiO₂ nanoparticles are very stable in suspension when referring to dissolution. However, the particles are not remaining suspended. It would stand to reason that increased ionic strength of the suspension solution may cause irreversible aggregation but even suspensions in distilled water had particle loss over time. It is for this reason that adherence to tube walls may cause particle loss over time. However, greater particle loss was observed as ionic strength increased as shown in Figure 6.7. when comparing the three particles for each water formulation. One possible mechanism for particle loss may be coprecipitation without inorganic salts that are precipitating from solution over time. Coprecipitation is a common method for preconcentration of nanoparticles before analysis or to separate particulate forms of an element from dissolved forms.²³³ It is likely that some nanoparticles inadvertently coprecipitated with inorganic salts and did not resuspend on the shaker. Sonication may have been successful in resuspending and recovering nanoparticles from tube walls or sediments, but that procedure was not explored in this study.

6.4. Conclusion and Future Studies

This study examined the influence of dissolved inorganics on three types of nanoparticles in polypropylene test tubes, however, the influence of dissolved organics on particle size and number concentration was not examined. Furthermore, for aging studies such as these, it may be wise to use glass beakers instead of plastic containers as the loss of nanoparticles may not be as great. It is difficult to model nanoparticles in real world waters when the container itself affects the suspension. Other issues with this study include the failure to measure transport efficiency in the additional water matrices, soft and hard water. Other studies have shown effects on the transport

efficiency due to the viscosity of the dispersion medium.²¹⁹ Lastly, the effect of sonication was not evaluated in this study but bath or probe sonication may prove beneficial for recovering adhered particles.

Chapter 7 : Conclusion

In this dissertation, titanium dioxide nanoparticles were modified with a wide assortment of organic ligands as chelators to improve the surface charge, hydrodynamic diameter, and dispersion characteristics. Dimercaptosuccinic acid, mercaptosuccinic acid, and citric acid had the best effect on not only increasing the ζ -potential of the measured nanoparticle dispersions but also decreasing their agglomeration and sedimentation. These findings may be useful in developing paints and coatings with dispersed titanium dioxide nanoparticles or to improve or retain nanoparticle properties for photocatalytic or other chemical processes such as in water treatment.

As the use of nanoparticles increases across all industries, their inadvertent release may also increase. In water treatment devices, nano-enabled processes are being investigated to increase efficiency and selectivity. It is vital to ensure that no nanoparticles are lost from these devices into produced water. Loss prevention is not only important for device sustainability but also for the safety of consumers. It is for this reason that a TiO₂ detection assay was developed using terephthalic acid as a hydroxyl radical scavenger and fluorescent probe. Using this assay, P25 nanoparticles can be detected at concentrations lower than 10 $\mu\text{g/L}$ using a portable and relatively inexpensive method. To date, this method has only been applied to simulate drinking water formulations but could be adapted to environmental water samples for preliminary testing in future studies.

Finally, the aging, transformation, and particle loss due to aggregation, sedimentation, or container adherence was explored using single particle inductively coupled mass spectrometry. Using three types of nanoparticles, the loss of particles from

suspension over 200 hours was measured as well as mean and most frequent particle sizes. This study showed that TiO₂ nanoparticles do not dissolve in suspension over this time period but rather agglomerate and are lost from suspension via two primary mechanisms, sedimentation or co-precipitation with inorganic salts, or adherence to container walls. This study may help researchers understand how particles transform over time, are removed from suspension, or adhered to the inner walls of pipes, plumbing, or water storage containers. Suffice it to say that nanoparticles are not physically or chemically inert but can change over time according to their environment.

References

- (1) Hochella, M. F.; Mogk, D. W.; Ranville, J.; Allen, I. C.; Luther, G. W.; Marr, L. C.; McGrail, B. P.; Murayama, M.; Qafoku, N. P.; Rosso, K. M. Natural, Incidental, and Engineered Nanomaterials and Their Impacts on the Earth System. *Science* **2019**, *363* (6434), eaau8299.
- (2) E56 Committee. *Terminology Relating to Nanotechnology*; ASTM International. <https://doi.org/10.1520/E2456-06R12>.
- (3) Jabbari, V.; Veleta, J. M.; Zarei-Chaleshtori, M.; Gardea-Torresdey, J.; Villagrán, D. Green Synthesis of Magnetic MOF@GO and MOF@CNT Hybrid Nanocomposites with High Adsorption Capacity towards Organic Pollutants. *Chem. Eng. J.* **2016**, *304*, 774–783. <https://doi.org/10.1016/j.cej.2016.06.034>.
- (4) Akter, T.; Saupe, G. B. Exceptional Sensitizer Dye Loading via a New Porous Titanium–Niobium Metal Oxide with Tris(2,2'-Bipyridyl)Ruthenium(II) in the Structure. *ACS Appl. Nano Mater.* **2018**, *1* (10), 5620–5630. <https://doi.org/10.1021/acsanm.8b01242>.
- (5) Lu, A.; Salabas, E. emsp14L; Schüth, F. Magnetic Nanoparticles: Synthesis, Protection, Functionalization, and Application. *Angew. Chem. Int. Ed.* **2007**, *46* (8), 1222–1244.
- (6) Barmparis, G. D.; Lodziana, Z.; Lopez, N.; Remediakis, I. N. Nanoparticle Shapes by Using Wulff Constructions and First-Principles Calculations. *Beilstein J. Nanotechnol.* **2015**, *6* (1), 361–368.
- (7) Gilbertson, L. M.; Albalghiti, E. M.; Fishman, Z. S.; Perreault, F.; Corredor, C.; Posner, J. D.; Elimelech, M.; Pfefferle, L. D.; Zimmerman, J. B. Shape-Dependent Surface Reactivity and Antimicrobial Activity of Nano-Cupric Oxide. *Environ. Sci. Technol.* **2016**, *50* (7), 3975–3984.
- (8) Luk'yanchuk, B.; Zheludev, N. I.; Maier, S. A.; Halas, N. J.; Nordlander, P.; Giessen, H.; Chong, C. T. The Fano Resonance in Plasmonic Nanostructures and Metamaterials. *Nat. Mater.* **2010**, *9* (9), 707.
- (9) Fan, J. A.; Wu, C.; Bao, K.; Bao, J.; Bardhan, R.; Halas, N. J.; Manoharan, V. N.; Nordlander, P.; Shvets, G.; Capasso, F. Self-Assembled Plasmonic Nanoparticle Clusters. *science* **2010**, *328* (5982), 1135–1138.
- (10) Alvarez, P. J. J.; Chan, C. K.; Elimelech, M.; Halas, N. J.; Villagrán, D. Emerging Opportunities for Nanotechnology to Enhance Water Security. *Nat. Nanotechnol.* **2018**, *13* (8), 634. <https://doi.org/10.1038/s41565-018-0203-2>.
- (11) Lu, H. M.; Jiang, Q. Size-Dependent Surface Energies of Nanocrystals. *J. Phys. Chem. B* **2004**, *108* (18), 5617–5619. <https://doi.org/10.1021/jp0366264>.

- (12) Zhang, X.; Li, W.; Kou, H.; Shao, J.; Deng, Y.; Zhang, X.; Ma, J.; Li, Y.; Zhang, X. Temperature and Size Dependent Surface Energy of Metallic Nano-Materials. *J. Appl. Phys.* **2019**, *125* (18), 185105. <https://doi.org/10.1063/1.5090301>.
- (13) Llansola-Portoles, M. J.; Bergkamp, J. J.; Finkelstein-Shapiro, D.; Sherman, B. D.; Kodis, G.; Dimitrijevic, N. M.; Gust, D.; Moore, T. A.; Moore, A. L. Controlling Surface Defects and Photophysics in TiO₂ Nanoparticles. *J. Phys. Chem. A* **2014**, *118* (45), 10631–10638. <https://doi.org/10.1021/jp506284q>.
- (14) Jiang, W.; Mashayekhi, H.; Xing, B. Bacterial Toxicity Comparison between Nano- and Micro-Scaled Oxide Particles. *Environ. Pollut.* **2009**, *157* (5), 1619–1625. <https://doi.org/10.1016/j.envpol.2008.12.025>.
- (15) Guozhong, C. *Nanostructures And Nanomaterials: Synthesis, Properties And Applications*; World Scientific, 2004.
- (16) Schwirn, K.; Tietjen, L.; Beer, I. Why Are Nanomaterials Different and How Can They Be Appropriately Regulated under REACH? *Environ. Sci. Eur.* **2014**, *26* (1), 4. <https://doi.org/10.1186/2190-4715-26-4>.
- (17) Taylor, A. B.; Siddiquee, A. M.; Chon, J. W. M. Below Melting Point Photothermal Reshaping of Single Gold Nanorods Driven by Surface Diffusion. *ACS Nano* **2014**, *8* (12), 12071–12079. <https://doi.org/10.1021/nn5055283>.
- (18) Couchman, P. R.; Jesser, W. A. Thermodynamic Theory of Size Dependence of Melting Temperature in Metals. *Nature* **1977**, *269* (5628), 481. <https://doi.org/10.1038/269481a0>.
- (19) Dai, H.; Zhao, J.; Huang, T.; Yu, X.; Sun, J.; Fang, H.; Zhu, Z.; Zhang, M.; Yu, K. Plasmonic Conglobation of Ultrathin Ag Nanofilms Far below Their Melting Points by Infrared Illumination. *Appl. Sci.* **2018**, *8* (6), 897. <https://doi.org/10.3390/app8060897>.
- (20) Crosby, A. J.; Lee, J.-Y. Polymer Nanocomposites: The “Nano” Effect on Mechanical Properties. *Polym. Rev.* **2007**, *47* (2), 217–229. <https://doi.org/10.1080/15583720701271278>.
- (21) Haque, M. A.; Saif, M. T. A. Thermo-Mechanical Properties of Nano-Scale Freestanding Aluminum Films. *Thin Solid Films* **2005**, *484* (1), 364–368. <https://doi.org/10.1016/j.tsf.2005.02.036>.
- (22) Quinten, M. Optical Properties of Nanoparticle Systems : Mie and Beyond <https://cds.cern.ch/record/1412315> (accessed Jun 20, 2019).
- (23) Kelly, K. L.; Coronado, E.; Zhao, L. L.; Schatz, G. C. The Optical Properties of Metal Nanoparticles: The Influence of Size, Shape, and Dielectric Environment. *J. Phys. Chem. B* **2003**, *107* (3), 668–677. <https://doi.org/10.1021/jp026731y>.
- (24) Titus, D.; James Jebaseelan Samuel, E.; Roopan, S. M. Chapter 12 - Nanoparticle Characterization Techniques. In *Green Synthesis, Characterization and Applications of Nanoparticles*; Shukla, A. K., Iravani, S., Eds.; Micro and

- Nano Technologies; Elsevier, 2019; pp 303–319. <https://doi.org/10.1016/B978-0-08-102579-6.00012-5>.
- (25) Talapin, D. V.; Shevchenko, E. V. Introduction: Nanoparticle Chemistry. *Chem. Rev.* **2016**, *116* (18), 10343–10345. <https://doi.org/10.1021/acs.chemrev.6b00566>.
- (26) Keller, A. A.; McFerran, S.; Lazareva, A.; Suh, S. Global Life Cycle Releases of Engineered Nanomaterials. *J. Nanoparticle Res.* **2013**, *15* (6), 1692. <https://doi.org/10.1007/s11051-013-1692-4>.
- (27) Giese, B.; Klaessig, F.; Park, B.; Kaegi, R.; Steinfeldt, M.; Wigger, H.; Gleich, A. von; Gottschalk, F. Risks, Release and Concentrations of Engineered Nanomaterial in the Environment. *Sci. Rep.* **2018**, *8* (1), 1–18. <https://doi.org/10.1038/s41598-018-19275-4>.
- (28) Inshakova, E.; Inshakov, O. World Market for Nanomaterials: Structure and Trends. *MATEC Web Conf.* **2017**, *129*, 02013. <https://doi.org/10.1051/mateconf/201712902013>.
- (29) Westerhoff, P.; Alvarez, P.; Li, Q.; Gardea-Torresdey, J.; Zimmerman, J. Overcoming Implementation Barriers for Nanotechnology in Drinking Water Treatment. *Environ. Sci. Nano* **2016**, *3* (6), 1241–1253.
- (30) Zhang, Y.; Wu, B.; Xu, H.; Liu, H.; Wang, M.; He, Y.; Pan, B. Nanomaterials-Enabled Water and Wastewater Treatment. *NanoImpact* **2016**, *3–4*, 22–39. <https://doi.org/10.1016/j.impact.2016.09.004>.
- (31) Brame, J.; Li, Q.; Alvarez, P. J. J. Nanotechnology-Enabled Water Treatment and Reuse: Emerging Opportunities and Challenges for Developing Countries. *Trends Food Sci. Technol.* **2011**, *22* (11), 618–624. <https://doi.org/10.1016/j.tifs.2011.01.004>.
- (32) Chou, C.-S.; Guo, M.-G.; Liu, K.-H.; Chen, Y.-S. Preparation of TiO₂ Particles and Their Applications in the Light Scattering Layer of a Dye-Sensitized Solar Cell. *Appl. Energy* **2012**, *92*, 224–233.
- (33) Dimitrijevic, N. M.; Rozhkova, E.; Rajh, T. Dynamics of Localized Charges in Dopamine-Modified TiO₂ and Their Effect on the Formation of Reactive Oxygen Species. *J. Am. Chem. Soc.* **2009**, *131* (8), 2893–2899.
- (34) Bar-Ilan, O.; Louis, K. M.; Yang, S. P.; Pedersen, J. A.; Hamers, R. J.; Peterson, R. E.; Heideman, W. Titanium Dioxide Nanoparticles Produce Phototoxicity in the Developing Zebrafish. *Nanotoxicology* **2012**, *6* (6), 670–679.
- (35) Weir, A.; Westerhoff, P.; Fabricius, L.; Hristovski, K.; Von Goetz, N. Titanium Dioxide Nanoparticles in Food and Personal Care Products. *Environ. Sci. Technol.* **2012**, *46* (4), 2242–2250.
- (36) Nakata, K.; Fujishima, A. TiO₂ Photocatalysis: Design and Applications. *J. Photochem. Photobiol. C Photochem. Rev.* **2012**, *13* (3), 169–189.

- (37) Westerhoff, P.; Song, G.; Hristovski, K.; Kiser, M. A. Occurrence and Removal of Titanium at Full Scale Wastewater Treatment Plants: Implications for TiO₂ Nanomaterials. *J. Environ. Monit.* **2011**, *13* (5), 1195–1203.
- (38) von Goetz, N.; Lorenz, C.; Windler, L.; Nowack, B.; Heuberger, M.; Hungerbuhler, K. Migration of Ag-and TiO₂-(Nano) Particles from Textiles into Artificial Sweat under Physical Stress: Experiments and Exposure Modeling. *Environ. Sci. Technol.* **2013**, *47* (17), 9979–9987.
- (39) Shandilya, N.; Le Bihan, O.; Bressot, C.; Morgenev, M. Emission of Titanium Dioxide Nanoparticles from Building Materials to the Environment by Wear and Weather. *Environ. Sci. Technol.* **2015**, *49* (4), 2163–2170.
- (40) Lowry, G. V.; Gregory, K. B.; Apte, S. C.; Lead, J. R. Transformations of Nanomaterials in the Environment. **2012**.
- (41) Lazar, M. A.; Varghese, S.; Nair, S. S. Photocatalytic Water Treatment by Titanium Dioxide: Recent Updates. *Catalysts* **2012**, *2* (4), 572–601. <https://doi.org/10.3390/catal2040572>.
- (42) Doudrick, K.; Monzón, O.; Mangonon, A.; Hristovski, K.; Westerhoff, P. Nitrate Reduction in Water Using Commercial Titanium Dioxide Photocatalysts (P25, P90, and Hombikat UV100). *J. Environ. Eng.* **2011**, *138* (8), 852–861.
- (43) Tugaoen, H. O.; Garcia-Segura, S.; Hristovski, K.; Westerhoff, P. Challenges in Photocatalytic Reduction of Nitrate as a Water Treatment Technology. *Sci. Total Environ.* **2017**, *599*, 1524–1551.
- (44) Shukla, R. K.; Sharma, V.; Pandey, A. K.; Singh, S.; Sultana, S.; Dhawan, A. ROS-Mediated Genotoxicity Induced by Titanium Dioxide Nanoparticles in Human Epidermal Cells. *Toxicol. In Vitro* **2011**, *25* (1), 231–241. <https://doi.org/10.1016/j.tiv.2010.11.008>.
- (45) Shape-engineered titanium dioxide nanoparticles (TiO₂-NPs)_ cytotoxicity and genotoxicity in bronchial epithelial cells | Elsevier Enhanced Reader <https://reader.elsevier.com/reader/sd/pii/S0278691519301036?token=821BA94276D1122EBF81969FBC28B5A6003C502E4D0D8C645A8D7291148AA62732822D7A927AF86370DC964F2996D569> (accessed Jun 12, 2019). <https://doi.org/10.1016/j.fct.2019.02.043>.
- (46) Shi, H.; Magaye, R.; Castranova, V.; Zhao, J. Titanium Dioxide Nanoparticles: A Review of Current Toxicological Data. *Part. Fibre Toxicol.* **2013**, *10* (1), 15. <https://doi.org/10.1186/1743-8977-10-15>.
- (47) Cao, Y.; Li, X.; Bian, Z.; Fuhr, A.; Zhang, D.; Zhu, J. Highly Photocatalytic Activity of Brookite/Rutile TiO₂ Nanocrystals with Semi-Embedded Structure. *Appl. Catal. B Environ.* **2016**, *180*, 551–558. <https://doi.org/10.1016/j.apcatb.2015.07.003>.
- (48) Ohno, T.; Sarukawa, K.; Tokieda, K.; Matsumura, M. Morphology of a TiO₂ Photocatalyst (Degussa, P-25) Consisting of Anatase and Rutile Crystalline Phases. *J. Catal.* **2001**, *203* (1), 82–86. <https://doi.org/10.1006/jcat.2001.3316>.

- (49) Westerhoff, P.; Atkinson, A.; Fortner, J.; Wong, M. S.; Zimmerman, J.; Gardea-Torresdey, J.; Ranville, J.; Herckes, P. Low Risk Posed by Engineered and Incidental Nanoparticles in Drinking Water. *Nat. Nanotechnol.* **2018**, *13* (8), 661. <https://doi.org/10.1038/s41565-018-0217-9>.
- (50) Lee, S.-Y.; Park, S.-J. TiO₂ Photocatalyst for Water Treatment Applications. *J. Ind. Eng. Chem.* **2013**, *19* (6), 1761–1769. <https://doi.org/10.1016/j.jiec.2013.07.012>.
- (51) Kaplan, R.; Erjavec, B.; Dražić, G.; Grdadolnik, J.; Pintar, A. Simple Synthesis of Anatase/Rutile/Brookite TiO₂ Nanocomposite with Superior Mineralization Potential for Photocatalytic Degradation of Water Pollutants. *Appl. Catal. B Environ.* **2016**, *181*, 465–474. <https://doi.org/10.1016/j.apcatb.2015.08.027>.
- (52) Zhao, W.; Ma, W.; Chen, C.; Zhao, J.; Shuai, Z. Efficient Degradation of Toxic Organic Pollutants with Ni₂O₃/TiO₂-XB_x under Visible Irradiation. *J. Am. Chem. Soc.* **2004**, *126* (15), 4782–4783. <https://doi.org/10.1021/ja0396753>.
- (53) Alonso-Tellez, A.; Masson, R.; Robert, D.; Keller, N.; Keller, V. Comparison of Hombikat UV100 and P25 TiO₂ Performance in Gas-Phase Photocatalytic Oxidation Reactions. *J. Photochem. Photobiol. Chem.* **2012**, *250*, 58–65. <https://doi.org/10.1016/j.jphotochem.2012.10.008>.
- (54) Wu, T.; Liu, G.; Zhao, J.; Hidaka, H.; Serpone, N. Photoassisted Degradation of Dye Pollutants. V. Self-Photosensitized Oxidative Transformation of Rhodamine B under Visible Light Irradiation in Aqueous TiO₂ Dispersions. *J. Phys. Chem. B* **1998**, *102* (30), 5845–5851. <https://doi.org/10.1021/jp980922c>.
- (55) Ani, I. J.; Akpan, U. G.; Olutoye, M. A.; Hameed, B. H. Photocatalytic Degradation of Pollutants in Petroleum Refinery Wastewater by TiO₂- and ZnO-Based Photocatalysts: Recent Development. *J. Clean. Prod.* **2018**, *205*, 930–954. <https://doi.org/10.1016/j.jclepro.2018.08.189>.
- (56) Cunningham, J.; Al-Sayyed, G.; Srijaranai, S.; Al-Sayyed, G.; Srijaranai, S. Adsorption of Model Pollutants onto TiO₂ Particles in Relation to Photoremediation of Contaminated Water <https://www.taylorfrancis.com/> (accessed Jun 20, 2019). <https://doi.org/10.1201/9781351069847-24>.
- (57) Tucci, F. G. and P. Titanium Dioxide Nanoparticles: a Risk for Human Health? <http://www.eurekaselect.com/140530/article> (accessed Jun 20, 2019).
- (58) Cox, A.; Venkatachalam, P.; Sahi, S.; Sharma, N. Silver and Titanium Dioxide Nanoparticle Toxicity in Plants: A Review of Current Research. *Plant Physiol. Biochem.* **2016**, *107*, 147–163. <https://doi.org/10.1016/j.plaphy.2016.05.022>.
- (59) Coppens, P.; Planchenstainer, F. The Labelling of Nanomaterials under EU Law, with a Particular Focus on France. *Eur. Food Feed Law Rev.* **2019**, *14* (2), 152–159.
- (60) EFSA Statement on the Review of the Risks Related to the Exposure to the Food Additive Titanium Dioxide (E 171) Performed by the French Agency for Food,

- Environmental and Occupational Health and Safety (ANSES). *EFSA J.* **2019**, *17* (6), e05714. <https://doi.org/10.2903/j.efsa.2019.5714>.
- (61) Seo, J.; Chung, H.; Kim, M.; Lee, J.; Choi, I.; Cheon, J. Development of Water-Soluble Single-Crystalline TiO₂ Nanoparticles for Photocatalytic Cancer-Cell Treatment. *Small* **2007**, *3* (5), 850–853.
- (62) Thurn, K. T.; Paunesku, T.; Wu, A.; Brown, E. M. B.; Lai, B.; Vogt, S.; Maser, J.; Aslam, M.; Dravid, V.; Bergan, R.; Woloschak, G. E. Labeling TiO₂ Nanoparticles with Dyes for Optical Fluorescence Microscopy and Determination of TiO₂–DNA Nanoconjugate Stability. *Small* **2009**, *5* (11), 1318–1325. <https://doi.org/10.1002/smll.200801458>.
- (63) Blatnik, J.; Luebke, L.; Simonet, S.; Nelson, M.; Price, R.; Leek, R.; Zeng, L.; Wu, A.; Brown, E. Dye Surface Coating Enables Visible Light Activation of TiO₂ Nanoparticles Leading to Degradation of Neighboring Biological Structures. *Microsc. Microanal.* **2012**, *18* (1), 134–142. <https://doi.org/10.1017/S1431927611012414>.
- (64) Kurepa, J.; Paunesku, T.; Vogt, S.; Arora, H.; Rabatic, B. M.; Lu, J.; Wanzer, M. B.; Woloschak, G. E.; Smalle, J. A. Uptake and Distribution of Ultrasmall Anatase TiO₂ Alizarin Red S Nanoconjugates in Arabidopsis Thaliana. *Nano Lett.* **2010**, *10* (7), 2296–2302. <https://doi.org/10.1021/nl903518f>.
- (65) Domingos, R. F.; Tufenkji, N.; Wilkinson, K. J. Aggregation of Titanium Dioxide Nanoparticles: Role of a Fulvic Acid. *Environ. Sci. Technol.* **2009**, *43* (5), 1282–1286. <https://doi.org/10.1021/es8023594>.
- (66) Řehoř, I.; Vilímová, V.; Jendelová, P.; Kubíček, V.; Jiráček, D.; Herynek, V.; Kapcalová, M.; Kotek, J.; Černý, J.; Hermann, P.; Lukeš, I. Phosphonate–Titanium Dioxide Assemblies: Platform for Multimodal Diagnostic–Therapeutic Nanoprobes. *J. Med. Chem.* **2011**, *54* (14), 5185–5194. <https://doi.org/10.1021/jm200449y>.
- (67) Kamps, K.; Leek, R.; Luebke, L.; Price, R.; Nelson, M.; Simonet, S.; Eggert, D. J.; Ateşin, T. A.; Brown, E. M. B. Surface Modification of the TiO₂nanoparticle Surface Enables Fluorescence Monitoring of Aggregation and Enhanced Photoreactivity. *Integr. Biol.* **2013**, *5* (1), 133–143. <https://doi.org/10.1039/c2ib20166f>.
- (68) Keller, A. A.; Lazareva, A. Predicted Releases of Engineered Nanomaterials: From Global to Regional to Local. *Environ. Sci. Technol. Lett.* **2014**, *1* (1), 65–70. <https://doi.org/10.1021/ez400106t>.
- (69) Hristozov, D.; Malsch, I. Hazards and Risks of Engineered Nanoparticles for the Environment and Human Health. *Sustainability* **2009**, *1* (4), 1161–1194. <https://doi.org/10.3390/su1041161>.
- (70) Warheit, D. B. Hazard and Risk Assessment Strategies for Nanoparticle Exposures: How Far Have We Come in the Past 10 Years? *F1000Research* **2018**, *7*. <https://doi.org/10.12688/f1000research.12691.1>.

- (71) Tsang, M. P.; Hristozov, D.; Zabeo, A.; Koivisto, A. J.; Jensen, A. C. Ø.; Jensen, K. A.; Pang, C.; Marcomini, A.; Sonnemann, G. Probabilistic Risk Assessment of Emerging Materials: Case Study of Titanium Dioxide Nanoparticles. *Nanotoxicology* **2017**, *11* (4), 558–568. <https://doi.org/10.1080/17435390.2017.1329952>.
- (72) Shah, S. N. A.; Shah, Z.; Hussain, M.; Khan, M. Hazardous Effects of Titanium Dioxide Nanoparticles in Ecosystem <https://www.hindawi.com/journals/bca/2017/4101735/abs/> (accessed Jun 26, 2019). <https://doi.org/10.1155/2017/4101735>.
- (73) Contado, C. Nanomaterials in Consumer Products: A Challenging Analytical Problem. *Front. Chem.* **2015**, *3*. <https://doi.org/10.3389/fchem.2015.00048>.
- (74) Singh, G.; Stephan, C.; Westerhoff, P.; Carlander, D.; Duncan, T. V. Measurement Methods to Detect, Characterize, and Quantify Engineered Nanomaterials in Foods. *Compr. Rev. Food Sci. Food Saf.* **2014**, *13* (4), 693–704. <https://doi.org/10.1111/1541-4337.12078>.
- (75) Cascio, C.; Gilliland, D.; Rossi, F.; Calzolari, L.; Contado, C. Critical Experimental Evaluation of Key Methods to Detect, Size and Quantify Nanoparticulate Silver. *Anal. Chem.* **2014**, *86* (24), 12143–12151. <https://doi.org/10.1021/ac503307r>.
- (76) Corredor, C.; Borysiak, M. D.; Wolfer, J.; Westerhoff, P.; Posner, J. D. Colorimetric Detection of Catalytic Reactivity of Nanoparticles in Complex Matrices. *Environ. Sci. Technol.* **2015**, *49* (6), 3611–3618. <https://doi.org/10.1021/es504350j>.
- (77) Bi, Y.; Westerhoff, P. High-Throughput Analysis of Photocatalytic Reactivity of Differing TiO₂ Formulations Using 96-Well Microplate Reactors. *Chemosphere* **2019**, *223*, 275–284. <https://doi.org/10.1016/j.chemosphere.2019.02.016>.
- (78) Yoo, D.; Lee, J.-H.; Shin, T.-H.; Cheon, J. Theranostic Magnetic Nanoparticles. *Acc. Chem. Res.* **2011**, *44* (10), 863–874. <https://doi.org/10.1021/ar200085c>.
- (79) Tsai, W.-B.; Kao, J.-Y.; Wu, T.-M.; Cheng, W.-T. Dispersion of Titanium Oxide Nanoparticles in Aqueous Solution with Anionic Stabilizer via Ultrasonic Wave <https://www.hindawi.com/journals/jnp/2016/6539581/> (accessed Jan 31, 2020). <https://doi.org/10.1155/2016/6539581>.
- (80) Qin, Y.; Sun, L.; Li, X.; Cao, Q.; Wang, H.; Tang, X.; Ye, L. Highly Water-Dispersible TiO₂ Nanoparticles for Doxorubicin Delivery: Effect of Loading Mode on Therapeutic Efficacy. *J. Mater. Chem.* **2011**, *21* (44), 18003–18010.
- (81) Mohan, R.; Drbohlavova, J.; Hubalek, J. Water-Dispersible TiO₂ Nanoparticles via a Biphasic Solvothermal Reaction Method. *Nanoscale Res. Lett.* **2013**, *8* (1), 503.
- (82) Stephan, C.; Neubauer, K.; Shelton, C. Single Particle Inductively Coupled Plasma Mass Spectrometry: Understanding How and Why. *PerkinElmer White Pap.* **2014**.

- (83) Laborda, F.; Bolea, E.; Jiménez-Lamana, J. Single Particle Inductively Coupled Plasma Mass Spectrometry: A Powerful Tool for Nanoanalysis. *Anal. Chem.* **2014**, *86* (5), 2270–2278. <https://doi.org/10.1021/ac402980q>.
- (84) Chou, C.-S.; Guo, M.-G.; Liu, K.-H.; Chen, Y.-S. Preparation of TiO₂ Particles and Their Applications in the Light Scattering Layer of a Dye-Sensitized Solar Cell. *Appl. Energy* **2012**, *92*, 224–233.
- (85) Dimitrijevic, N. M.; Rozhkova, E.; Rajh, T. Dynamics of Localized Charges in Dopamine-Modified TiO₂ and Their Effect on the Formation of Reactive Oxygen Species. *J. Am. Chem. Soc.* **2009**, *131* (8), 2893–2899.
- (86) Bar-Ilan, O.; Louis, K. M.; Yang, S. P.; Pedersen, J. A.; Hamers, R. J.; Peterson, R. E.; Heideman, W. Titanium Dioxide Nanoparticles Produce Phototoxicity in the Developing Zebrafish. *Nanotoxicology* **2012**, *6* (6), 670–679.
- (87) Weir, A.; Westerhoff, P.; Fabricius, L.; Hristovski, K.; Von Goetz, N. Titanium Dioxide Nanoparticles in Food and Personal Care Products. *Environ. Sci. Technol.* **2012**, *46* (4), 2242–2250.
- (88) Nakata, K.; Fujishima, A. TiO₂ Photocatalysis: Design and Applications. *J. Photochem. Photobiol. C Photochem. Rev.* **2012**, *13* (3), 169–189.
- (89) Romanello, M. B.; de Cortalezzi, M. M. F. An Experimental Study on the Aggregation of TiO₂ Nanoparticles under Environmentally Relevant Conditions. *Water Res.* **2013**, *47* (12), 3887–3898.
- (90) Loosli, F.; Le Coustumer, P.; Stoll, S. TiO₂ Nanoparticles Aggregation and Disaggregation in Presence of Alginate and Suwannee River Humic Acids. pH and Concentration Effects on Nanoparticle Stability. *Water Res.* **2013**, *47* (16), 6052–6063.
- (91) Danielsson, K.; Gallego-Urrea, J. A.; Hasselov, M.; Gustafsson, S.; Jonsson, C. M. Influence of Organic Molecules on the Aggregation of TiO₂ Nanoparticles in Acidic Conditions. *J. Nanoparticle Res.* **2017**, *19* (4), 133.
- (92) Geng, Z.; Yang, X.; Boo, C.; Zhu, S.; Lu, Y.; Fan, W.; Huo, M.; Elimelech, M.; Yang, X. Self-Cleaning Anti-Fouling Hybrid Ultrafiltration Membranes via Side Chain Grafting of Poly (Aryl Ether Sulfone) and Titanium Dioxide. *J. Membr. Sci.* **2017**, *529*, 1–10.
- (93) Hamadani, M.; Karimzadeh, S.; Jabbari, V.; Villagrán, D. Synthesis of Cysteine, Cobalt and Copper-Doped TiO₂ Nanophotocatalysts with Excellent Visible-Light-Induced Photocatalytic Activity. *Mater. Sci. Semicond. Process.* **2016**, *41*, 168–176.
- (94) Yun, E.-T.; Yoo, H.-Y.; Kim, W.; Kim, H.-E.; Kang, G.; Lee, H.; Lee, S.; Park, T.; Lee, C.; Kim, J.-H. Visible-Light-Induced Activation of Periodate That Mimics Dye-Sensitization of TiO₂: Simultaneous Decolorization of Dyes and Production of Oxidizing Radicals. *Appl. Catal. B Environ.* **2017**, *203*, 475–484.

- (95) Vieira, G. B.; José, H. J.; Peterson, M.; Baldissarelli, V. Z.; Alvarez, P.; Moreira, R. D. F. P. M. CeO₂/TiO₂ Nanostructures Enhance Adsorption and Photocatalytic Degradation of Organic Compounds in Aqueous Suspension. *J. Photochem. Photobiol. Chem.* **2017**.
- (96) Jabbari, V.; Hamadani, M.; Karimzadeh, S.; Villagrán, D. Enhanced Charge Carrier Efficiency and Solar Light-Induced Photocatalytic Activity of TiO₂ Nanoparticles through Doping of Silver Nanoclusters and C–N–S Nonmetals. *J. Ind. Eng. Chem.* **2016**, *35*, 132–139.
- (97) Long, M.; Brame, J.; Qin, F.; Bao, J.; Li, Q.; Alvarez, P. J. J. Phosphate Changes Effect of Humic Acids on TiO₂ Photocatalysis: From Inhibition to Mitigation of Electron–Hole Recombination. *Environ. Sci. Technol.* **2017**, *51* (1), 514–521. <https://doi.org/10.1021/acs.est.6b04845>.
- (98) Marks, R.; Yang, T.; Westerhoff, P.; Doudrick, K. Comparative Analysis of the Photocatalytic Reduction of Drinking Water Oxoanions Using Titanium Dioxide. *Water Res.* **2016**, *104*, 11–19.
- (99) O’Neal Tugaoen, H.; Garcia-Segura, S.; Hristovski, K.; Westerhoff, P. Compact Light-Emitting Diode Optical Fiber Immobilized TiO₂ Reactor for Photocatalytic Water Treatment. *Sci. Total Environ.* **2018**, *613–614*, 1331–1338. <https://doi.org/10.1016/j.scitotenv.2017.09.242>.
- (100) Yang, Y.; Javed, H.; Zhang, D.; Li, D.; Kamath, R.; McVey, K.; Sra, K.; Alvarez, P. J. Merits and Limitations of TiO₂-Based Photocatalytic Pretreatment of Soils Impacted by Crude Oil for Expediting Bioremediation. *Front. Chem. Sci. Eng.* **2017**, *11* (3), 387–394.
- (101) Kibanova, D.; Cervini-Silva, J.; Destailats, H. Efficiency of Clay–TiO₂ Nanocomposites on the Photocatalytic Elimination of a Model Hydrophobic Air Pollutant. *Environ. Sci. Technol.* **2009**, *43* (5), 1500–1506.
- (102) Thio, B. J. R.; Zhou, D.; Keller, A. A. Influence of Natural Organic Matter on the Aggregation and Deposition of Titanium Dioxide Nanoparticles. *J. Hazard. Mater.* **2011**, *189* (1), 556–563.
- (103) French, R. A.; Jacobson, A. R.; Kim, B.; Isley, S. L.; Penn, R. L.; Baveye, P. C. Influence of Ionic Strength, PH, and Cation Valence on Aggregation Kinetics of Titanium Dioxide Nanoparticles. *Environ. Sci. Technol.* **2009**, *43* (5), 1354–1359.
- (104) Dunphy Guzman, K. A.; Finnegan, M. P.; Banfield, J. F. Influence of Surface Potential on Aggregation and Transport of Titania Nanoparticles. *Environ. Sci. Technol.* **2006**, *40* (24), 7688–7693.
- (105) SCHWARZ, S.; PETZOLD, G.; WIENHOLD, U. Stabilizing Titanium Dioxide. *Eur. Coat. J.* **2004**, No. 7–8, 34–36.
- (106) Kim, M.-S.; Louis, K.; Pedersen, J.; Hamers, R.; Peterson, R.; Heideman, W. Using Citrate-Functionalized TiO₂ Nanoparticles to Study the Effect of Particle Size on Zebrafish Embryo Toxicity. *Analyst* **2014**, *139* (5), 964–972.

- (107) Kotsokechagia, T.; Cellesi, F.; Thomas, A.; Niederberger, M.; Tirelli, N. Preparation of Ligand-Free TiO₂ (Anatase) Nanoparticles through a Nonaqueous Process and Their Surface Functionalization. *Langmuir* **2008**, *24* (13), 6988–6997.
- (108) Dimitrijevic, N. M.; Saponjic, Z. V.; Bartels, D. M.; Thurnauer, M. C.; Tiede, D. M.; Rajh, T. Revealing the Nature of Trapping Sites in Nanocrystalline Titanium Dioxide by Selective Surface Modification. *J. Phys. Chem. B* **2003**, *107* (30), 7368–7375.
- (109) Rajh, T.; Chen, L. X.; Lukas, K.; Liu, T.; Thurnauer, M. C.; Tiede, D. M. Surface Restructuring of Nanoparticles: An Efficient Route for Ligand–Metal Oxide Crosstalk. *J. Phys. Chem. B* **2002**, *106* (41), 10543–10552. <https://doi.org/10.1021/jp021235v>.
- (110) Moser, J.; PUNCHIHewa, S.; Infelta, P. P.; Graetzel, M. Surface Complexation of Colloidal Semiconductors Strongly Enhances Interfacial Electron-Transfer Rates. *Langmuir* **1991**, *7* (12), 3012–3018.
- (111) Seo, J.; Chung, H.; Kim, M.; Lee, J.; Choi, I.; Cheon, J. Development of Water-Soluble Single-Crystalline TiO₂ Nanoparticles for Photocatalytic Cancer-Cell Treatment. *Small* **2007**, *3* (5), 850–853.
- (112) Raza, M.; Bachinger, A.; Zahn, N.; KICKELBICK, G. Interaction and UV-Stability of Various Organic Capping Agents on the Surface of Anatase Nanoparticles. *Materials* **2014**, *7* (4), 2890–2912.
- (113) Lai, Y.-C.; Lai, C.-S.; Tai, J.-T.; Nguyen, T. P.; Wang, H.-L.; Lin, C.-Y.; Tsai, T.-Y.; Ho, H.-C.; Wang, P.-H.; Liao, Y.-C. Understanding Ligand–Nanoparticle Interactions for Silica, Ceria, and Titania Nanopowders. *Adv. Powder Technol.* **2015**, *26* (6), 1676–1686.
- (114) Fauconnier, N.; Pons, J.; Roger, J.; Bee, A. Thiolation of Maghemite Nanoparticles by Dimercaptosuccinic Acid. *J. Colloid Interface Sci.* **1997**, *194* (2), 427–433.
- (115) Maurizi, L.; Bisht, H.; Bouyer, F.; Millot, N. Easy Route to Functionalize Iron Oxide Nanoparticles via Long-Term Stable Thiol Groups. *Langmuir* **2009**, *25* (16), 8857–8859.
- (116) Sakai, N.; Ikeda, T.; Teranishi, T.; Tatsuma, T. Sensitization of TiO₂ with Pt, Pd, and Au Clusters Protected by Mercapto- and Dimercaptosuccinic Acid. *ChemPhysChem* **2011**, *12* (13), 2415–2418.
- (117) Valois, C. R.; Braz, J. M.; Nunes, E. S.; Vinolo, M. A.; Lima, E. C.; Curi, R.; Kuebler, W. M.; Azevedo, R. B. The Effect of DMSA-Functionalized Magnetic Nanoparticles on Transendothelial Migration of Monocytes in the Murine Lung via a β 2 Integrin-Dependent Pathway. *Biomaterials* **2010**, *31* (2), 366–374.
- (118) Watanabe, N.; Kaneko, T.; Uchimaru, Y.; Yanagida, S.; Yasumori, A.; Sugahara, Y. Preparation of Water-Dispersible TiO₂ Nanoparticles from Titanium

Tetrachloride Using Urea Hydrogen Peroxide as an Oxygen Donor. *CrystEngComm* **2013**, *15* (48), 10533–10540.

- (119) Jing, J.; Feng, J.; Li, W.; William, W. Y. Low-Temperature Synthesis of Water-Dispersible Anatase Titanium Dioxide Nanoparticles for Photocatalysis. *J. Colloid Interface Sci.* **2013**, *396*, 90–94.
- (120) Aposhian, H. V.; Aposhian, M. M. Meso-2, 3-Dimercaptosuccinic Acid: Chemical, Pharmacological and Toxicological Properties of an Orally Effective Metal Chelating Agent. *Annu. Rev. Pharmacol. Toxicol.* **1990**, *30* (1), 279–306.
- (121) Van der Linde, A.; Pillen, S.; Gerrits, G.; Bouwes Bavinck, J. Stevens-Johnson Syndrome in a Child with Chronic Mercury Exposure and 2, 3-Dimercaptopropane-1-Sulfonate (DMPS) Therapy. *Clin. Toxicol.* **2008**, *46* (5), 479–481.
- (122) Wang, N.; Hsu, C.; Zhu, L.; Tseng, S.; Hsu, J.-P. Influence of Metal Oxide Nanoparticles Concentration on Their Zeta Potential. *J. Colloid Interface Sci.* **2013**, *407*, 22–28.
- (123) Domingos, R. F.; Baalousha, M. A.; Ju-Nam, Y.; Reid, M. M.; Tufenkji, N.; Lead, J. R.; Leppard, G. G.; Wilkinson, K. J. Characterizing Manufactured Nanoparticles in the Environment: Multimethod Determination of Particle Sizes. *Environ. Sci. Technol.* **2009**, *43* (19), 7277–7284.
- (124) Sentein, C.; Guizard, B.; Giraud, S.; Yé, C.; Ténégal, F. Dispersion and Stability of TiO₂ Nanoparticles Synthesized by Laser Pyrolysis in Aqueous Suspensions; IOP Publishing, 2009; Vol. 170, p 012013.
- (125) Szakal, C.; McCarthy, J. A.; Ugelow, M. S.; Konicek, A. R.; Louis, K.; Yezer, B.; Herzing, A. A.; Hamers, R. J.; Holbrook, R. D. Preparation and Measurement Methods for Studying Nanoparticle Aggregate Surface Chemistry. *J. Environ. Monit.* **2012**, *14* (7), 1914–1925.
- (126) Elimelech, M.; Gregory, J.; Jia, X.; Williams, R. A. CHAPTER 3 - Surface Interaction Potentials. In *Particle Deposition and Aggregation*; Butterworth-Heinemann, 1995; pp 33–67. <https://doi.org/10.1016/B978-0-7506-0743-8.50007-8>.
- (127) Nielsen, M. K.; Arneborg, N. The Effect of Citric Acid and PH on Growth and Metabolism of Anaerobic *Saccharomyces Cerevisiae* and *Zygosaccharomyces Bailii* Cultures. *Food Microbiol.* **2007**, *24* (1), 101–105.
- (128) Zhang, Y.; Chen, Y.; Westerhoff, P.; Hristovski, K.; Crittenden, J. C. Stability of Commercial Metal Oxide Nanoparticles in Water. *Water Res.* **2008**, *42* (8–9), 2204–2212.
- (129) Lee, C.-G.; Javed, H.; Zhang, D.; Kim, J.-H.; Westerhoff, P.; Li, Q.; Alvarez, P. J. Porous Electrospun Fibers Embedding TiO₂ for Adsorption and Photocatalytic Degradation of Water Pollutants. *Environ. Sci. Technol.* **2018**, *52* (7), 4285–4293.

- (130) Nichols, G.; Byard, S.; Bloxham, M. J.; Botterill, J.; Dawson, N. J.; Dennis, A.; Diart, V.; North, N. C.; Sherwood, J. D. A Review of the Terms Agglomerate and Aggregate with a Recommendation for Nomenclature Used in Powder and Particle Characterization. *J. Pharm. Sci.* **2002**, *91* (10), 2103–2109.
- (131) Keller, A. A.; Wang, H.; Zhou, D.; Lenihan, H. S.; Cherr, G.; Cardinale, B. J.; Miller, R.; Ji, Z. Stability and Aggregation of Metal Oxide Nanoparticles in Natural Aqueous Matrices. *Environ. Sci. Technol.* **2010**, *44* (6), 1962–1967.
- (132) Suttiponpanit, K.; Jiang, J.; Sahu, M.; Suvachittanont, S.; Charinpanitkul, T.; Biswas, P. Role of Surface Area, Primary Particle Size, and Crystal Phase on Titanium Dioxide Nanoparticle Dispersion Properties. *Nanoscale Res Lett* **2010**, *6* (1), 27. <https://doi.org/10.1007/s11671-010-9772-1>.
- (133) Degen, A.; Kosec, M. Effect of PH and Impurities on the Surface Charge of Zinc Oxide in Aqueous Solution. *J. Eur. Ceram. Soc.* **2000**, *20* (6), 667–673.
- (134) Liao, D.; Wu, G.; Liao, B. Zeta Potential of Shape-Controlled TiO₂ Nanoparticles with Surfactants. *Colloids Surf. Physicochem. Eng. Asp.* **2009**, *348* (1–3), 270–275.
- (135) Nur, Y.; Lead, J.; Baalousha, M. Evaluation of Charge and Agglomeration Behavior of TiO₂ Nanoparticles in Ecotoxicological Media. *Sci. Total Environ.* **2015**, *535*, 45–53.
- (136) Honary, S.; Zahir, F. Effect of Zeta Potential on the Properties of Nano-Drug Delivery Systems-a Review (Part 2). *Trop. J. Pharm. Res.* **2013**, *12* (2), 265–273.
- (137) Turley, R.; Benavides, R.; Hernández-Viezcás, J. Á.; Gardea-Torresdey, J. L. Insights on Ligand Interactions with Titanium Dioxide Nanoparticles via Dynamic Light Scattering and Electrophoretic Light Scattering. *Microchem. J.* **2018**.
- (138) Williams, R.; Jencks, W.; Westheimer, F. PKa Data Compiled by R. Williams Available Online <https://www.chem.wisc.edu/areas/reichpkatablepkacompile-1-Williams.pdf> Accessed 10 Febr. 2018 **2004**.
- (139) Taurozzi, J. S.; Hackley, V. A.; Wiesner, M. Preparation of Nanoparticle Dispersions from Powdered Material Using Ultrasonic Disruption. *NIST Spec. Publ.* **2012**, *1200–2* (2), 15.
- (140) Taurozzi, J. S.; Hackley, V. A.; Wiesner, M. R. Ultrasonic Dispersion of Nanoparticles for Environmental, Health and Safety Assessment—Issues and Recommendations. *Nanotoxicology* **2011**, *5* (4), 711–729.
- (141) Taurozzi, J. S.; Hackley, V. A.; Wiesner, M. Preparation of a Nanoscale TiO₂ Aqueous Dispersion for Toxicological or Environmental Testing. *NIST Spec. Publ.* **2012**, *1200–3* (3), 11.
- (142) Kosmulski, M. The PH Dependent Surface Charging and Points of Zero Charge. VII. Update. *Adv. Colloid Interface Sci.* **2018**, *251*, 115–138. <https://doi.org/10.1016/j.cis.2017.10.005>.

- (143) Pradhan, S.; Hedberg, J.; Blomberg, E.; Wold, S.; Odnevall Wallinder, I. Effect of Sonication on Particle Dispersion, Administered Dose and Metal Release of Non-Functionalized, Non-Inert Metal Nanoparticles. *J. Nanoparticle Res.* **2016**, *18* (9). <https://doi.org/10.1007/s11051-016-3597-5>.
- (144) Roebben, G.; Ramirez-Garcia, S.; Hackley, V. A.; Roesslein, M.; Klaessig, F.; Kestens, V.; Lynch, I.; Garner, C. M.; Rawle, A.; Elder, A.; Colvin, V. L.; Kreyling, W.; Krug, H. F.; Lewicka, Z. A.; McNeil, S.; Nel, A.; Patri, A.; Wick, P.; Wiesner, M.; Xia, T.; Oberdörster, G.; Dawson, K. A. Interlaboratory Comparison of Size and Surface Charge Measurements on Nanoparticles Prior to Biological Impact Assessment. *J. Nanoparticle Res.* **2011**, *13* (7), 2675. <https://doi.org/10.1007/s11051-011-0423-y>.
- (145) Karlsson, H. L.; Cronholm, P.; Hedberg, Y.; Tornberg, M.; De Battice, L.; Svedhem, S.; Wallinder, I. O. Cell Membrane Damage and Protein Interaction Induced by Copper Containing Nanoparticles—Importance of the Metal Release Process. *Toxicology* **2013**, *313* (1), 59–69. <https://doi.org/10.1016/j.tox.2013.07.012>.
- (146) Dickson, D.; Liu, G.; Li, C.; Tachiev, G.; Cai, Y. Dispersion and Stability of Bare Hematite Nanoparticles: Effect of Dispersion Tools, Nanoparticle Concentration, Humic Acid and Ionic Strength. *Sci. Total Environ.* **2012**, *419*, 170–177. <https://doi.org/10.1016/j.scitotenv.2012.01.012>.
- (147) Betts, J. N.; Johnson, M. G.; Rygiewicz, P. T.; King, G. A.; Andersen, C. P. Potential for Metal Contamination by Direct Sonication of Nanoparticle Suspensions. *Environ. Toxicol. Chem.* **2013**, *32* (4), 889–893. <https://doi.org/10.1002/etc.2123>.
- (148) Alvarez, P. J. J.; Chan, C. K.; Elimelech, M.; Halas, N. J.; Villagrán, D. Emerging Opportunities for Nanotechnology to Enhance Water Security. *Nat. Nanotechnol.* **2018**, *13* (8), 634–641. <https://doi.org/10.1038/s41565-018-0203-2>.
- (149) Santhosh, C.; Velmurugan, V.; Jacob, G.; Jeong, S. K.; Grace, A. N.; Bhatnagar, A. Role of Nanomaterials in Water Treatment Applications: A Review. *Chem. Eng. J.* **2016**, *306*, 1116–1137. <https://doi.org/10.1016/j.cej.2016.08.053>.
- (150) Montenegro-Ayo, R.; Morales-Gomero, J. C.; Alarcon, H.; Cotillas, S.; Westerhoff, P.; Garcia-Segura, S. Scaling up Photoelectrocatalytic Reactors: A TiO₂ Nanotube-Coated Disc Compound Reactor Effectively Degrades Acetaminophen. *Water* **2019**, *11* (12), 2522. <https://doi.org/10.3390/w11122522>.
- (151) Loeb, S. K.; Alvarez, P. J. J.; Brame, J. A.; Cates, E. L.; Choi, W.; Crittenden, J.; Dionysiou, D. D.; Li, Q.; Li-Puma, G.; Quan, X.; Sedlak, D. L.; David Waite, T.; Westerhoff, P.; Kim, J.-H. The Technology Horizon for Photocatalytic Water Treatment: Sunrise or Sunset? *Environ. Sci. Technol.* **2019**, *53* (6), 2937–2947. <https://doi.org/10.1021/acs.est.8b05041>.
- (152) An, Y.; de Ridder, D. J.; Zhao, C.; Schoutteten, K.; Bussche, J. V.; Zheng, H.; Chen, G.; Vanhaecke, L. Adsorption and Photocatalytic Degradation of

- Pharmaceuticals and Pesticides by Carbon Doped-TiO₂ Coated on Zeolites under Solar Light Irradiation. *Water Sci. Technol.* **2016**, 73 (12), 2868–2881. <https://doi.org/10.2166/wst.2016.146>.
- (153) Bessergenev, V. G.; Mateus, M. C.; Morgado, I. M.; Hantusch, M.; Burkel, E. Photocatalytic Reactor, CVD Technology of Its Preparation and Water Purification from Pharmaceutical Drugs and Agricultural Pesticides. *Chem. Eng. J.* **2017**, 312, 306–316. <https://doi.org/10.1016/j.cej.2016.11.148>.
- (154) Da Silva, E. S.; Prevot, V.; Forano, C.; Wong-Wah-Chung, P.; Burrows, H. D.; Sarakha, M. Heterogeneous Photocatalytic Degradation of Pesticides Using Decatungstate Intercalated Macroporous Layered Double Hydroxides. *Environ. Sci. Pollut. Res.* **2014**, 21 (19), 11218–11227. <https://doi.org/10.1007/s11356-014-2971-z>.
- (155) Jasim, S. Y.; Irabelli, A.; Yang, P.; Ahmed, S.; Schweitzer, L. Presence of Pharmaceuticals and Pesticides in Detroit River Water and the Effect of Ozone on Removal. *Ozone Sci. Eng.* **2006**, 28 (6), 415–423. <https://doi.org/10.1080/01919510600985945>.
- (156) Beltrán, F. J.; Rey, A. Free Radical and Direct Ozone Reaction Competition to Remove Priority and Pharmaceutical Water Contaminants with Single and Hydrogen Peroxide Ozonation Systems. *Ozone Sci. Eng.* **2018**, 40 (4), 251–265. <https://doi.org/10.1080/01919512.2018.1431521>.
- (157) Sylvester, P.; Westerhoff, P.; Möller, T.; Badruzzaman, M.; Boyd, O. A Hybrid Sorbent Utilizing Nanoparticles of Hydrous Iron Oxide for Arsenic Removal from Drinking Water. *Environ. Eng. Sci.* **2006**, 24 (1), 104–112. <https://doi.org/10.1089/ees.2007.24.104>.
- (158) Guan, X.; Du, J.; Meng, X.; Sun, Y.; Sun, B.; Hu, Q. Application of Titanium Dioxide in Arsenic Removal from Water: A Review. *J. Hazard. Mater.* **2012**, 215–216, 1–16. <https://doi.org/10.1016/j.jhazmat.2012.02.069>.
- (159) NuTiO Titanium Dioxide Commercial Cleaning Technology <https://www.nanotechproject.org/cpi/products/nutio-titanium-dioxide-commercial-cleaning-technology/> (accessed Apr 3, 2020).
- (160) Gehrke, I.; Geiser, A.; Somborn-Schulz, A. Innovations in Nanotechnology for Water Treatment. *Nanotechnol. Sci. Appl.* **2015**, 8, 1–17. <https://doi.org/10.2147/NSA.S43773>.
- (161) Riaz, S.; Park, S.-J. An Overview of TiO₂-Based Photocatalytic Membrane Reactors for Water and Wastewater Treatments. *J. Ind. Eng. Chem.* **2020**, 84, 23–41. <https://doi.org/10.1016/j.jiec.2019.12.021>.
- (162) Stancl, H. O.; Hristovski, K.; Westerhoff, P. Hexavalent Chromium Removal Using UV-TiO₂/Ceramic Membrane Reactor. *Environ. Eng. Sci.* **2015**, 32 (8), 676–683. <https://doi.org/10.1089/ees.2014.0507>.

- (163) Gerrity, D.; Ryu, H.; Crittenden, J.; Abbaszadegan, M. Photocatalytic Inactivation of Viruses Using Titanium Dioxide Nanoparticles and Low-Pressure UV Light. *J. Environ. Sci. Health Part A* **2008**, *43* (11), 1261–1270. <https://doi.org/10.1080/10934520802177813>.
- (164) Stefan, M. I. *Advanced Oxidation Processes for Water Treatment: Fundamentals and Applications*; IWA Publishing, 2017.
- (165) Puralytics <https://web.archive.org/web/20200407124624/https://puralytics.com/> (accessed May 7, 2020).
- (166) Gar Alalm, M.; Tawfik, A.; Ookawara, S. Enhancement of Photocatalytic Activity of TiO₂ by Immobilization on Activated Carbon for Degradation of Pharmaceuticals. *J. Environ. Chem. Eng.* **2016**, *4* (2), 1929–1937. <https://doi.org/10.1016/j.jece.2016.03.023>.
- (167) Abdel-Maksoud, Y. K.; Imam, E.; Ramadan, A. R. Sand Supported TiO₂ Photocatalyst in a Tray Photo-Reactor for the Removal of Emerging Contaminants in Wastewater. *Catal. Today* **2018**, *313*, 55–62. <https://doi.org/10.1016/j.cattod.2017.10.029>.
- (168) Binas, V.; Venieri, D.; Kotzias, D.; Kiriakidis, G. Modified TiO₂ Based Photocatalysts for Improved Air and Health Quality. *J. Materiomics* **2017**, *3* (1), 3–16. <https://doi.org/10.1016/j.jmat.2016.11.002>.
- (169) Islam, Md. T.; Dominguez, A.; Turley, R. S.; Kim, H.; Sultana, K. A.; Shuvo, M.; Alvarado-Tenorio, B.; Montes, M. O.; Lin, Y.; Gardea-Torresdey, J.; Noveron, J. C. Development of Photocatalytic Paint Based on TiO₂ and Photopolymer Resin for the Degradation of Organic Pollutants in Water. *Sci. Total Environ.* **2020**, *704*, 135406. <https://doi.org/10.1016/j.scitotenv.2019.135406>.
- (170) Powell, C. D.; Atkinson, A. J.; Ma, Y.; Marcos-Hernandez, M.; Villagran, D.; Westerhoff, P.; Wong, M. S. Magnetic Nanoparticle Recovery Device (MagNERD) Enables Application of Iron Oxide Nanoparticles for Water Treatment. *J. Nanoparticle Res.* **2020**, *22* (2), 48. <https://doi.org/10.1007/s11051-020-4770-4>.
- (171) Gondikas, A. P.; Kammer, F. von der; Reed, R. B.; Wagner, S.; Ranville, J. F.; Hofmann, T. Release of TiO₂ Nanoparticles from Sunscreens into Surface Waters: A One-Year Survey at the Old Danube Recreational Lake. *Environ. Sci. Technol.* **2014**, *48* (10), 5415–5422. <https://doi.org/10.1021/es405596y>.
- (172) Bourgeault, A.; Cousin, C.; Geertsen, V.; Cassier-Chauvat, C.; Chauvat, F.; Durupthy, O.; Chanéac, C.; Spalla, O. The Challenge of Studying TiO₂ Nanoparticle Bioaccumulation at Environmental Concentrations: Crucial Use of a Stable Isotope Tracer. *Environ. Sci. Technol.* **2015**, *49* (4), 2451–2459. <https://doi.org/10.1021/es504638f>.
- (173) Shi, X.; Li, Z.; Chen, W.; Qiang, L.; Xia, J.; Chen, M.; Zhu, L.; Alvarez, P. J. Fate of TiO₂ Nanoparticles Entering Sewage Treatment Plants and Bioaccumulation in Fish in the Receiving Streams. *NanoImpact* **2016**, *3*, 96–103.

- (174) B. Reed, R.; P. Martin, D.; J. Bednar, A.; D. Montaña, M.; Westerhoff, P.; F. Ranville, J. Multi-Day Diurnal Measurements of Ti-Containing Nanoparticle and Organic Sunscreen Chemical Release during Recreational Use of a Natural Surface Water. *Environ. Sci. Nano* **2017**, *4* (1), 69–77. <https://doi.org/10.1039/C6EN00283H>.
- (175) Venkatesan, A. K.; Reed, R. B.; Lee, S.; Bi, X.; Hanigan, D.; Yang, Y.; Ranville, J. F.; Herckes, P.; Westerhoff, P. Detection and Sizing of Ti-Containing Particles in Recreational Waters Using Single Particle ICP-MS. *Bull. Environ. Contam. Toxicol.* **2018**, *100* (1), 120–126. <https://doi.org/10.1007/s00128-017-2216-1>.
- (176) Sun, H.; Zhang, X.; Niu, Q.; Chen, Y.; Crittenden, J. C. Enhanced Accumulation of Arsenate in Carp in the Presence of Titanium Dioxide Nanoparticles. *Water. Air. Soil Pollut.* **2007**, *178* (1), 245–254. <https://doi.org/10.1007/s11270-006-9194-y>.
- (177) Zeman, T.; Loh, E.-W.; Čierný, D.; Šerý, O. Penetration, Distribution and Brain Toxicity of Titanium Nanoparticles in Rodents' Body: A Review. *IET Nanobiotechnol.* **2018**, *12* (6), 695–700. <https://doi.org/10.1049/iet-nbt.2017.0109>.
- (178) Laomettachit, T.; Puri, I. K.; Liangruksa, M. A Two-Step Model of TiO₂ Nanoparticle Toxicity in Human Liver Tissue. *Toxicol. Appl. Pharmacol.* **2017**, *334*, 47–54. <https://doi.org/10.1016/j.taap.2017.08.018>.
- (179) Younes, M.; Aggett, P.; Aguilar, F.; Crebelli, R.; Dusemund, B.; Filipič, M.; Frutos, M. J.; Galtier, P.; Gott, D.; Gundert-Remy, U.; Kuhnle, G. G.; Lambré, C.; Leblanc, J.-C.; Lillegaard, I. T.; Moldeus, P.; Mortensen, A.; Oskarsson, A.; Stankovic, I.; Waalkens-Berendsen, I.; Wright, M.; Lodi, F.; Rincon, A. M.; Smeraldi, C.; Woutersen, R. A. Evaluation of Four New Studies on the Potential Toxicity of Titanium Dioxide Used as a Food Additive (E 171). *EFSA J.* **2018**, *16* (7), e05366. <https://doi.org/10.2903/j.efsa.2018.5366>.
- (180) Karimipour, M.; Zirak Javanmard, M.; Ahmadi, A.; Jafari, A. Oral Administration of Titanium Dioxide Nanoparticle through Ovarian Tissue Alterations Impairs Mice Embryonic Development. *Int. J. Reprod. Biomed.* **2018**, *16* (6), 397–404.
- (181) Flores, K.; Turley, R. S.; Valdes, C.; Ye, Y.; Cantu, J.; Hernandez-Viezcas, J. A.; Parsons, J. G.; Gardea-Torresdey, J. L. Environmental Applications and Recent Innovations in Single Particle Inductively Coupled Plasma Mass Spectrometry (SP-ICP-MS). *Appl. Spectrosc. Rev.* **2019**, *0* (0), 1–26. <https://doi.org/10.1080/05704928.2019.1694937>.
- (182) Aznar, R.; Barahona, F.; Geiss, O.; Ponti, J.; José Luis, T.; Barrero-Moreno, J. Quantification and Size Characterisation of Silver Nanoparticles in Environmental Aqueous Samples and Consumer Products by Single Particle-ICPMS. *Talanta* **2017**, *175*, 200–208. <https://doi.org/10.1016/j.talanta.2017.07.048>.
- (183) Ramos, K.; Gómez-Gómez, M. M.; Cámara, C.; Ramos, L. Silver Speciation and Characterization of Nanoparticles Released from Plastic Food Containers by Single Particle ICPMS. *Talanta* **2016**, *151*, 83–90. <https://doi.org/10.1016/j.talanta.2015.12.071>.

- (184) Bulbul, G.; Eskandarloo, H.; Abbaspourrad, A. A Novel Paper Based Colorimetric Assay for the Detection of TiO₂ Nanoparticles. *Anal. Methods* **2018**, *10* (3), 275–280. <https://doi.org/10.1039/C7AY02700A>.
- (185) Yoe, J. H.; Armstrong, A. R. Colorimetric Determination of Titanium with Disodium-1,2-Dihydroxybenzene-3,5-Disulfonate. *Anal. Chem.* **1947**, *19* (2), 100–102. <https://doi.org/10.1021/ac60002a009>.
- (186) HAMANO, T.; MITSUHASHI, Y.; Aoki, N.; YAMAMOTO, S.; TSUJI, S.; ITO, Y.; OJI, Y. Colorimetric Micro-Determination of Titanium Dioxide in Foods. *NIPPON SHOKUJIN KOGYO GAKKAISHI* **1990**, *37* (2), 162–166.
- (187) Bocca, B.; Caimi, S.; Senofonte, O.; Alimonti, A.; Petrucci, F. ICP-MS Based Methods to Characterize Nanoparticles of TiO₂ and ZnO in Sunscreens with Focus on Regulatory and Safety Issues. *Sci. Total Environ.* **2018**, *630*, 922–930. <https://doi.org/10.1016/j.scitotenv.2018.02.166>.
- (188) Dan, Y.; Shi, H.; Stephan, C.; Liang, X. Rapid Analysis of Titanium Dioxide Nanoparticles in Sunscreens Using Single Particle Inductively Coupled Plasma–Mass Spectrometry. *Microchem. J.* **2015**, *122*, 119–126. <https://doi.org/10.1016/j.microc.2015.04.018>.
- (189) Page, S. E.; Arnold, W. A.; McNeill, K. Terephthalate as a Probe for Photochemically Generated Hydroxyl Radical. *J. Environ. Monit.* **2010**, *12* (9), 1658–1665. <https://doi.org/10.1039/C0EM00160K>.
- (190) Barreto, J. C.; Smith, G. S.; Strobel, N. H. P.; McQuillin, P. A.; Miller, T. A. Terephthalic Acid: A Dosimeter for the Detection of Hydroxyl Radicals in Vitro. *Life Sci.* **1994**, *56* (4), PL89–PL96. [https://doi.org/10.1016/0024-3205\(94\)00925-2](https://doi.org/10.1016/0024-3205(94)00925-2).
- (191) Lin, X. H.; Lee, S. N.; Zhang, W.; Li, S. F. Y. Photocatalytic Degradation of Terephthalic Acid on Sulfated Titania Particles and Identification of Fluorescent Intermediates. *J. Hazard. Mater.* **2016**, *303*, 64–75. <https://doi.org/10.1016/j.jhazmat.2015.10.025>.
- (192) Heringa, M. B.; Peters, R. J. B.; Bleys, R. L. A. W.; van der Lee, M. K.; Tromp, P. C.; van Kesteren, P. C. E.; van Eijkeren, J. C. H.; Undas, A. K.; Oomen, A. G.; Bouwmeester, H. Detection of Titanium Particles in Human Liver and Spleen and Possible Health Implications. *Part. Fibre Toxicol.* **2018**, *15* (1), 15. <https://doi.org/10.1186/s12989-018-0251-7>.
- (193) Pal, A.; Pal, M.; Mukherjee, P.; Bagchi, A.; Raha, A. Determination of the Hardness of Drinking Packaged Water of Kalyani Area, West Bengal. *Asian J. Pharm. Pharmacol.* **2018**, *4* (2), 203–206.
- (194) Li, S.; Timoshkin, I. V.; Maclean, M.; Macgregor, S. J.; Wilson, M. P.; Given, M. J.; Wang, T.; Anderson, J. G. Fluorescence Detection of Hydroxyl Radicals in Water Produced by Atmospheric Pulsed Discharges. *IEEE Trans. Dielectr. Electr. Insul.* **2015**, *22* (4), 1856–1865. <https://doi.org/10.1109/TDEI.2015.005147>.

- (195) López, R.; Gómez, R. Band-Gap Energy Estimation from Diffuse Reflectance Measurements on Sol–Gel and Commercial TiO₂: A Comparative Study. *J. Sol-Gel Sci. Technol.* **2012**, *61* (1), 1–7. <https://doi.org/10.1007/s10971-011-2582-9>.
- (196) de la Calle, I.; Menta, M.; Klein, M.; Séby, F. Screening of TiO₂ and Au Nanoparticles in Cosmetics and Determination of Elemental Impurities by Multiple Techniques (DLS, SP-ICP-MS, ICP-MS and ICP-OES). *Talanta* **2017**, *171*, 291–306. <https://doi.org/10.1016/j.talanta.2017.05.002>.
- (197) Zhang, J.; Zhou, P.; Liu, J.; Yu, J. New Understanding of the Difference of Photocatalytic Activity among Anatase, Rutile and Brookite TiO₂. *Phys. Chem. Chem. Phys.* **2014**, *16* (38), 20382–20386. <https://doi.org/10.1039/C4CP02201G>.
- (198) Vequizo, J. J. M.; Matsunaga, H.; Ishiku, T.; Kamimura, S.; Ohno, T.; Yamakata, A. Trapping-Induced Enhancement of Photocatalytic Activity on Brookite TiO₂ Powders: Comparison with Anatase and Rutile TiO₂ Powders. *ACS Catal.* **2017**, *7* (4), 2644–2651. <https://doi.org/10.1021/acscatal.7b00131>.
- (199) Burns Robert A.; Crittenden John C.; Hand David W.; Selzer Volker H.; Sutter Lawrence L.; Salman Salman R. Effect of Inorganic Ions in Heterogeneous Photocatalysis of TCE. *J. Environ. Eng.* **1999**, *125* (1), 77–85. [https://doi.org/10.1061/\(ASCE\)0733-9372\(1999\)125:1\(77\)](https://doi.org/10.1061/(ASCE)0733-9372(1999)125:1(77)).
- (200) Lutze, H. V.; Kerlin, N.; Schmidt, T. C. Sulfate Radical-Based Water Treatment in Presence of Chloride: Formation of Chlorate, Inter-Conversion of Sulfate Radicals into Hydroxyl Radicals and Influence of Bicarbonate. *Water Res.* **2015**, *72*, 349–360. <https://doi.org/10.1016/j.watres.2014.10.006>.
- (201) Wang, J.; Zhu, H.; Hurren, C.; Zhao, J.; Pakdel, E.; Li, Z.; Wang, X. Degradation of Organic Dyes by P25-Reduced Graphene Oxide: Influence of Inorganic Salts and Surfactants. *J. Environ. Chem. Eng.* **2015**, *3* (3), 1437–1443. <https://doi.org/10.1016/j.jece.2015.05.008>.
- (202) Hanigan, D.; Truong, L.; Schoepf, J.; Nosaka, T.; Mulchandani, A.; Tanguay, R. L.; Westerhoff, P. Trade-Offs in Ecosystem Impacts from Nanomaterial versus Organic Chemical Ultraviolet Filters in Sunscreens. *Water Res.* **2018**, *139*, 281–290. <https://doi.org/10.1016/j.watres.2018.03.062>.
- (203) Sun, T. Y.; Gottschalk, F.; Hungerbühler, K.; Nowack, B. Comprehensive Probabilistic Modelling of Environmental Emissions of Engineered Nanomaterials. *Environ. Pollut.* **2014**, *185*, 69–76. <https://doi.org/10.1016/j.envpol.2013.10.004>.
- (204) Bi, X.; Ma, H.; Westerhoff, P. Dry Powder Assay Rapidly Detects Metallic Nanoparticles in Water by Measuring Surface Catalytic Reactivity. *Environ. Sci. Technol.* **2018**, *52* (22), 13289–13297. <https://doi.org/10.1021/acs.est.8b03915>.
- (205) Piccinno, F.; Gottschalk, F.; Seeger, S.; Nowack, B. Industrial Production Quantities and Uses of Ten Engineered Nanomaterials in Europe and the World. *J. Nanoparticle Res.* **2012**, *14* (9), 1109. <https://doi.org/10.1007/s11051-012-1109-9>.

- (206) B. Saleh, N.; Khalid, A.; Tian, Y.; Ayres, C.; V. Sabaraya, I.; Pietari, J.; Hanigan, D.; Chowdhury, I.; G. Apul, O. Removal of Poly- and per-Fluoroalkyl Substances from Aqueous Systems by Nano-Enabled Water Treatment Strategies. *Environ. Sci. Water Res. Technol.* **2019**, *5* (2), 198–208. <https://doi.org/10.1039/C8EW00621K>.
- (207) Pulizzi, F.; Sun, W. Treating Water with Nano. *Nat. Nanotechnol.* **2018**, *13* (8), 633–633. <https://doi.org/10.1038/s41565-018-0238-4>.
- (208) Theron, J.; Walker, J. A.; Cloete, T. E. Nanotechnology and Water Treatment: Applications and Emerging Opportunities. *Crit. Rev. Microbiol.* **2008**, *34* (1), 43–69. <https://doi.org/10.1080/10408410701710442>.
- (209) Qu, X.; Brame, J.; Li, Q.; Alvarez, P. J. J. Nanotechnology for a Safe and Sustainable Water Supply: Enabling Integrated Water Treatment and Reuse. *Acc. Chem. Res.* **2013**, *46* (3), 834–843. <https://doi.org/10.1021/ar300029v>.
- (210) Tiwari, D. K.; Behari, J.; Sen, P. *Application of Nanoparticles in Waste Water Treatment 1*.
- (211) Luksiene, Z. 16 - Nanoparticles and Their Potential Application as Antimicrobials in the Food Industry. In *Food Preservation*; Grumezescu, A. M., Ed.; Nanotechnology in the Agri-Food Industry; Academic Press, 2017; pp 567–601. <https://doi.org/10.1016/B978-0-12-804303-5.00016-X>.
- (212) Katsnelson, B. A.; Privalova, L. I.; Sutunkova, M. P.; Minigalieva, I. A.; Gurvich, V. B.; Shur, V. Y.; Shishkina, E. V.; Makeyev, O. H.; Valamina, I. E.; Varaksin, A. N.; Panov, V. G. Experimental Research into Metallic and Metal Oxide Nanoparticle Toxicity In Vivo. In *Bioactivity of Engineered Nanoparticles*; Yan, B., Zhou, H., Gardea-Torresdey, J. L., Eds.; Nanomedicine and Nanotoxicology; Springer: Singapore, 2017; pp 259–319. https://doi.org/10.1007/978-981-10-5864-6_11.
- (213) Love, S. A.; Maurer-Jones, M. A.; Thompson, J. W.; Lin, Y.-S.; Haynes, C. L. Assessing Nanoparticle Toxicity. *Annu. Rev. Anal. Chem.* **2012**, *5* (1), 181–205. <https://doi.org/10.1146/annurev-anchem-062011-143134>.
- (214) Chakraborty, C.; Sharma, A. R.; Sharma, G.; Lee, S.-S. Zebrafish: A Complete Animal Model to Enumerate the Nanoparticle Toxicity. *J. Nanobiotechnology* **2016**, *14* (1), 65. <https://doi.org/10.1186/s12951-016-0217-6>.
- (215) Buchman, J. T.; Hudson-Smith, N. V.; Landy, K. M.; Haynes, C. L. Understanding Nanoparticle Toxicity Mechanisms To Inform Redesign Strategies To Reduce Environmental Impact. *Acc. Chem. Res.* **2019**, *52* (6), 1632–1642. <https://doi.org/10.1021/acs.accounts.9b00053>.
- (216) Mahapatra, I.; Sun, T. Y.; Clark, J. R. A.; Dobson, P. J.; Hungerbuehler, K.; Owen, R.; Nowack, B.; Lead, J. Probabilistic Modelling of Prospective Environmental Concentrations of Gold Nanoparticles from Medical Applications as a Basis for Risk Assessment. *J. Nanobiotechnology* **2015**, *13* (1), 93. <https://doi.org/10.1186/s12951-015-0150-0>.

- (217) Hagendorfer, H.; Kaegi, R.; Parlinska, M.; Sinnet, B.; Ludwig, C.; Ulrich, A. Characterization of Silver Nanoparticle Products Using Asymmetric Flow Field Flow Fractionation with a Multidetector Approach – a Comparison to Transmission Electron Microscopy and Batch Dynamic Light Scattering. *Anal. Chem.* **2012**, *84* (6), 2678–2685. <https://doi.org/10.1021/ac202641d>.
- (218) Hadioui, M.; Leclerc, S.; Wilkinson, K. J. Multimethod Quantification of Ag⁺ Release from Nanosilver. *Talanta* **2013**, *105*, 15–19. <https://doi.org/10.1016/j.talanta.2012.11.048>.
- (219) Merrifield, R. C.; Stephan, C.; Lead, J. Determining the Concentration Dependent Transformations of Ag Nanoparticles in Complex Media: Using SP-ICP-MS and Au@Ag Core–Shell Nanoparticles as Tracers. *Environ. Sci. Technol.* **2017**, *51* (6), 3206–3213. <https://doi.org/10.1021/acs.est.6b05178>.
- (220) Römer, I.; White, T. A.; Baalousha, M.; Chipman, K.; Viant, M. R.; Lead, J. R. Aggregation and Dispersion of Silver Nanoparticles in Exposure Media for Aquatic Toxicity Tests. *J. Chromatogr. A* **2011**, *1218* (27), 4226–4233. <https://doi.org/10.1016/j.chroma.2011.03.034>.
- (221) J. Stark, W.; R. Stoessel, P.; Wohlleben, W.; Hafner, A. Industrial Applications of Nanoparticles. *Chem. Soc. Rev.* **2015**, *44* (16), 5793–5805. <https://doi.org/10.1039/C4CS00362D>.
- (222) Baalousha, M.; Sikder, M.; Prasad, A.; Lead, J.; Merrifield, R.; Chandler, G. T. The Concentration-Dependent Behaviour of Nanoparticles. *Environ. Chem.* **2015**, *13* (1), 1–3. <https://doi.org/10.1071/EN15142>.
- (223) Zou, X.; Shi, J.; Zhang, H. Morphological Evolution and Reconstruction of Silver Nanoparticles in Aquatic Environments: The Roles of Natural Organic Matter and Light Irradiation. *J. Hazard. Mater.* **2015**, *292*, 61–69. <https://doi.org/10.1016/j.jhazmat.2015.03.005>.
- (224) US Environmental Protection Agency. Methods for Measuring the Acute Toxicity of Effluents and Receiving Waters to Freshwater and Marine Organisms. *EPA-821-R-02-012* **2002**.
- (225) Tharaud, M.; P. Gondikas, A.; F. Benedetti, M.; Kammer, F. von der; Hofmann, T.; Cornelis, G. TiO₂ Nanomaterial Detection in Calcium Rich Matrices by SpICPMS. A Matter of Resolution and Treatment. *J. Anal. At. Spectrom.* **2017**, *32* (7), 1400–1411. <https://doi.org/10.1039/C7JA00060J>.
- (226) Laborda, F.; Jiménez-Lamana, J.; Bolea, E.; R. Castillo, J. Critical Considerations for the Determination of Nanoparticle Number Concentrations, Size and Number Size Distributions by Single Particle ICP-MS. *J. Anal. At. Spectrom.* **2013**, *28* (8), 1220–1232. <https://doi.org/10.1039/C3JA50100K>.
- (227) Lee, W.-W.; Chan, W.-T. Calibration of Single-Particle Inductively Coupled Plasma-Mass Spectrometry (SP-ICP-MS). *J. Anal. At. Spectrom.* **2015**, *30* (6), 1245–1254. <https://doi.org/10.1039/C4JA00408F>.

- (228) Pace, H. E.; Rogers, N. J.; Jarolimek, C.; Coleman, V. A.; Higgins, C. P.; Ranville, J. F. Determining Transport Efficiency for the Purpose of Counting and Sizing Nanoparticles via Single Particle Inductively Coupled Plasma Mass Spectrometry. *Anal. Chem.* **2011**, *83* (24), 9361–9369. <https://doi.org/10.1021/ac201952t>.
- (229) Croteau, M.-N.; Misra, S. K.; Luoma, S. N.; Valsami-Jones, E. Silver Bioaccumulation Dynamics in a Freshwater Invertebrate after Aqueous and Dietary Exposures to Nanosized and Ionic Ag. *Environ. Sci. Technol.* **2011**, *45* (15), 6600–6607. <https://doi.org/10.1021/es200880c>.
- (230) Römer, I.; Gavin, A. J.; White, T. A.; Merrifield, R. C.; Chipman, J. K.; Viant, M. R.; Lead, J. R. The Critical Importance of Defined Media Conditions in Daphnia Magna Nanotoxicity Studies. *Toxicol. Lett.* **2013**, *223* (1), 103–108. <https://doi.org/10.1016/j.toxlet.2013.08.026>.
- (231) Fabrega, J.; Zhang, R.; Renshaw, J. C.; Liu, W.-T.; Lead, J. R. Impact of Silver Nanoparticles on Natural Marine Biofilm Bacteria. *Chemosphere* **2011**, *85* (6), 961–966. <https://doi.org/10.1016/j.chemosphere.2011.06.066>.
- (232) Gaiser, B. K.; Fernandes, T. F.; Jepson, M.; Lead, J. R.; Tyler, C. R.; Stone, V. Assessing Exposure, Uptake and Toxicity of Silver and Cerium Dioxide Nanoparticles from Contaminated Environments. *Environ. Health* **2009**, *8* (1), S2. <https://doi.org/10.1186/1476-069X-8-S1-S2>.
- (233) Laborda, F.; Bolea, E.; Cepriá, G.; Gómez, M. T.; Jiménez, M. S.; Pérez-Arantegui, J.; Castillo, J. R. Detection, Characterization and Quantification of Inorganic Engineered Nanomaterials: A Review of Techniques and Methodological Approaches for the Analysis of Complex Samples. *Anal. Chim. Acta* **2016**, *904*, 10–32. <https://doi.org/10.1016/j.aca.2015.11.008>.

Vita

Reagan Scott Turley was born in Salt Lake City, Utah, the second of four children. He received a Bachelor of Science in Chemistry with a minor in Mathematics in 2015 from Brigham Young University in Provo, Utah. During his undergraduate studies he performed research on the synthesis, characterization, and utility of zinc oxide nanomaterials. While at BYU, Reagan interned with the Utah Bureau of Forensic Services and assisted in the development of an FTIR library of controlled substances, extracted hash oil for preliminary testing training kits, and added samples to a nationwide vehicle paint database.

Reagan joined the Ph.D. program in Chemistry at the University of Texas at El Paso in Spring 2016. He became a student researcher for the NSF Engineering Research Center for Nanotechnology Enabled Water Treatment (NEWTEC) under the advisement of Dr. Jorge Gardea-Torresdey. During his doctoral studies, he helped produce a series of instructional videos for freshman year chemistry courses as a teaching assistant. Reagan presented his research at two conferences, an ACS regional conference in El Paso, TX, and at the 8th annual Sustainable Nanotechnology Organization conference in San Diego, CA. As of this writing, he has one first-author publication and seven other publications as a co-author.

Email address: reaganturley@runbox.com